# Master's Thesis : Dynamics and control of low inertia power networks with high penetration of renewable energy sources

**Auteur :** Dragozis, Romane
**Promoteur(s) :** Ernst, Damien
**Faculté :** Faculté des Sciences appliquées
**Diplôme :** Master : ingénieur civil électricien, à finalité spécialisée en "electronic systems and devices"
**Année académique :** 2019-2020
**URI/URL :** http://hdl.handle.net/2268.2/9051

# Dynamics and control of low inertia power networks with high penetration of renewable energy sources

Graduation Studies conducted for obtaining the Master's degree in Electrical Engineering by

ROMANE DRAGOZIS

Supervisor :
DAMIEN ERNST

Jury members :
THIERRY VAN CUTSEM
CHRISTOPHE DRUET

University of Liège
Faculty of Applied Sciences
Academic year 2019 - 2020

# Abstract

Nowadays, power systems are mainly composed of conventional power plants connected to the grid through synchronous machines. However, renewable energy sources see their establishment grow with time, especially wind power and photovoltaic (PV) plants but also energy storage systems, to reduce $CO_2$ and other greenhouse gases emissions. These technologies are connected to the grid through power electronics devices, that decouple them from the network and protect them from any inertia response contrary to synchronous machines. This lack of inertia jeopardizes the system stability and has harmful effects in terms of the frequency response but also on the voltage stability.

This work thus focuses on the study of such transmission networks with high penetration of renewable energy sources. The first chapter targets on the network stability theory. It includes an overview of the main system parameters as well as their effect on the network stability and focuses especially on the frequency response and the voltage stability.

The second chapter is dedicated to the influence of inertia in the network. Definition of inertia in power systems is given using the swing equation as well as the interpretation of inertia together with the link between this measure and system frequency or voltage. The load participation in the frequency response is also discussed as it has an influence on the system and finally the aggregated model of a whole power system is given.

In the third chapter, three main sections are developed, focusing on low inertia networks. The first one consists of the consequences that the lack of inertia has on power systems stability, in terms of frequency, voltage, over-current and black-start capabilities, system parameters and power reserves. It thus focuses on the way the system reacts to severe faults where the second section introduces energy buffer technologies together with solutions that can be implemented for 100 % power electronics-based systems to participate in frequency and voltage regulation. Finally, the third section focuses on the particular case of the converters connecting the renewable energy source to the grid either in grid-following or grid-forming mode. The definition and the characteristics of each converter as well as the motivation behind using grid-forming converters is given. The models of each converter used in the simulations is described as well in this chapter.

The application to the Nordic network is discussed in the fourth chapter. The simulation tools that are used are presented in addition to the topology of the studied network. Its initial operation is illustrated and then two types of simulations are presented. The first one consists in depopulating a region of the network of synchronous machines and replacing them with renewable energy sources connected through converters while the other configuration makes use of a HVDC link that imports active power out of an interconnection. Each configuration is studied in terms of frequency response and voltage control and various technologies mixes are proposed to obtain the most appropriate one.

Finally, the fifth chapter gives an overall overview of the remaining and encountered challenges linked to the high penetration of inverter-based energy sources while the last chapter concludes the entire work.

# Acknowledgments

First and foremost, I would like to express my special thanks and gratitude to my supervisor Pr. *Damien Ernst* who gave me the opportunity to carry this thesis out on this enriching and topical subject. I am grateful for his permanent enthusiasm about my work, his positivity, his availability and his guidance helping me to organise and finalize this thesis in the best way possible.

My appreciation and gratitude are extended to Pr. *Thierry Van Cutsem* and his assistant *Bertand Bastin*. They both helped me use the software `RAMSES` and `ARTERE` as well as the models they have implemented. They were also crucial to figure out the physics behind each component. Thanks to their availability, advice and generosity, I could achieve to complete this thesis as I wanted to.

Then, I would like to express my gratitude to the University of Liege but more especially to the Montefiore Institute. I would like to thank the professors for their professionalism, the availability of the laboratories necessary for my learning and for training my skills during these last five years throughout which I came to know about a large range of different matters

I would like to include a special thanks to *Luc Martin* but more especially *Dimitri Monie*. Both have read this thesis to check the content out, the English and the orthography. I would not have been able to delve into my thesis topic with such a precision without their precious help.

Last but no least, I would like to thank my family and my boyfriend for supporting me in this work during these last months.

# Contents

# List of Figures

# List of Tables

# Introduction

A growing proportion of renewable energy sources is constituting today's power systems such as wind power and PV plants especially in order to reduce the $CO_2$ and other greenhouse gases emissions. Indeed, in 2015, the EU-28 countries total capacity reached 128.8 GW of wind power and 87.9 GW of PV, both representing 23.8 % of the total european electricity generation capacity [28]. As it has already increased because of the reduction of these technologies' costs, this capacity is expected to grow up significantly with the next ten years : the installed capacity could reach 323 GW of PV and 192 GW of wind power in 2030, corresponding respectively to 30 % and 18 % of the total European demand [10, 16]. These renewable energy sources are connected to the grid through power electronics devices that decouple them from the network. This effect is not similar to the conventional power plants that use synchronous generators which direct connection to the grid inherently stabilizes the system when a contingency occurs in the network, such as power imbalance or a short-circuit [28]. By replacing these conventional power plants with renewable energy sources, the overall system inertia being reduced, it jeopardizes the stability of the system since it is an inherent parameter that dampens the harmful effects of a fault. As detailed later, huge frequency deviations and voltage instabilities endangering the grid stability and the power balancing are more likely to occur with the high penetration of renewable energy sources in the system. In order to deal with these problems, Transmission System Operators, or TSOs, have until now limited the level of inverter-based power plants in some countries, usually between 20 % and 50 % of the total generation capacity [28].

The goal of this master thesis is to study the network stability of high-voltage transmission power systems with high integration of renewable energy sources and apply the outcomes to an existing network where conventional power plants are replaced with renewable energy sources. FIGURE 1 illustrates the evolution of such a network moving from mainly conventional sources of power characterized by a high inertia to an inverter-based grid with a majority of renewable sources of energy as wind, PV and storage units.
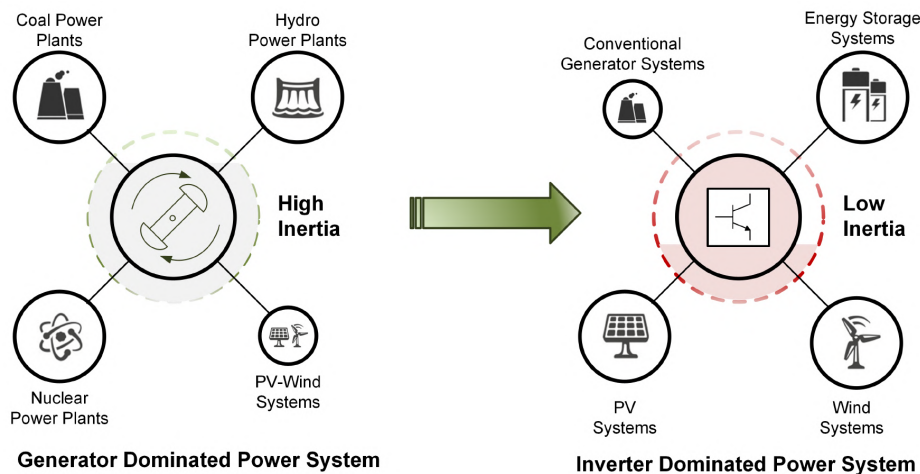


Figure 1: Illustration of the change in the power system from conventional power plants towards 100 % inverter-based power system [25].

1

# Chapter 1

# Network stability

Stability in a power network consists in maintaining it in a permanent operating equilibrium, which means keeping steady voltages and frequency relatively constant and maintaining synchronism between synchronous machines. All these conditions need to be fulfilled in order to keep the system robust and to work in a reliable and secure operation [14]. The main system parameters, as shown in the schema represented in FIGURE 1.1, are thus *frequency*, *voltage* and *rotor angle*. Angle stability can be divided in two categories : small-signal stability and transient stability ; voltage stability is studied depending on the magnitude of the disturbance and finally each system parameter is characterized by either a short or long term time span, except for the angle stability.
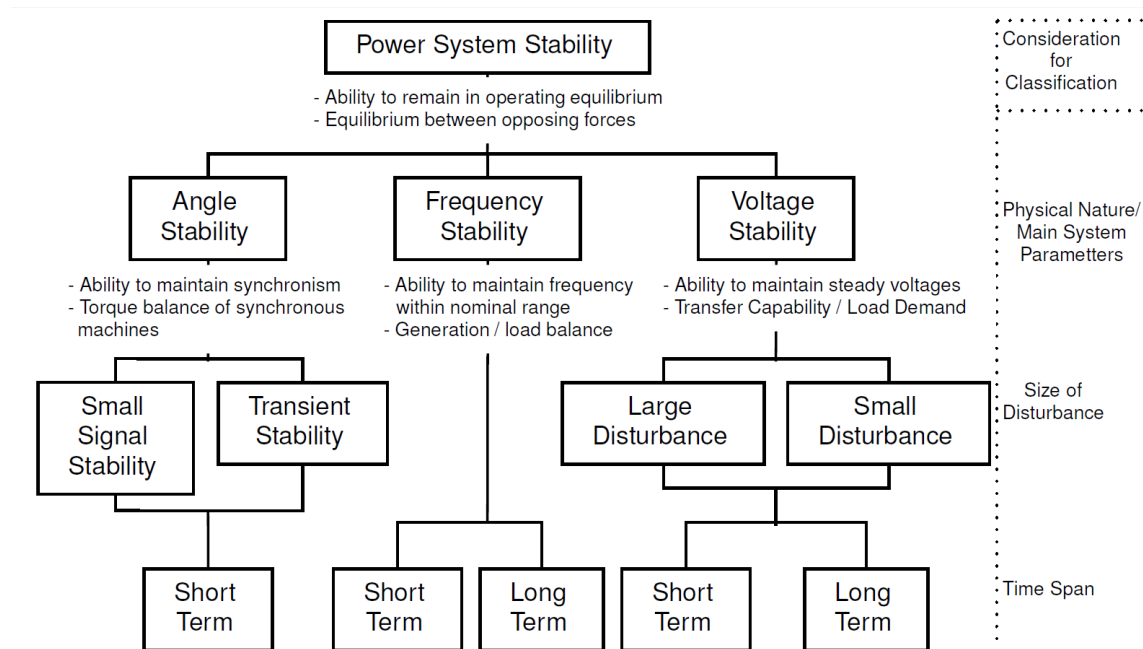
Figure 1.1: Classification of the power system stability (physical nature, size of disturbance and time span) [14].

Either cost- or market-based, ancillary services are provided by generators and loads in the grid whenever balancing or network issues occur and to ensure the whole stability of the system is restored in any condition. [9]. But these services are mainly provided by conventional generators and loads in today's networks, which is likely to change in the future with the high penetration of renewable energy sources. Indeed, these energy sources are well capable of providing ancillary services and keep the whole power system stable and in a reliable operation [16].

When a power imbalance occurs in the network, the system frequency control is carried out by stabilizing it through fast-acting closed-loop controllers, including governors participating in primary frequency reserves, and by restoring it to a steady-state value by means of slow-acting centralized controllers, so-called Automatic Generator Control (AGC) or secondary services [16]. This particular type of ancillary service is detailed in the next section.

Bus voltages are also system parameters that need to be controlled within a certain safety range to protect the grid from outages and blackouts.  Indeed, too high voltages can lead to degradation and damage in equipment present in the network while too low voltages cause higher Joule losses and can disturb the nominal operation of the grid [16, 30]. This type of voltage stability is also developed in the next section.

Finally, rotor angle stability is required to maintain synchronism between synchronous machines after a disturbance occurred in the interconnected network and is characterized solely by a short term time span. Since this work only focuses on frequency response and voltage stability, rotor angle stability is not considered and not developed beyond this chapter.

## 1.1 Frequency response

When an imbalance occurs in an AC network, i.e. when the produced and the generated powers mismatch, the network frequency will either drop or increase from its nominal value, i.e. 50 or 60 Hz depending on the geographic location. In order to solve this change and thus restore the frequency to its nominal value, system operators have implemented three frequency control schemes, each one taking part in the system restoration during a specific time slot [6]. Indeed, the grid frequency is required to remain within an acceptable range, i.e. deviations of 5 % from the nominal value [30], in order to keep the system stable. If large frequency deviations occur, they can cause issues in the grid that could potentially lead to fault cascades and even blackouts [29]. FIGURE 1.2 illustrates the different types of frequency response after a frequency dip, with the corresponding time slots.
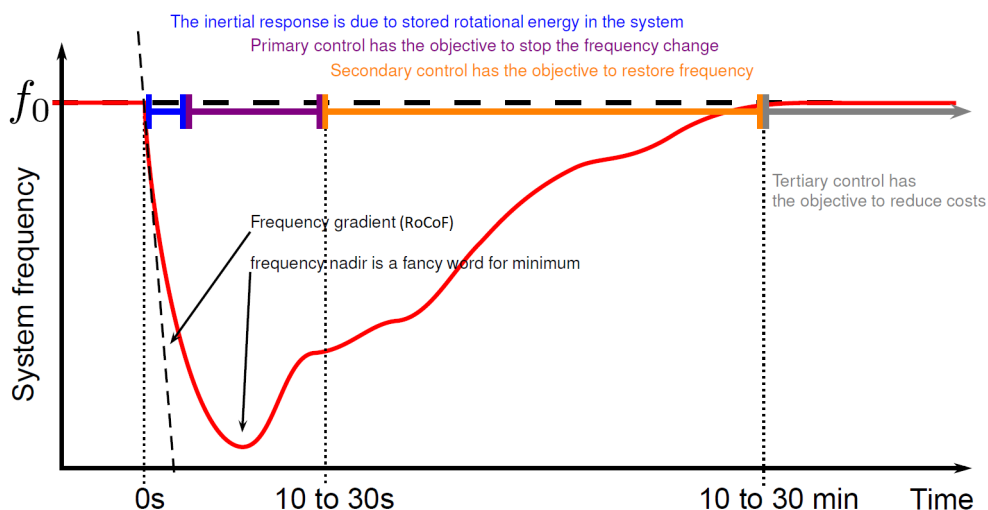


Figure 1.2: Illustration of the inertial and the frequency responses, the Rate of Change of Frequency and the frequency nadir [20].

First, before any frequency response of the governors occurs, the synchronous machines that are connected to the grid limit the frequency drop because of their inertia. This is called the *inertial response* of the network. This response acts within milliseconds to tens of seconds after the imbalance started and depends on the overall system inertia which dampens the frequency deviation from its nominal value. This effect is explained in more details in SECTION 2.1.

Concerning the governors frequency response, the first reserves that are automatically activated are *primary frequency reserves*. These occur within few seconds, typically 10 to 30 seconds after the occurrence of the imbalance. It consists of a governor responsible for changing the active power output of the generators participating in the frequency response depending on the local frequency variation in order to reduce the frequency deviation and stabilize the system frequency. In the case where the frequency is common to the AC area, these generators will change their output power regardless of the power imbalance location. The response of the generators depends on their own frequency-droop characteristic which gives information about the change in generated active power according to the change in frequency [10].

Afterwards *secondary frequency reserves* take place automatically, like the primary ones. Also known as Automatic Generation Control (AGC), these reserves last within 10 to 30 minutes and aim at restoring the grid frequency to its nominal value and the tie-line power exchanges with the other control zones to their set-point values. These reserves are activated by the means of an integral controller responsible for changing the turbine governor set-points in order to restore the frequency [10].

Finally, *tertiary frequency reserves* are the last step of the frequency control. These take place after the secondary reserves ended activity and consist in manually dispatching the generated power set operating points while coordinating the power production in order to handle present and future disturbances in the system and prevent congestion. For doing so, emergency control and protection schemes as load shedding can be triggered. Also, manual generator rescheduling using cheaper sources can be carried out within 45 to 75 minutes after the imbalance started [25, 29]. This kind of frequency response is not studied in this work.

Frequency reserves thus depend on several system parameters, including the total system inertia, the percentage MW size trips, the headroom, the governor control availability and withdrawal, the speed of primary frequency response, the frequency controllability of asynchronous connections and finally the fast acting energy storage plant availability [24].

## 1.2 Voltage stability

During normal as well as disturbed conditions, voltage stability is defined as the capability of a power system to keep voltage in stable magnitudes. Indeed, loads and generators are directly impacted in case voltage instabilities occur in the network. On the one hand, voltage is required to be as close as possible to its nominal value so that it ensures loads consume the required amount of power, since those are sensitive to voltage variations around its nominal values [7]. On the other hand, the dynamic behaviour of energy sources, in terms of active and reactive power injections, are directly related to voltage stability during disturbed conditions. System operators thus have the responsible role of avoiding any case of voltage instability or collapse, i.e. progressive voltage rise or fall until reaching critical values, ensuring the power grid operation keeps safe and reliable. They control the voltage so that it remains between specific limits in both transient and steady states with the aid of producers connected to the grid [12]. In general, the voltage is kept between 0.9 and 1.1 pu in steady-state and is regulated through several devices that directly or indirectly provide reactive power including shunt condensers, synchronous condensers, tap-changing transformers, flexible alternating current transmission system (FACTS) and VSC HVDC converter stations.

# Chapter 2

# Influence of inertia on the network

This chapter aims at summarizing the influence that inertia has on an electric network. The definition of inertia applied to power systems is first detailed using the swing equation. Some orders of magnitude depending on several parameters including the type of power plant, its rated power and the way these influence the value of the inertia are also given. Then, the link between inertia and frequency as well as voltage is presented followed by a reminder on the participation of loads in the frequency response. Finally, an aggregated model is proposed to help understand what factors influence the whole system inertia.

## 2.1  Definition of inertia in power systems

Synchronous generators such as those connected to nuclear, coal, gas and hydropower systems are composed of rotating masses which are directly linked to the inertial frequency response of the system after a power imbalance occurs due to their elecromechanical coupling [16]. Indeed, these rotating masses are characterized by a certain amount of kinetic energy, and during a frequency deviation from its nominal value, the synchronous machine either absorbs or injects kinetic energy from or to the grid, respectively, in order to damp this frequency change [28].

The rotational energy $E_k$ of a synchronous machine rotating at the speed $\omega$ is given by the following formula :

$$E_k = \frac{1}{2} J \omega^2, \tag{2.1}$$

where $J$ is the moment of inertia of the machine in [kg·m$^2$].

The corresponding inertia is defined by the ratio between the rotational energy $E_k$ in [MJ] at nominal speed $\omega_0$ and the rated power of the machine $S$ in [MVA] :

$$H = \frac{E_{k,0}}{S} = \frac{1}{2} \frac{J \omega_0^2}{S} \tag{2.2}$$

Inertia is measured in seconds and tells how long the synchronous machine is able to supply its rated power with the kinetic energy stored in its rotational masses [29]. From [28], inertia is defined as "the resistance of a physical object to a change of motion, in its speed and direction". In our case where the physical objects are the rotational masses and the resistance, to the change in rotational speed corresponds to the moment of inertia.

Inertia depends on the type, the size and the speed of the machine. Typical values are presented in TABLE 2.1 and range from 2 to 10 seconds. As can be noted from this table and from FIGURE 2.1 that represents the inertia

as a function of the rating for different generator types, inertia is usually inversely proportional to the rating of the machine, which is directly related to EQ. 2.2.

Table 2.1: Typical values of inertia depending on the power plant type [10].

| Power plant | Rating $S$ [MW] | Inertia $H$ [s] |
|---|---|---|
| Thermal | 500 - 1500 | 2 - 2.3 |
| Thermal | 1000 | 4 - 5 |
| Thermal | 10 | 4 |
| Thermal | Not mentioned | 4 - 5 |
| Thermal (2 poles) | Not mentioned | 2.5 - 6 |
| Thermal (4 poles) | Not mentioned | 4 - 10 |
| Thermal (steam) | 130 | 4 |
| Thermal (steam) | 60 | 3.3 |
| Thermal (combined cycle) | 115 | 4.3 |
| Thermal (gas) | 90 - 120 | 5 |
| Thermal | Not mentioned | 2 - 8 |
| Hydroelectric ($450 < n < 514$ rpm) | 10 - 65 | 2 - 4.3 |
| Hydroelectric ($200 < n < 400$ rpm) | 10 - 75 | 2 - 4 |
| Hydroelectric ($138 < n < 180$ rpm) | 10 - 90 | 2 - 3.3 |
| Hydroelectric ($80 < n < 120$ rpm) | 10 - 85 | 1.75 - 3 |
| Hydroelectric | Not mentioned | 4.75 |
| Hydroelectric ($n < 200$ rpm) | Not mentioned | 2 - 3 |
| Hydroelectric ($n > 200$ rpm) | Not mentioned | 2 - 4 |
| Hydroelectric | Not mentioned | 2 - 4 |
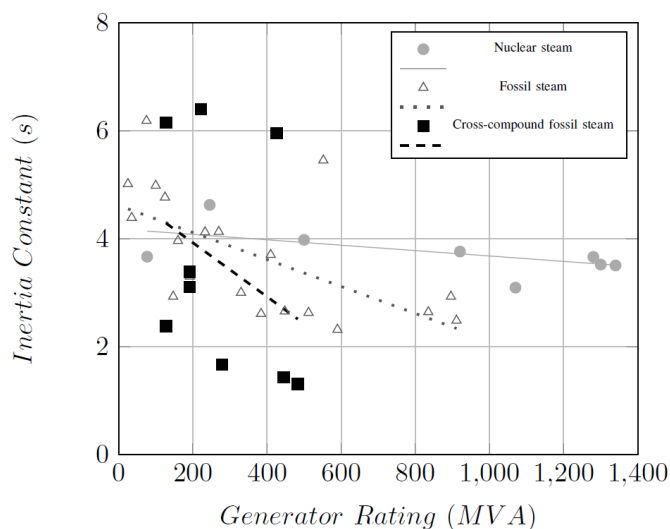


Figure 2.1: Inertia values for different power plants at different ratings [27].

In order to relate power imbalance to frequency deviation, the *swing equation* is derived. This equation describes the relation between the inertial response of the machine and the rotational speed $\omega$ after a power imbalance. The swing equation is developed from the derivative of the kinetic energy of the machine, see EQ. 2.1, and, assuming a non time-varying moment of inertia $J$, results in the following equation[1] :

$$\frac{dE_k}{dt} = J\omega\frac{d\omega}{dt} = P_m - P_e,$$ (2.3)

where $P_m$ and $P_e$ are respectively the mechanical power supplied by the machine and the electric power demand.

Using EQ. 2.2, it is possible to express the swing equation at nominal frequency $\omega_0$ as a function of inertia $H$ with a first order approximation :

$$\frac{2HS}{\omega_0}\frac{d\omega}{dt} = \frac{2HS}{f_0}\frac{df}{dt} = P_{m,0} - P_e$$ (2.4)

This shows that inertia $H$ is directly related to the rate of change of frequency $\frac{df}{dt}$, resulting from a power imbalance $P_{m,0} - P_e$ [29], which corresponds to the inertial response of the system after an imbalance. Indeed, because of the synchronism, the mechanical rotational speed is directly coupled to the electrical angular frequency. So, in order to participate in the frequency control, generators are equipped with a speed governor that measures the rotational speed of the shaft and a servomotor that controls the amount of fluid sent to the turbine by means of a throttle [6]. Each of them reacts depending on its inertia and electric distance to the disturbance by altering their load angle and speed. From EQ. 2.4, it can be concluded that if the overall system is characterized by low inertia, the system frequency change will be less damped and the frequency swings will be higher compared to a high inertia network [28]. Also, rotating masses inherently providing stored energy together with the voltage source characteristic of a synchronous machine protect from voltage magnitude perturbations and provide sources of power that can be used to limit voltage steps. Therefore inertia is a key parameter that influences both the network frequency and voltages [12].

## 2.2   Loads participating in the frequency response

In some cases, loads are also participating in the frequency response and thus in the stability of the power system. The demand response capability of the load depends on its type and dynamics [28]. This is especially the case for motor loads such as induction motors, fans or pumps, where the change in electrical power is directly impacted by the frequency because of the motor speed changes, in contrast with resistive loads which electrical power is independent from the frequency, such as in heating loads [20].

In the specific case where loads play a role in the frequency control, the total change in electric power $\Delta P_e$, where $\Delta$ stands for a small variation, is described by the following equation :

$$\Delta P_e = \Delta P_L + D \cdot \Delta\omega$$ (2.5)

where $\Delta P_L$ is the frequency-independent change in load and $D$ the load-damping constant, usually ranging from 1 to 2 [20], and $\Delta\omega$ the rotational speed variation.

---

[1]This equation can also be expressed in terms of torque instead of power, if both sides are multiplied by the angular frequency $\omega$.

Rewriting EQ. 2.4 in per-unit powers, i.e. dividing by the apparent power $S$, considering the nominal angular frequency $\omega_0 = 1$ pu and a small variations case, it becomes :

$$\frac{d\Delta\omega}{dt} = \frac{\Delta P_{m,0} - \Delta P_e}{2H} \tag{2.6}$$

Substituting EQ. 2.5 in the above equation, it gives :

$$\frac{d\Delta\omega}{dt} = \frac{\Delta P_{m,0} - \Delta P_L}{2H} - \frac{D \cdot \Delta\omega}{2H} \tag{2.7}$$

So, without any action of the governor, the frequency response is entirely determined by the inertial response, directly related to the inertia $H$ and the damping constant $D$.

## 2.3   Aggregated model

The swing equation derived in EQ. 2.7 can be used to describe an aggregated model of the whole network. Let's consider the case of $n$ generators, $j$ loads and $l$ connecting tie-lines. The swing equation applied to this aggregated model, i.e. the Aggregated Swing Equation (ASE) [29], becomes the following one :

$$\frac{d\Delta\omega}{dt} = \frac{\Delta P_{m,0} - \Delta P_L - \Delta P_{loss}}{2H_{sys}} - \frac{D_{sys} \cdot \Delta\omega}{2H_{sys}}, \tag{2.8}$$

where

$$\omega = \frac{\sum_{i=1}^{n} H_i \omega_i}{\sum_{i=1}^{n} H_i} \tag{2.9}$$

$$S = \sum_{i=1}^{n} S_i \tag{2.10}$$

$$H_{sys} = \frac{\sum_{i=1}^{n} H_i S_i}{S} \tag{2.11}$$

$$D_{sys} = \frac{\sum_{i=1}^{n} D_i S_i}{S} \tag{2.12}$$

$$P_{m,0} = \sum_{i=1}^{n} P_{m,0,i} \tag{2.13}$$

$$P_L = \sum_{i=1}^{j} P_{L,i} \tag{2.14}$$

$$P_{loss} = \sum_{i=1}^{l} P_{loss,i}, \tag{2.15}$$

where $H_{sys}$ is the system inertia, which depends on the number of generators and their inertia, and $D_{sys}$ is the system load-damping factor[2]. The higher amount of generator connected to the grid, the higher the system inertia, resulting in flatter frequency deviation after an imbalance event. This means that depending on the cause of the

---

[2]Some typical values of the system load-damping factor can be found in [10].

imbalance, the inertia of the system can differ during the day. In case of a load change, the generators adjust their output in order to restore the nominal frequency, as explained in CHAPTER 1, whereas in case of a change on the generator side, the inertia and the reserves in the AC network change, making the inertia fluctuate throughout the day [6, 28].

# Chapter 3

# Low inertia network

If a majority of inverter-based technologies are connected to the grid in lieu of synchronous machines, no more inherent control through rotational inertia is possible since a decoupling between the power generated by renewable energy sources (RES) and the grid takes place. Indeed, [10] states that, between 1996 and 2016, EU has reduced its system inertia by nearly 20 %, which is linked to the fact that power coming from RES has risen by 20 %.

In fact, from [27], it is mentioned that wind turbines are connected to the grid through back-to-back converters, usually either in the form of double fed induction generators (DFIG) or through full converter synchronous generators (FCSG). The latter prevents any inertial response from occurring after a frequency deviation because of this decoupling, even though the blades, the gearbox and the generator store some kinetic energy.

Solar panels, on their end, are not characterized by any inertial response since no rotating part is involved in their operation and thus no kinetic energy is stored : only capacitors are storing a few energy [28].

Finally, this referenced article also states that HVDC links, generally used to transport huge amounts of power from isolated renewable sources sites to loads, decouple several interconnected systems, preventing inertia from being directly accessible to some parts of the grid.

The first section below aims at listing some of the main impacts linked to the lack of inertia while the following one details the solutions proposed in order to counteract the harmful effects of inserting power electronics interfaced energy sources in the network. These include the alternatives of participating in the frequency control, improving the inertial response and keeping the voltage in an acceptable range so that the whole network is stable. Finally, the third section aims at applying some of these proposed solutions to converters connected to renewable energy sources. Two types of converters, i.e. converters in grid-following and grid-forming mode, are defined and the energy buffer behind the converter as well as its location of grid-forming converters in the grid are discussed. That section ends with the description of the model used to implement each type of converters.

## 3.1   Consequences on the network

### 3.1.1   Rate of Change of Frequency

The first consequence on the network that can be highlighted is directly linked to the *Rate of Change of Frequency* (RoCoF), illustrated in FIGURE 1.2. It corresponds to the derivative of the frequency just after the disturbance occurs and, assuming no frequency-dependent load exists, is directly derived from the swing equation derived in EQ. 2.4 :

$$RoCoF = \frac{df}{dt}\bigg|_{t=0^+} = \frac{\Delta P f_0}{2HS},\tag{3.1}$$

where $\Delta P$ is the power imbalance due to the disturbance and $H$ the system inertia as defined in EQ. 2.11. As it can be deduced from this relation, low inertia systems are subject to significantly large frequency deviations, jeopardizing the system stability and possibly leading to network issues. It makes it more challenging to control the frequency and thus stabilize the power system, since dynamics are faster [29].

Moreover, *system protection relays* are embedded in the network to prevent islanding[1] and their tripping depends on the value of the RoCoF, which theoretically corresponds to the highest frequency deviation following a disturbance. If it is too high, corresponding to a too steep frequency deviation, and exceeds a threshold value, the relay trips in order to protect synchronous machines characterized by mechanical limitations. In the case of a low inertia system, high RoCoF can thus activate these types of relays and disconnect distributed generation in cascade which can enhance the original frequency event or even damage some equipment [13, 27]. For instance, in [29], some simulations were carried out in a two-area system with decreasing inertia. These resulted in significant increase and more abrupt transient flows through the tie-line between both areas. These consequences could be detected by the grid as a short circuit directly leading to automatic protection device tripping.

Also, low inertia bringing too high RoCoF can lead to considerably lower frequency nadir. Both are illustrated in FIGURE 3.1 as a function of converter[2] connected generation for an imbalance of 0.1 pu for different values of the system synchronous machine inertia. The frequency nadir is defined as the lowest frequency reached when an imbalance occurs, causing a frequency drop, i.e. when the produced power is less than the consumed one. In a low inertia system, a smaller amount of governors participates in the frequency control and the remaining ones have less time to react causing a lower frequency nadir compared to a higher inertia case. The same phenomenon happens when the frequency increases, the maximum frequency being even higher in low inertia systems. Frequency relays can thus trip if the frequency nadir is too low, causing under-frequency load shedding, potential cascaded outages and blackouts in the worst case [25, 27]. Disconnection of generators and load shedding can also occur in case of low frequency nadir, which jeopardizes the system stability [11].

---

[1]From [28]: "Islanding occurs when a part of the power system becomes electrically isolated from the rest of the power system, yet continues to be energized by generators connected to the isolated subsystem. Consequently,the frequency will change rapidly as the local generation will not exactly balance the remaining load.".

[2]It is assumed that converters do not take part in the frequency response in these graphs.

(a) Nadir frequency in function of different levels of converter connected generation



(b) ROCOF measured over 500 ms in function of different levels of converter connected generation
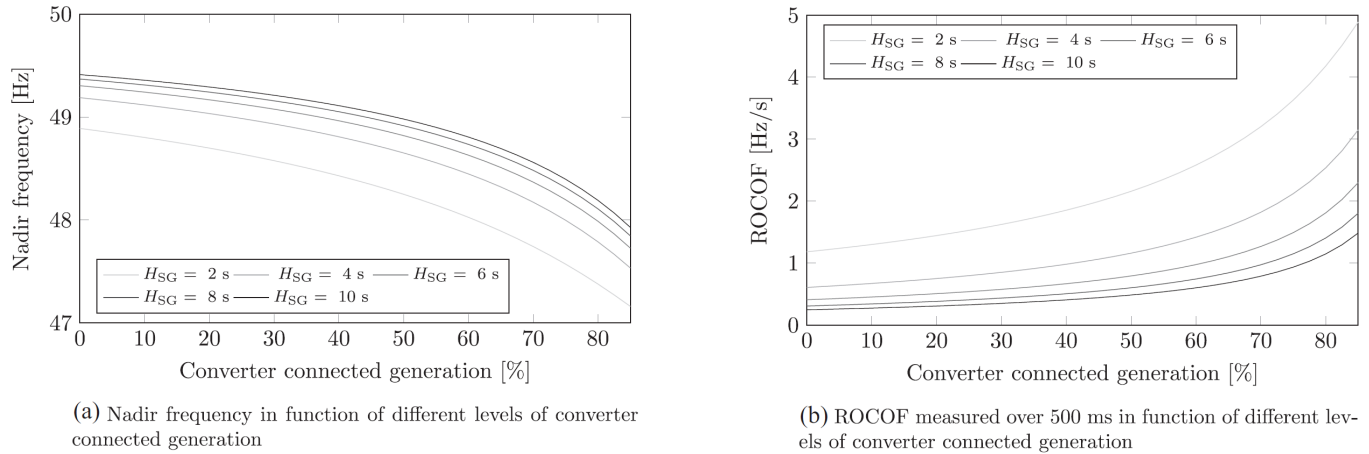
Figure 3.1: Evolution of the frequency nadir and the RoCoF as a function of converter connected generation for a power imbalance of 0.1 pu, for different values of system inertia [28].

### 3.1.2 Voltage stability issues

The second issue that arises in a network to which mainly renewable energy sources are connected relates to the voltage stability. Indeed, TSOs are concerned by several problems that involve voltage issues such as deeper and widespread voltage dips after severe transmission network faults and lack or excess of reactive power. They induce significant voltage differences between nodes, loss of devices in the context of fault-ride through capability. Also, this type of issue includes the reduction of the short circuit power levels and more significant voltage dips result in the tripping of under-voltage protection. Moreover, inadequate support to restore system voltage immediately after the occurrence of the fault is more likely to happen [12].

In [19], it is also stated that system control tasks such as voltage support and oscillation damping are also compromised when moving from a network mainly provided by power coming from synchronous generators compared to a 100 % power electronics-based network. Furthermore, the mechanism through which reactive power compensation is provided to the network changes with the high penetration of RES. In fact, conventional Automatic Voltage Regulators, so-called AVRs, of synchronous machines are characterized by lower dynamics compared to voltage control through converters. Thus, low inertia systems should be equipped with voltage and reactive power control devices that do not involve unstable dynamics while coupling them with the inertial response of synchronous machines. In this literature it is also mentioned that voltage variations at the Point of Common Coupling, i.e. the PCC, especially for the case of wind turbines, and potential excessive voltage control movements in the grid, as on-load tap-changers for regulating transformers for instance, are more likely to occur.

A significant issue that is discussed in detail in SECTION 3.3 related to the stiffness of the whole grid. Indeed, it is reduced when removing synchronous machines and replacing them with power electronics-based technologies that cannot rely anymore on a grid which AC voltage is imposed. There is thus a need for these kinds of energy sources to impose the voltage in such a way that all synchronous machines could be removed until reaching a zero-inertia system [12]. Also, the sensitivity to angle and impedances variations as well as synchronization of voltages created by all these converters have to be carefully taken into account to avoid respectively sudden increase of active power and frequency difference. That would cause very high power flows, leading to the disconnection or

even the destruction of these converters [7].

### 3.1.3 Over-current capability

Protection relays related to the over-current time are present in the grid to protect its components. Their circuit breaker tripping is set depending on this large amount of fault current that conventional machines can handle. However, synchronous machines are capable of withstanding very high currents during a fault, compared to their nominal current value. In contrast, renewable energy sources connected through converters are not able of resisting to such a high current. They are only capable of resisting to a small increase above their nominal output current. Thus, changes in the protection relays should be achieved when moving to an inverter-based power system since the acceptable fault current will be extremely reduced. Even though short-circuit currents can not be withstood by inverters, these have the capability of reacting very rapidly after a fault occurs, within one-fourth of a cycle, and to disconnect themselves from the grid to avoid their hardware destruction [16]. This particular topic is developed in SECTION 3.3 that focuses on converters operation.

### 3.1.4 Black-start capability

Blackouts and natural disasters, while occasional, may happen in the network at any time. After the grid went down, it is required to restart and supply power by the introduction of a *black-start* operation. Moving from the present network to an inverter-based one, it is required to ensure that this particular type of ancillary service can be triggered whenever it is needed and thus guarantee a reliable operation of the power system. Two particular services are required for the system to be able to trigger a black-start operation : acting as a voltage source and providing enough power so that it is able to start transformers and motors with high in-rush currents. These objectives are both reached with synchronous generators, when the load is properly sized. That same capability is required with the future inverter-based power systems, with the same reliability, either by providing enough starting current or by segregating loads, so that the grid could be re-powered [16].

### 3.1.5 Time-varying parameters

Another network issue cited in [29] is the time dependency of the system parameters. Indeed, when defining the swing equation in EQ. 2.3, it was assumed that the moment of inertia $J$ was not time-varying because of the direct coupling between generator speed and network frequency. When replacing conventional power plants with intermittent renewable sources of energy, this parameter is no more constant. Thus, the rotational inertia becomes time-varying, depending on the day, the season, the year, the weather conditions (wind speed, irradiance, ...), the state of charge in case of batteries, and whether the RES is online or not [25]. This effect has been illustrated in [10] for Germany in 2012, where inertia was varying between 2.5 and 6 seconds within the year. In [28, 27] it is also stated that, while in EQ. 2.2 the inertia is defined by the nominal speed of the machine, the speed range of a wind turbine is varying with time, so its kinetic energy and by consequence its inertia constant, as represented in FIGURE 3.2. Indeed, when rotating at minimum rotor speed, the kinetic energy stored in the wind turbine is 60 % lower than at nominal operation. On the other hand, as the wind speed increases, the rotor speed increases as well, resulting in a higher amount of stored kinetic energy that increases the inertia of the wind turbine.
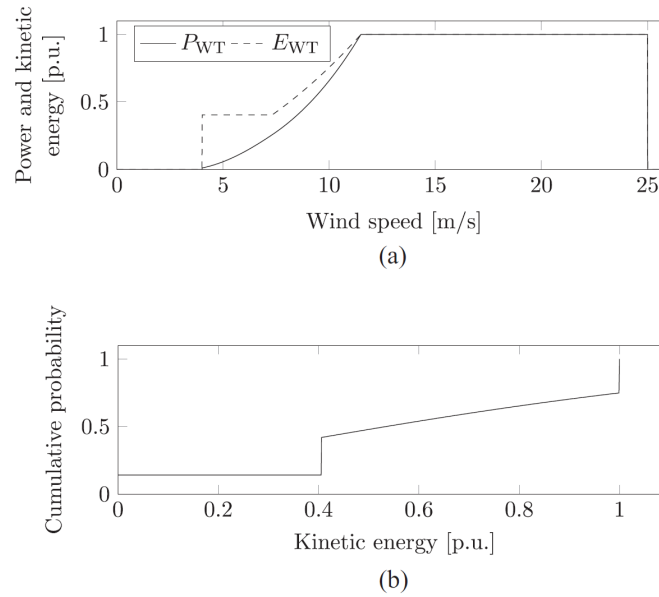
Figure 3.2: Kinetic energy stored in a variable speed wind turbine [28].

This effect has two main consequences. The first resides in the ability of the TSO to estimate the system inertia to plan purposes in the future network mainly composed of RES. Also, this jeopardizes the accuracy of the detection of frequency events and the measure of the Rate of Change of Frequency (RoCoF). Thus, accurate forecasts especially for PV and wind power are required in order to determine precisely the amount of lack of inertia and thus the techniques required to compensate it and provide ancillary services [25].

### 3.1.6  Power reserves

Finally, since the number of synchronous machines will decrease with the high penetration of renewable energy sources, less generators will be available to provide ancillary services such as frequency reserves or black-start operation. Solutions should be found in order to replace these synchronous machines with intermittent sources while keeping the system reliability as today's one, with enough reserves and even faster responses [13].

## 3.2 Proposed solutions

In order to overcome the previously listed problems due to the lack of inertia and find ways to reach a stable grid with 100 % renewable energy sources, solutions have been proposed. They first include some solutions linked to the energy buffer that can be used to allow a power plant to produce or reduce its active power production. These are, especially for PV plants and wind power generation, Energy Storage System (ESS) and the deloading technique. These two allow RES to participate in the frequency control without any requirement on permanent accurate resource forecast to guarantee power reserve availability. This way, wind, solar and batteries are able to provide active and reactive control as synchronous machines do [16].

Then, several solutions can be implemented in order to keep the system stable in voltage and frequency as well as to obtain inertial response from the power plants. Most techniques that are presented in the literature are droop control, fast frequency reserve and virtual inertia, in order for RES to participate in the frequency control and fill the lack of inertia by other means than the presence of synchronous machines. Indeed, [16] mentions that synthetic inertia responses can be implemented in a controller for wind turbines and batteries at any operating conditions and also for PV when it is curtailed with headroom. Also, synchronous condensers can be connected to the grid to achieve voltage support and other features that these devices can offer. Demand response and modification of protection relays are also presented in order to overcome problems listed in the previous section. All these techniques, including the energy buffers, are detailed in the next two subsections.

### 3.2.1 Energy buffer

Two types of energy buffers are discussed in this section : Energy Storage System, so-called ESS, and deloading techniques. Both can be used together with PV plants and wind turbines. However, it is important to note that wind turbines can be sorted in two different categories : fixed and variable speed. In the first case, the wind turbine is directly connected to the grid through an induction generator that allows the power plant to participate in the inertial response to a frequency deviation [8]. However this inertia is very small compared to synchronous machines. On the other hand, variable speed wind turbines do not inherently participate in the inertial response after an imbalance occurs since it is connected to the grid through either Permanent Magnet Synchronous Generator (PMSG) or Double Fed Induction Generator (DFIG) that allows it to change its output power over a wide range of wind speeds. Indeed, when connected through a PMSG, the generator stator is connected to a power electronic converter that injects power in the grid whereas through a DFIG a rotor circuit connects the generator to the grid.

In general, the inertia of a wind turbine is mainly determined by the blades and depends on its type, its size and the presence or absence of a gearbox. It usually ranges from 2 to 6 seconds, comparably to conventional power plants [28, 27]. Literature [10] presents a table with typical values of inertia for different wind turbine types and also shows a comparison of the system inertia with and without the hidden inertia in wind power plants. Even though wind turbines have kinetic energy stored in their rotating blades, this technology do not inherently release it as synchronous machines do. It requires the implementation of a controller providing inertia response. Two types can be implemented : fast power reserve and inertia emulation [8].

### 3.2.1.1 Energy Storage System

*Energy Storage System*, so-called ESS, is the first solution proposed to keep the power grid stable using power electronics converters. This is particularly relevant for photovoltaic technologies that do not contribute in the inertial response as they do not have any rotating parts. In order to make PV and wind power plants participate in the the frequency control and thus provide additional active power when required, fast-acting storage units are developed. These include batteries, super-capacitors and the flywheel Energy Storage System [10, 13, 28]. ESS reduces the effect of the renewable energy sources variability while providing amounts of power during an imbalance to stabilize and restore the system frequency. Thus, power is injected into the grid during periods when the RES does not produce enough energy and is absorbed when it generates an excess of power compared to the grid requirement at that moment. Several battery ESS technologies can be used in the frequency control : Lead Acid, Sodium Metal Halide, Sodium Sulfur and Li-ion. Each technology is characterized with a certain response time, storage period and efficiency, all summarized in TABLE 3.1 [23].

Table 3.1: Various battery Energy Storage Systems with their characteristics (response time, storage period and efficiency) [23].

|  | Lead Acid | Sodium Metal Halide | Sodium Sulfur | Li-ion |
|---|---|---|---|---|
| Response time [ms] | 100 | 100 | 100 | 100 |
| Storage period | 15 min-3 hr | 15 min-3 hr | 4-6 hr | 15 min-1 hr |
| Efficiency [%] | 85 | 85 | 70 | 90 |

The main drawbacks are that ESS needs to reload after providing all its available power reserves to the network and will fail to absorb power from the grid if the battery system is fully charged [8]. Also, in [25], it is mentioned that the cost can be very high. In order to solve this issue, the same paper mentions a type of ESS where batteries and ultra-capacitors are put in parallel in order to avoid the impact of fast-frequency on the lifetime of the ESS technology. Finally, the battery lifecycle, defined as "the number of complete charge/discharge cycles a battery can perform before its nominal capacity falls below 80 % of its initial rated capacity" [15] is also a parameter to take into account. Always finite, it is mainly influenced by the average current rating of the battery and its depth of discharge [23].

Talking about wind turbines, ESS technologies together with frequency reserves capabilities are a proposed solution, especially for the DFIG-connected wind turbines. At all speed ranges, the Energy Storage System would play a role by providing active power for the speed recovery in order to avoid a second frequency decrease. It would also play as a backup system from which power can be extracted during deficits [8]. The same paper mentions the combination of variable speed wind power plants with flywheel storage, controlled in parallel by a central control system. The flywheel storage could be used as energy buffer to provide frequency reserve services while the central control system distributes the power reserve margin between both technologies.

PV systems combined with ESS are also discussed in the literature [8]. It states that PV associated with Li-ion batteries are used to control active and reactive power and thus participate in frequency and voltage regulation services. That way, it can either inject or absorb power to or from the grid depending on its operation mode, respectively called up- and down-regulation, through a bidirectional converter.

### 3.2.1.2   Deloading technique

The technique of *deloading* either the PV or the wind power plant is also a potential solution to allow RES to have an energy buffer that can be used to participate in the frequency control. An example of this category is mentioned in [27]. It says that in Ireland, the Transmission System Operator (TSO) requires wind turbines to participate in the frequency response by deloading at nominal frequency, as illustrated in FIGURE 3.3 at 50 Hz. If the frequency drops below the frequency corresponding to point B, the wind turbine is able to participate in the frequency control by increasing its active power output according to the power-frequency characteristic[3] between points A and B.
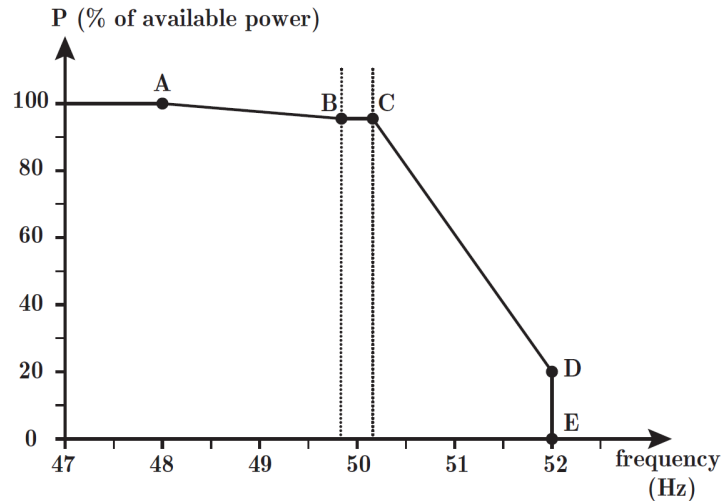


Figure 3.3: Power-frequency characteristic of wind turbines in Ireland [27].

In general, it is possible to apply this deloading technique to wind turbines in two different ways called pitch angle control and over-speed control [10].

The pitch angle control is illustrated in FIGURE 3.4. Increasing the pitch angle from $\beta_0$ to $\beta_1$, with constant speed $V_W$ and at maximum power point (MPP) rotor speed $\Omega_{MPP}$, the maximum available power $P_{MPP}$ moves to the deloaded power $P_{del}$. This way, if an imbalance occurs in the network causing a frequency deviation, some active power reserve is available for the frequency control to restore the system to balance.

---

[3]The droop control technique is developed in details in SECTION 3.2.2.1.
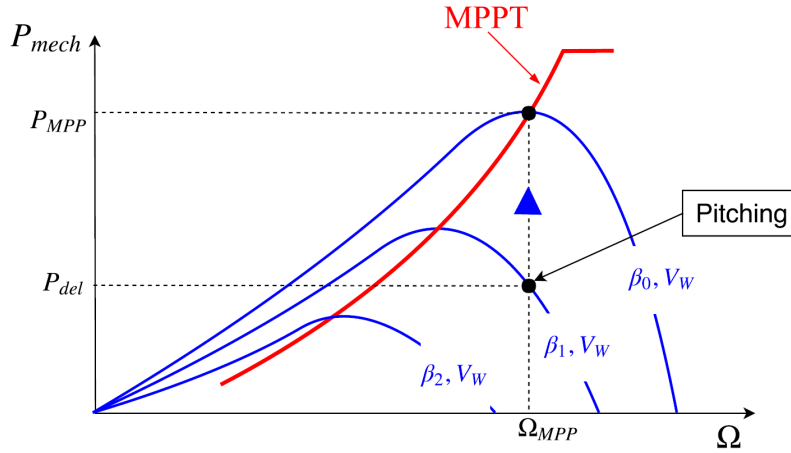
Figure 3.4: Deloading technique : pitch angle control for a wind turbine, with blades' angle $\beta_0 < \beta_1 < \beta_2$ [10].

On the other hand, over-speed control keeps the same pitch angle $\beta_0$ and the same speed $V_W$ but moves towards the right side of the MPP power $P_{MPP}$ as illustrated in FIGURE 3.5a. Thus the wind turbine works at rotor speed $\Omega_{del,1}$ and, in case of frequency deviation, the latter is reduced to $\Omega_{MPP}$, rotor speed corresponding to $P_{MPP}$, injecting the corresponding kinetic energy to the system for the frequency response. FIGURE 3.5b illustrates the case where under-speed control technique is used, i.e. when the wind turbine rotor speed is reduced to $\Omega_{del,2}$, which is below $\Omega_{MPP}$. This technique is known as a "detrimental strategy" since power is extracted from the turbine by increasing the rotor speed from $\Omega_{del,2}$ to $\Omega_{MPP}$, which reduces the frequency response and could lead to an opposite desired behaviour.



(a) Over-speed control.



(b) Under-speed control.
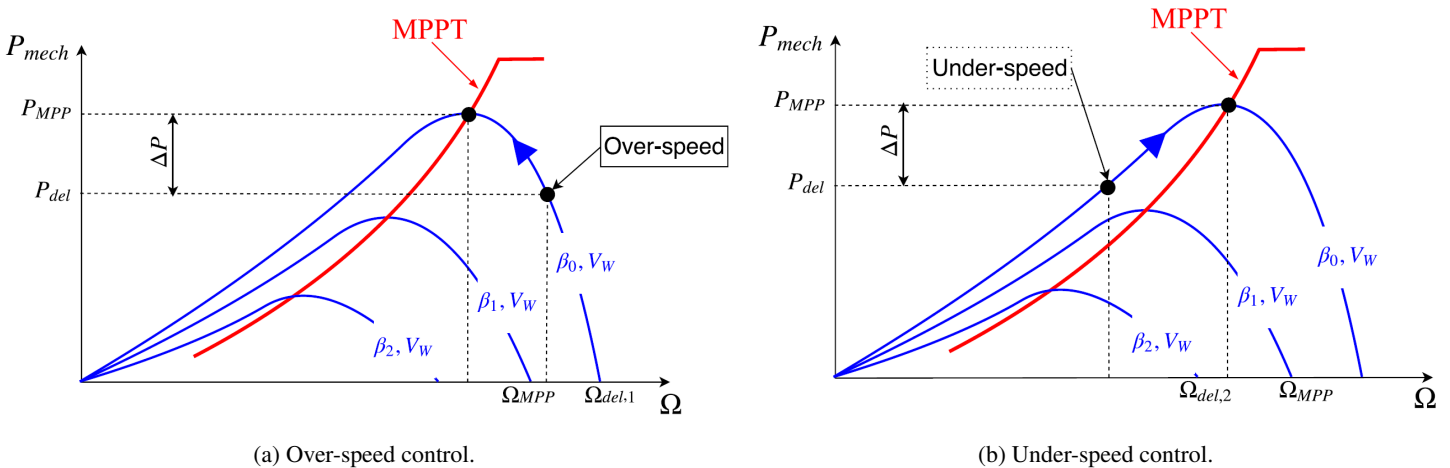
Figure 3.5: Deloading technique : speed control for a wind turbine [10].

In the same paper, deloading applied to PV power plants is also proposed as a solution to benefit from power reserves that can be released in case of frequency decreases. This could be done by changing the output voltage from the value corresponding to the maximum power point tracker (MPPT). Similarly to wind turbines, the PV power plant is working at a sub-optimal operating point, leading to some available power reserve that is used to deliver inertial response to the power grid in case of contingency leading to a frequency deviation. This technique is

illustrated in FIGURE 3.6, where the PV unit output power is reduced from $P_{MPP}$ to $P_{del}$, leading to some available active power $\Delta P = P_{MPP} - P_{del}$. Reducing the power to $P_{del}$ leads to a corresponding voltage different from $V_{MPP}$, either greater or smaller, respectively corresponding to $V_{del,1}$ and $V_{del,2}$. For stability reasons, deloading techniques are implemented choosing voltage $V_{del,1}$ higher than the MPP voltage.



(a) $V_{del,1} > V_{MPP}$.
(b) $V_{del,2} < V_{MPP}$.
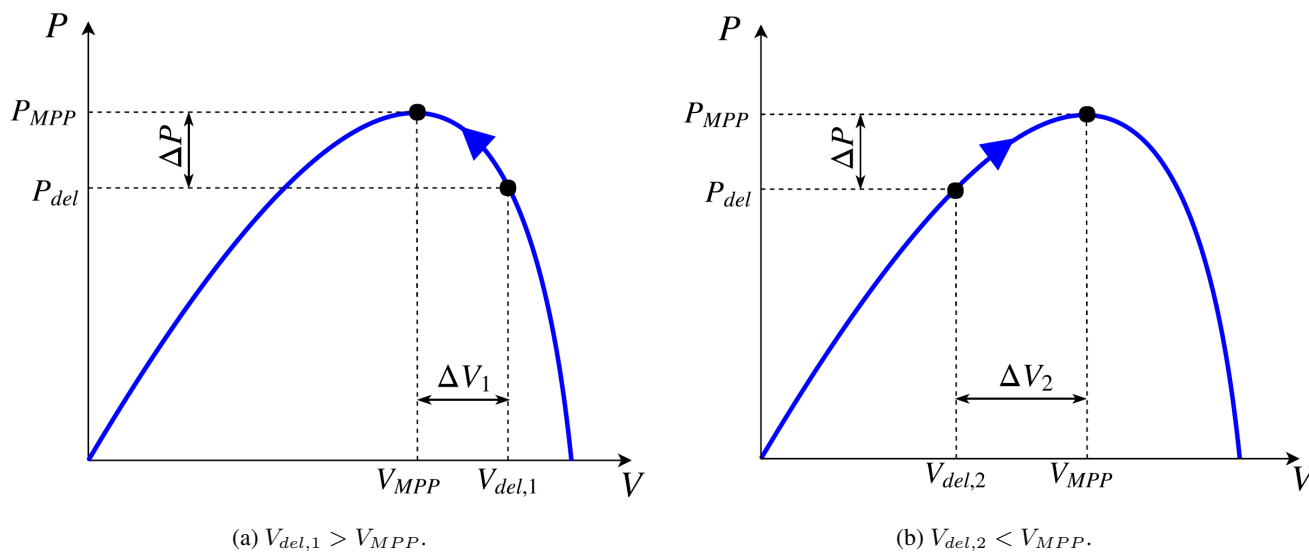
Figure 3.6: Deloading technique : voltage control for a PV plant [10].

For all techniques described in this section, deloading a power plant leads to operating it under its maximum available capacity causing a permanent power loss. This is the main drawback of this technique, even though it is highly reliable and allows the non-use of any power reserves. Thus, it does not make the RES as profitable as if the plant was working at MPPT level. Despite that disadvantage, [28] mentions that this technique for PV is more economically feasible than using battery units even though [27] states that keeping power reserves from renewable source power plants leads to a relative high cost in production support mechanisms. This literature also mentions that the deloading technique has the main advantage of delivering frequency control during a long period of time, and can be used to participate in both primary and secondary controls.

### 3.2.2  Solutions for the frequency response and the voltage control

In a low inertia system, frequency and voltage regulation techniques as well as inertial response need to be implemented. Some devices or methods can be used with RES in order to keep the network stable. These techniques are illustrated in FIGURE 3.7 and include droop control, fast power reserve, inertia emulation, the use of synchronous condensers, demand response and the modification of present protection relays. All of them are explained in details in the following subsections.
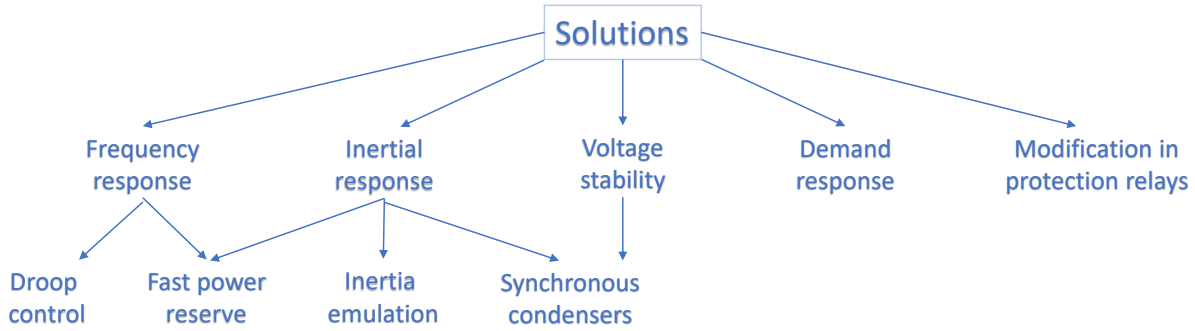


Figure 3.7: Schematic of the proposed solutions for renewable energy sources to participate in the network stability.

#### 3.2.2.1  Droop techniques

*Droop techniques* are the first type of frequency regulation techniques that can be implemented in the controller of a RES for it to participate in the frequency control like synchronous machines do. As for conventional synchronous generators equipped with a governor, a frequency deviation in the network following a disturbance is translated into a power output change, for example, a wind turbine, in such a way that it follows the characteristic represented in FIGURES 3.8a. This way, the wind turbine is able to activate frequency reserves that improve the frequency nadir and help recover the frequency to its nominal value. The corresponding output power change of the wind turbine $\Delta P$ proportional to the frequency change $\Delta f = f_{meas} - f_{nom}$ is computed by the following equation :

$$\Delta P = P - P_0 = -\frac{f_{meas} - f_{nom}}{R},$$
(3.2)

where $P_0$ and $f_{nom}$ are respectively the nominal output power and frequency of the power plant, $P$ the dispatched output power of the wind turbine, $f_{meas}$ the measured grid frequency and $R$ the chosen droop coefficient of the droop characteristic [8]. The block diagram of the droop control is shown in FIGURE 3.8b. A signal $P_{ref} = P_{MPP} + \Delta P$ is sent to the power converter of the turbine, giving to it information about the amount of stored kinetic energy it needs to release [10].

(a) Droop characteristic.                                    (b) Block diagram of droop control.
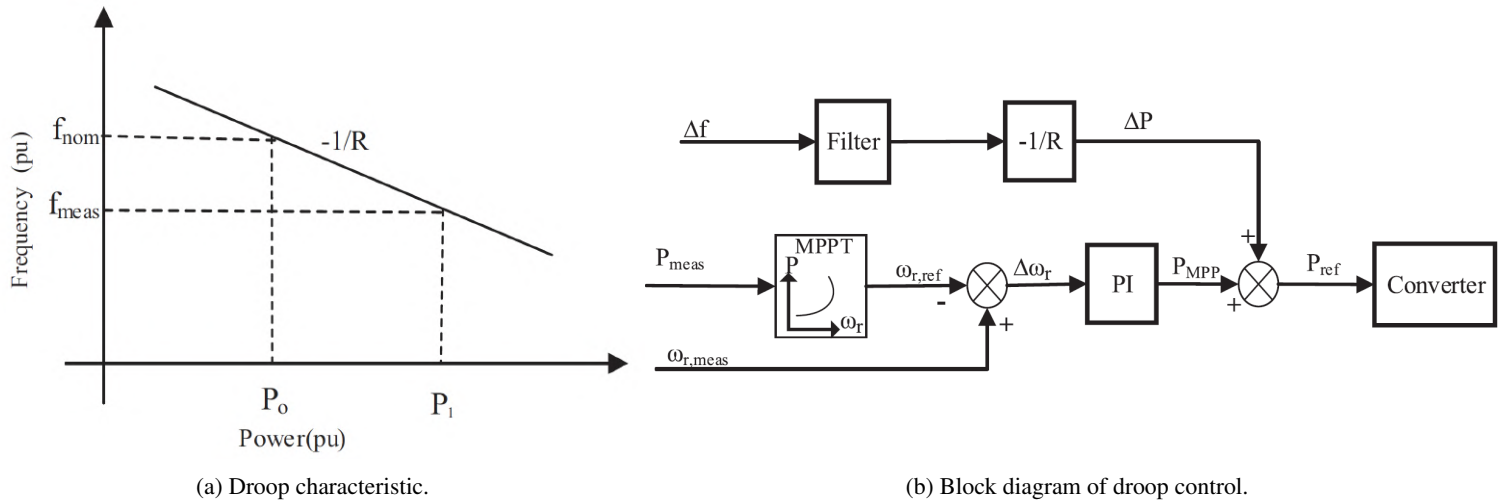
Figure 3.8: Droop technique : Power-frequency characteristic and block diagram [8].

For PVs, such control is especially mentioned in [8] where, together with a ESS, an active and reactive droop control is implemented in order to participate in frequency and voltage regulations by automatically regulating both active and reactive powers in the grid, during a lack of generation by the PV arrays. During an opposite event, i.e. when the demand is greater than the produced power, the inverter control switches so that is regulates both the frequency and the voltage depending on the active and reactive power set-points. This control then depends on the PV array output power and its battery state of charge (SOC). But droop control involves the implementation of a linear relationship between active power compared to frequency and reactive power compared to voltage. As a consequence, short timescale computations need to be carried out to make the droop-controlled inverters slow down, in particular in their transient response [16].

### 3.2.2.2 Virtual inertia

One solution to reach a stable 100 % inverter-based grid is to implement *virtual inertia*, also known as *synthetic inertia*. The aim is to mimic the imbalance power response of a synchronous machine, i.e. its inertia and damping characteristics, by implementing a controller connected to the grid-side through a feedback loop. Indeed, as represented in FIGURE 3.9, the virtual inertia is implemented in the inverter connected to the RES on one side and to the grid on the other side, where it usually measures the voltage, the current and the frequency [13]. Doing so, a few seconds after the imbalance, an additional amount of power is autonomously produced in order to stabilize the system after a frequency deviation, i.e. primary frequency reserves can be activated [7, 25]. Thus, the total inertia of the system is computed by taking into account conventional generators inertia and emulated inertia connected to the RES [10].
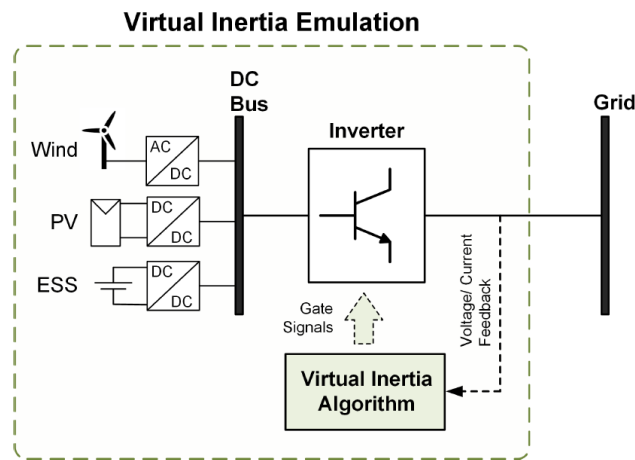
Figure 3.9: Virtual inertia concept [25].

Different types of virtual inertia can be implemented to make power converters behave as synchronous machines. Each of them has its pros and cons, as summarized in TABLE 3.2.

The first category of virtual inertia is called the *synchronverter*. This one is based on the synchronous machine itself as it uses its own electromechanical relationships to emulate inertia. Thus, this voltage-source model behaves as a conventional synchronous machine from the point of view of the grid [25]. This type of virtual inertia uses the model of the synchronous machine defining relations between torque, flux equations, virtual impedances as well as potential exciters. The parameters linked to the inertial response of the emulated machine, i.e. the moment of inertia and the damping factor, can be tuned in order to get an model as effective and stable as a synchronous machine. The main advantage of this model is to take as inputs voltage and frequency without needing the measurement of the RoCoF, responsible for bringing measurement issues and undesirable noise [13]. Also, numerical instabilities can be encountered because of the complexity of the exact replication of the synchronous machine behaviour. Moreover, synchronization to the grid is achieved in the basic implementation of synchronverters by means of a Phase Locked Loop (PLL). However, instabilities can occurs if it is poorly tuned. Solutions are proposed to counteract this effect, such as *self-synchronized synchroventers*. Finally, since this kind of virtual inertia is a voltage-source one, it is not inherently protected against transient overcurrents. It requires some protection schemes in order to work safely continuously [25].

The second type of virtual inertia is the *swing equation-based* model. While this technique is less complex than the previous one, it requires the measurement of the RoCoF, implying proper tuning of both control and signal processing parameters. The stability is usually studied while ignoring the damping factor, i.e. in a worst-case approach, while the so-called virtual synchronous generators include the damping part of the equation [13].

The third category is the *frequency-dependent active power response*, which does not use the relation between the physical devices, compared to both previous techniques. The main advantage of this technique is that the only constraints are the generation/storage technology and the capability of the power converter. This approach includes power-frequency, synchronous power and virtual oscillation controllers [13].

Table 3.2: Different types of virtual inertia, advantages and disadvantages [13].

| Method | Advantages | Disadvantages |
|---|---|---|
| Synchronverters | Accurate and coherent electromechanical model<br><br>No RoCoF measurement<br><br>PLL only for synchronization | Numerical instabilities issues<br><br>No overcurrent protection (voltage-source model) |
| Swing equation-based model | Easier to apply and tune than synchronverters<br>Connects to stability terminology | Potential swings while poor tuning<br>No overcurrent protection (voltage-source model)<br>RoCoF measurement |
| Frequency-active power model | Adaptivity and wide-range of applicability<br><br>Droop control : easy to apply<br><br>Technology limits could be considered | Non-common approach in grid control<br>Potential need of communication infrastructure<br><br>PLL use (potential instability) |

Virtual inertia has the main disadvantage of including delays due to the underlying signal processing. For instance, Phase Locked Loops, when used, can cause delays that have deteriorating effects on the operation of the power response. Also, it must be noted that some amount of energy is required to provide active power when needed, with an appropriate coordinate control between this energy and the inverter. This energy can either come from deloading devices, masked kinetic energy stored in the rotating masses of the blades of wind turbines or be stored in batteries (for instance, inverter-fed storage systems or super-capacitor), or flywheels [11, 28]. For instance, stored kinetic energy in the rotating blades of a wind turbine can range from 2 to 6 seconds and is thus non-negligible [8]. In the same paper, two different kinds of inertia emulation are presented, including either one or two-loops in the control diagram. The first one allows to participate in the primary reserves while the second also allows to participate in the restoration of the network frequency.

### 3.2.2.3 Fast power reserve

Only applicable to wind turbines, the *fast power reserve* technique is another potential solution for short-term inertial response and for supporting frequency. Illustrated in FIGURES 3.10a and 3.10b, the technique works as follows : during a decrease in frequency, when the frequency deviation exceeds a certain threshold, the wind turbine raises its output active power from its maximum power point tracking $P_{MPPT}$ to $P_{cmd}$ and delivers its kinetic energy stored in its rotating blades to the grid during a time slot $t_{dec}$, leading to the rotor speed drop down to $\Omega_{WT,min}$. This specific period of time during which the wind turbine participates in the frequency regulation is called the over-production period. Then, the wind turbine goes back to its nominal operation by decreasing its output power and thus increasing its rotor speed back to $\Omega_{MPPT}$, during $t_{acc}$ [8, 10].

(a) $P - \Omega$ characteristic [10].



(b) Wind turbine output power as a function of time [8].
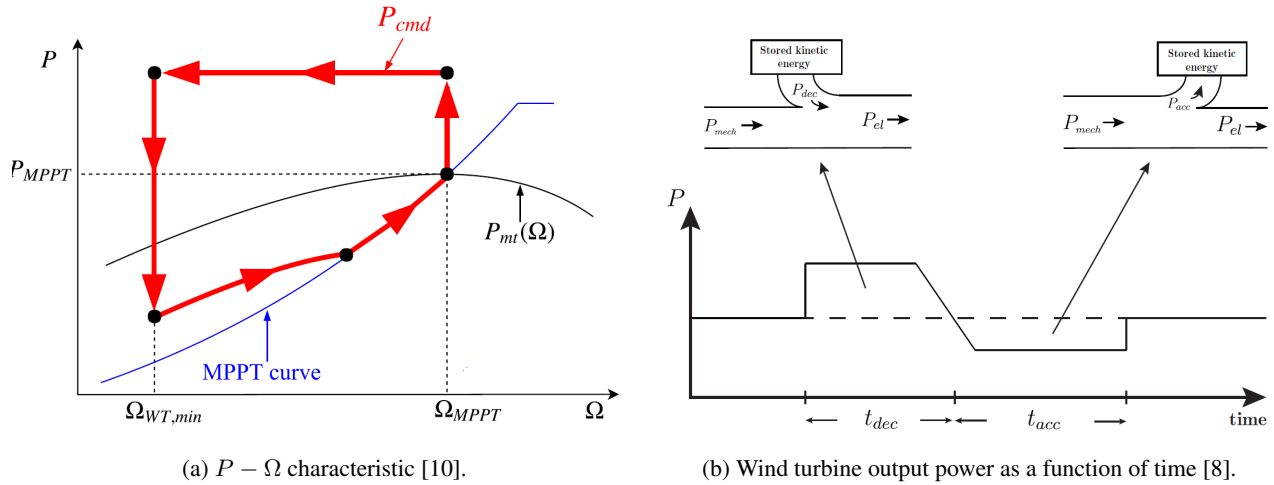
Figure 3.10: Fast power reserve : wind turbine output power as a function of rotor speed and time.

The main drawback of this technique remains in its short term operation, as the wind turbine is not able to participate in the frequency control during a long period of time and especially during its recovery or under-production period $t_{acc}$. The participation of the wind turbine thus depends on the available amount of stored kinetic energy in its rotating masses.

#### 3.2.2.4   Synchronous condensers

*Synchronous condensers*, also called *synchronous compensators*, are devices already existing in today's networks. Their behaviour is the same as synchronous machines except that their shaft is spinning freely. Hence, they do not produce any active power on their own but are mainly used to contribute in voltage regulation in electric trans- mission power systems by absorbing or producing reactive power whenever it is required. Their inertia together with their voltage regulation capabilities can thus be used respectively to recover the lack of inertia due to the replacement of synchronous generators with RES and maintain a stable power grid [13]. Indeed, synchronous condensers can be characterized by an inertia ranging from 1 to 6.5 seconds, which is comparable to synchronous machines[4]. Also, these machines can provide an effective support when restoring the grid, especially by contribut- ing to short-circuit current infeed which compensates the limited current capacity of converters. Moreover, these machines provide strength to the network which is reduced by implanting more RES connected through converters [16]. Thus, these devices operating together with HVDC links on wind power, PV plants and ESS technologies connected to the grid with converters could be a solution to ensure a stable 100 % RES power system [12]. Of course, additional investments are necessary, including the placement of additional synchronous condensers in the network, such that it remains stable whatever fault occurs, and the potential need to increase the rated power at which these devices are operating in order to support voltage anywhere in the grid. [16] mentions the potential solution of converting large retired thermal plants into synchronous condensers for the aforementioned purposes. [1] mentions synchronous condensers up to 350 MVA and [5] of 240 MVA.

---

[4]Indeed, EQ. 2.2 can also be used to compute the inertia of a synchronous condenser.

### 3.2.2.5 Modification of protection relays

As explained in SECTION 3.1.1, reduced system inertia leads to higher RoCoF and larger frequency swings which can induce tripping of relays that protect the systems devices and that ensure the system stability. If the RoCoF is still higher than today, a change in the protection relays should be carried out while moving toward a low inertia grid. Nowadays, RoCoF relays are typically set between 0.1 and 1 Hz/s for 50 Hz systems and depending on the grid inertia [27]. For instance, for the island grid of Ireland and because of the anticipated growing in wind power capacity in 2025, it is stated that thresholds of RoCoF relays need to be increased. Indeed, the current threshold is set to 0.5 Hz/s and should be increased to 1 Hz/s if 75 % of the generation becomes inverter-based [28]. As a solution, adaptive Automatic Load Shedding (ALS) is especially mentioned in [13]. Compared to static ALS, this type of ALS considers the actual system in time delay and load to be shed causing less customer disturbance. It offers more selectivity by the means of algorithms that measure data from the monitoring system considering the voltage and frequency dependency of loads.

### 3.2.2.6 Demand response

*Demand side* solutions are also proposed in order to react to system imbalances and be a part of the frequency control. It is defined in [4] by the "ability to control and manipulate demand side loads to continuously turn them off/on or change their consumption based on the situation and in response to power quality, system security, voltage and frequency, technical and economic constraints, applied by grid operators". This technique, while similar, cannot be compared with load shedding, applied in abnormal power system operation and in emergency conditions. In demand response, frequency-sensitive loads equipped with a self-regulating control can contribute to the frequency regulation, like in induction motors. Also, frequency-sensitive relays can be inserted into the grid, their role being to disconnect loads when frequency thresholds are exceeded [4]. Another solution comes from a project involving electric vehicles as suggested by the Danish ELECTRA Integrated Research Programme. It proposes control algorithms for these vehicles chargers to provide Fast Frequency Response (FFR) and virtual inertia. These chargers, usually operating at a nominal current of 16 A, could be controlled and change their operation into 1 A discrete steps depending on the frequency (resp. RoCoF) when providing FFR (resp. virtual inertia) [13]. Finally, another solution is proposed in [27] where it is mentioned that control of voltage-independent load can be carried out to support frequency. Thus, by opting for demand response instead of generators-side response, frequency deviation can be efficiently reduced, along with $CO_2$ emissions, energy consumption and energy reserves, directly decreasing the system operational costs [4].

## 3.3   Implementation of solutions in grid-forming converters

With the penetration of more renewable energy sources replacing synchronous machines, solutions have been presented for them to participate in the frequency control, voltage regulation and in the inertial response of the system, so that the whole transmission system is kept stable. As soon as wind turbines, PV arrays and batteries are connected through converters, as represented in FIGURE 3.11, implementation of some of those solutions within these converters is one of the main potential ways for reaching a 100 % RES grid.
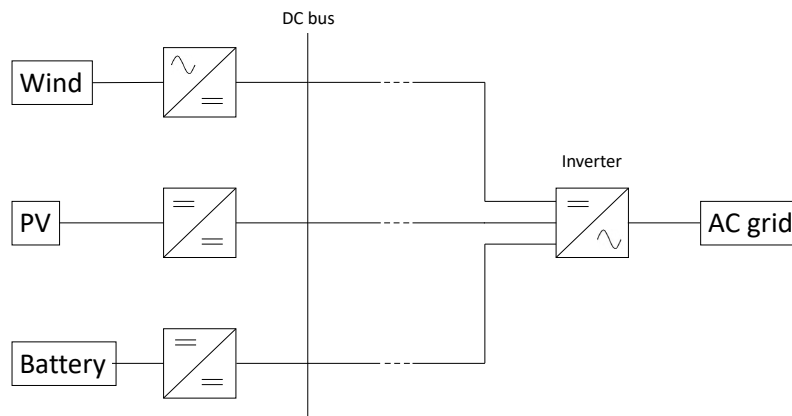


Figure 3.11: Schematic of a connection between a renewable energy source and the AC grid through converters.

This section aims at defining these converters that can operate in two different modes, grid-following and grid-forming, and describes their respective features as well as their advantages and drawbacks. The motivation for setting up grid-forming converters into the power grid is presented as well. Then, the energy buffer technology connected on the other side of the converter is discussed as well as where grid-forming converters should ideally be located in the grid. Finally, the models used for the grid-following and grid-forming converters implemented as injectors in the RAMSES software are presented.

### 3.3.1   Principles of grid-following converters and motivation for setting up grid-forming converters

Renewable energy sources such as PV, wind power and batteries are connected to the stiff AC grid through Voltage-Source Converters, so called VSCs. Nowadays, this energy conversion is done through *grid-following* converters. They act as ideal source of current connected in parallel to the grid with a high impedance. They control their output current and its phase angle in order to meet the required active and reactive powers [19]. The phasor diagram related to the operation of the grid-following inverter is represented in FIGURE 3.12.
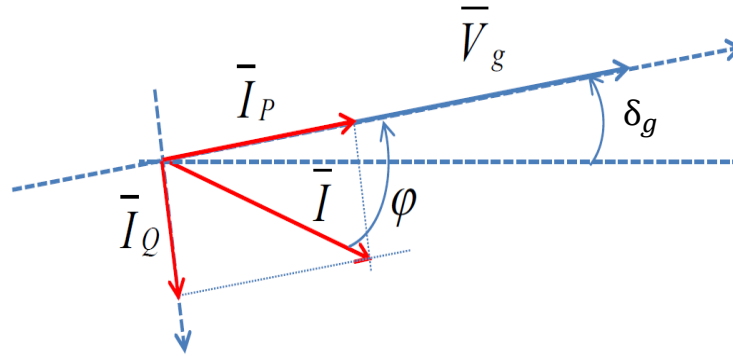
Figure 3.12: Phasor diagram of the grid-following converter [32].

The operation of a grid-following converter is composed of several steps : the AC grid voltage $\bar{V}_g$ imposed by synchronous machines, thus its amplitude $V_g$ as well as its phase angle $\delta_g$, are both measured through a Phased-locked Loop (PLL) at the terminal of the converter. This converter operates by following the grid angle and voltage instead of controlling it, as the designation suggests. Indeed, current $\bar{I}$ is injected by the converter into the network at a certain phase shift so that the active component $\bar{I}_P$ aligns with $\bar{V}_g$ and, at the same time, the reactive component $\bar{I}_q$ is in quadrature with the grid voltage. This way, a simple control like the one represented by the block diagram in FIGURE 3.13 can be implemented in order to obtain an active power corresponding to the active power set-point $P^*$.
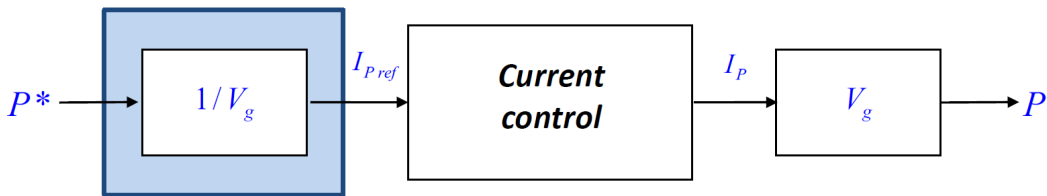


Figure 3.13: Block diagram of a simple control of a converter in grid-following mode [32].

However, since it requires a signal from the AC grid to determine its output, this type of inverter is not able to work standalone and it is thus impossible to reach a 100 % penetration of RES with only this kind of inverter. Indeed, the voltage measured by grid-following converters would become more volatile, which would cause frequency differences between converters and produce high power flows, leading to lots of changes in their output current. Producing a cascade effect in the whole system, this could cause an entire system collapse. Also, a relative change in the dynamics would occur if synchronous machines were replaced only with grid-following inverters. Indeed, these machines act relatively slowly while the inverters are characterized by much faster dynamics. This could impact the whole operation of the grid since loss of synchronization could occur because of the rigid fast inverter controllers present in the grid. It is thus required to implement even faster controllers that would be able to track a fast-moving reference [26]. Moreover, since grid-following inverters follow the angle of the stiff AC grid, they could no longer work without synchronous machines working in the network since they would not have any angle to be synchronized with. There is thus a need to implement converters that would be able to force this

frequency for the proper operation of the grid-following inverters found in the grid [7]. Finally, it is noteworthy to mention that the power plant is able to provide ancillary services and/or regulate the grid voltage, even if, in the case of the simple model described in this section, the active power set-point does not change with the frequency. Indeed, inertial response could be implemented through a controller but it would require the implementation of a PLL to measure changes in frequency and then modify $P^*$. Since the grid-following converter measures the grid voltage angle, this measure is not inherent to its simple model and the implementation of such services would require to derive the measured grid angle to obtain the grid frequency. However, since frequency permanently oscillates around its nominal value, this derivative computation would amplify the measure noises and would thus imply the implementation of filters that would modify the inertial action of the grid-following converter [32].

In order to avoid these effects, a solution has been proposed in the literature, the so-called *grid-forming* converter. This inverter's behaviour is different from the previous one as it acts as an independent and ideal AC voltage source with a low-output impedance [19]. Indeed, in this case, the converter imposes a certain voltage and frequency and does not require the signal from an external source of power anymore, as it is the case for grid-following converters with synchronous machines. The frequency is thus no longer related to any physical rotational part but would correspond to a set-point value of the control system and the output voltage could be used as voltage reference [7]. FIGURE 3.14 illustrates the difference between the operation of grid-following and grid-forming converters. In the above configuration, the grid angle and the voltage are both measured through a PLL and the grid-following converter injects a current such that the set-point active and reactive powers, respectively $P^*$ and $Q^*$, are met by the means of an advanced grid support control scheme. In contrast, the grid-forming inverter uses active power-frequency and reactive power-voltage droop controls to set the right frequency and admissible voltages depending on the measured active and reactive powers respectively. Thus, grid-forming converters control the frequency and the voltage instead of following those parameters imposed by the grid [22].
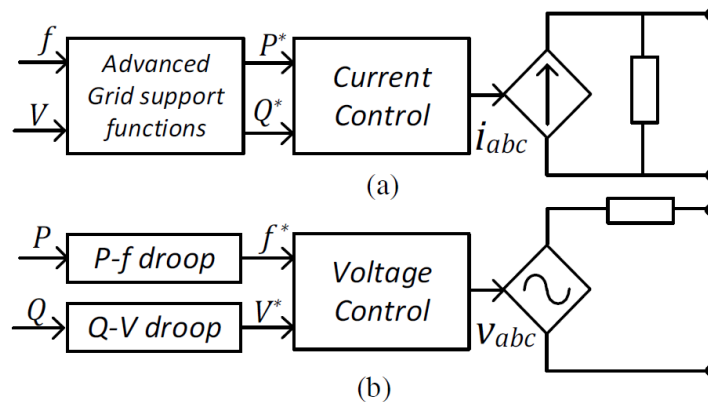


Figure 3.14: Inverter controllers in (a) grid-following and (b) grid-forming configuration [22].

It means this kind of controller could manage to autonomously regulate both the voltage and the frequency without the help of synchronous machines, and this in any grid conditions, i.e. in normal, disturbed and emergency operations. It requires to be compatible with all the technologies connected to the pre-existing network, such as synchronous machines and condensers, grid-following converters, and so on. Moreover, it could operate in black-start mode with sufficient energy buffer to restore the whole system after a blackout and it would have synchronization, load-sharing and frequency-power droop capabilities like synchronous machines. Furthermore,

because of their voltage-source operation, these converters could operate in fast response time enabling control at shorter time-scales compared to classical frequency control given by synchronous machines with grid-following inverters. Indeed, the latter require additional control loops to measure the voltage, the current and the frequency of the grid that inherently slows down the dynamics of the converter [17, 18, 26]. Finally, each type of converters is characterized by a good fault ride-through performance as they are able to withstand balanced or unbalanced undervoltage and overvoltage faults as well as frequency excursions. They also have the capability of injecting reactive current during a fault in order to allow faster voltage recovery after the fault. Thus, the safe and stable operation of the grid is ensured with the replacement of synchronous machines with converters [16].

The main issue regarding grid-forming converters is that their current can change rapidly after a contingency, since it is the only parameter which is not controlled by the converter, but determined by the network. Indeed, the voltage change is limited by the inertial behaviour implemented in the converter itself [12]. Thus, increasing the voltage angle, the active power injected into the grid increases but the converter could be already providing its maximum active power. At that moment, protection systems would disconnect it from the grid since they are not able to withstand overload capabilities and thus high currents as synchronous machines do. In fact, a synchronous machine allows to reach currents of about 250 % of their nominal value and two times more in the case of a short-circuit in both rotor and stator windings, for a certain period of time, due their to their thermal inertia. In the case of converters, the maximum current that they can withstand is about 110 % of their nominal value, because of the semiconductors[5] they hold. Higher current values reached following a grid event would cause the device to disconnect from the network or even its hardware to be destroyed, if no high-costly oversizing or over-current mitigation techniques are implemented [7]. [22] suggests to implement advanced control schemes such as virtual impedance current limiting but also mentions that these schemes could bring instabilities at large scale. In [16], it is stated that advanced protection schemes using current differential and methods detecting and clearing grid faults could also be a way to fix these high current issues. Finally, [18] suggests to allow deeper voltage drops during motor starts in order to overcome the high-current rating requirements.

### 3.3.2   Energy buffer technology

Since grid-following and grid-forming converters connected to renewable energy sources are able to participate in the frequency control, an energy buffer technology needs to be chosen in order for the converter to be able to produce or absorb power whenever it is required. Three candidate technologies are proposed [12]:

- The first possibility is to benefit the power overproduction capability of the power plant, i.e. its headroom ;

- The second consists in moving the operating point of the power plant so that it overproduces power whenever it is required ;

- The third choice is the installation of an ESS device connected in parallel to the power plant.

The first option requires that the power plant that provides power has the ability to increase it before reaching its operational limit. The second possibility linked to the deloading technique is not the preferred one for the same reasons as the ones detailed in SECTION 3.2.1.2 : moving away from the maximum power point tracking

---

[5]Indeed, from [16], the DC/AC converter manages the power flow through fast-acting controlling switching devices.

automatically implies that the total capacity of the power plant is not exploited. Indeed, today's inverter-based power sources operate in a MPP mode to produce the maximum possible amount of energy. Thus, modifying the optimal operation of the power plant induces a permanent reduction of its exploitation and therefore an additional cost linked to this reduced amount of power production capability. Convincing producers to permanently reduce their maximum output power could thus be difficult [26]. Considering the third option, the same paper mentions that grid-forming converters based on battery storage technology could be available in the market already, megawatt-sized, being able to black-start motor loads and to energize high-voltage transformers. It piqued the interest for some projects, some researchers working on the parallel operation of several grid-forming inverters. Indeed, by adding more converters, it could help each one to withstand a higher current as it is required within the period following an event in the grid. Thus, as also mentioned in [7], appending batteries or any other ESS technology could be the most convenient choice.

### 3.3.3 Location of the grid-forming converters

As the motivation of connecting grid-forming converters to the grid is stated, the location of these converters in the network is the next topic to be studied. If grid-following converters are already connected to the power network, some of them could be replaced with grid-forming converters. If not, it is important to know where grid-forming converters should ideally be added to any existing network. In [12], it is explained that grid-forming converters should be optimally spatially distributed in the grid and thus be placed as equally as possible across the whole system. Indeed, in such an arrangement, the network would be able to stay stable after any event bringing large angular jumps and it would ensure the security of any inverter-based system close to severe fault events such as a generator/interconnector trips or a short circuit. In fact, grid-forming converters would have the capability of transiently supplying power at this local level in order to reduce changes in bus bar angles. If the converter is connected far from the fault location, power must be transmitted over a long electrical distance, increasing the bus bar angles changes. This reasoning makes sense since it directly relates to the following equation :

$$P = \frac{V \cdot E}{X} sin\delta, \tag{3.3}$$

where $P$ is the active power transmitted in a transmission line, $V$ and $E$ are the bus voltages at each side of the line, $X$ its reactance[6] and $\delta$ is the voltage angle difference between both buses. From this equation, for the same amount of power $P$, a larger electrical distance being translated into a higher reactance $X$ leads to larger voltage angle deviation. Therefore, since the location of events that arise in the network is unpredictable, it is confirmed that grid-forming converters should be placed with an equal spatial distribution over the whole network area. However, if such an arrangement is not possible, the best configuration would be to place these converters in the centre of the network area in order to have similar average distances to any disturbance. This way, no particular area of the network is favoured compared to the others in terms of power security, especially in case of one part of the system being islanded from the rest.

---

[6]It is assumed that the transmission line is only characterized by an impedance where the resistance is negligible compared to its reactance.

### 3.3.4   Modelling of the Voltage-Source Converters

The models of the Voltage-Source Converters in grid-following and grid-forming mode used in the simulations are presented in this section. For both of them, the converter is implemented in the RAMSES software as an injector, since the renewable energy source to which the converter is connected is not considered in the software. The general model is illustrated in FIGURE 3.15.
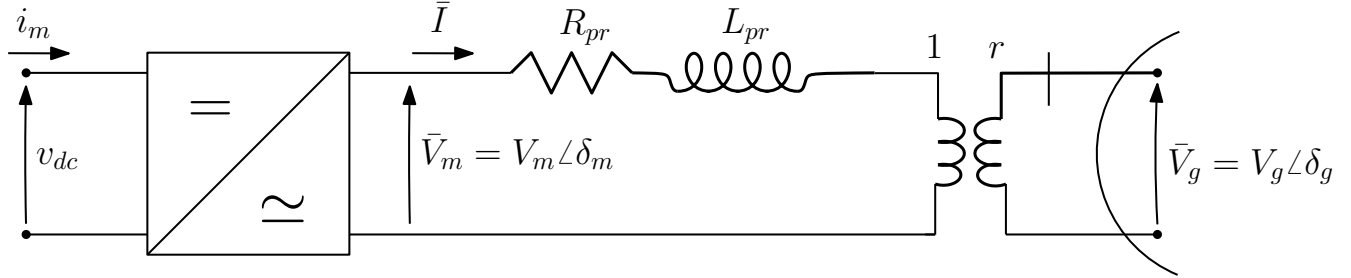


Figure 3.15: Phase reactor of the source of power, the Voltage-Source Converter and the transformer connected to the AC grid [2, 3].

The renewable energy source is represented by the constant voltage $v_{dc}$ and the current $i_m$, the converter is connected to this source and produces a modulated voltage $\bar{V}_m$ and injects a current $\bar{I} = i_x + j \cdot i_y$ into the grid. $R_{pr}$ and $L_{pr}$ are the phase reactor resistance and inductance, respectively, representing the losses in the Voltage-Source Converter and the losses due to the transformer, which transformer ratio $r$ is set to 1 with a proper choice of the base voltages. Finally, $\bar{V}_g = v_x + j \cdot v_y$ corresponds to the voltage at Point of Common Coupling with the AC grid. For both models, several frequencies are defined in the implementation and these are the following :

- $\tilde{\omega}_g$ is the per-unit grid angular frequency estimated by the PLL with the aid of the grid voltage components $v_x$ and $v_y$ ;

- $\omega_N$ is the nominal angular frequency in [rad/s], chosen as the base angular frequency in this model ;

- $\omega_{ref}$ is the reference angular frequency at which the orthogonal axis ($x$,$y$) rotate in [rad/s].

In both models, the converter is assumed lossless and the voltage $v_{dc}$ is assumed to be constant. The base power on the DC side is chosen to be the nominal active power $P_{nom}$ of the converter while on the AC side the base power corresponds to the nominal apparent power $S_{nom}$ of the converter [2, 3]. An example of the operation of both types of VSCs is presented in APPENDIX B.

#### 3.3.4.1   Grid-following converter

The block diagram describing the general operation of the grid-following converter is represented in FIGURE 3.16. The grid-following converter is composed of several elements : a Phase Locked Loop, a current controller and an active and reactive powers controller. The PLL measures the voltage angle of the grid $\delta_g$ in order to set the reference frame so that its $d$-axis is aligned with the grid voltage $\bar{V}_g$. This way, in steady state, the grid angle $\tilde{\delta}_g$ estimated by the PLL matches $\delta_g$ such that the $d$-axis and $q$-axis components of the grid voltage $\bar{V}$ in the reference

frame of the PLL are equal to $v_d = V$ and $v_q = 0$. In that specific case, since the active and reactive powers $P$ and $Q$, respectively, produced by the VSC can be computed by the means of the following equations :

$$P = v_d i_d + v_q i_q \tag{3.4}$$

$$Q = v_q i_d - v_d i_q \tag{3.5}$$

The active power produced by the VSC is directly controlled through $i_d$ and the reactive power through $i_q$.
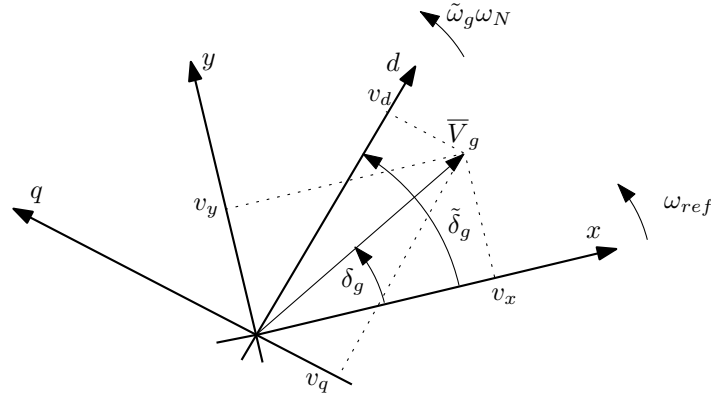


Figure 3.16: Phasor diagram of the operation of the grid-following converter [2].

The block diagrams of the active and reactive powers control are represented in FIGURE 3.17. In the future simulations, the grid-following converter model implementing these control loop is always referenced as "GFol".



(a) Active power control.

(b) Reactive power control.
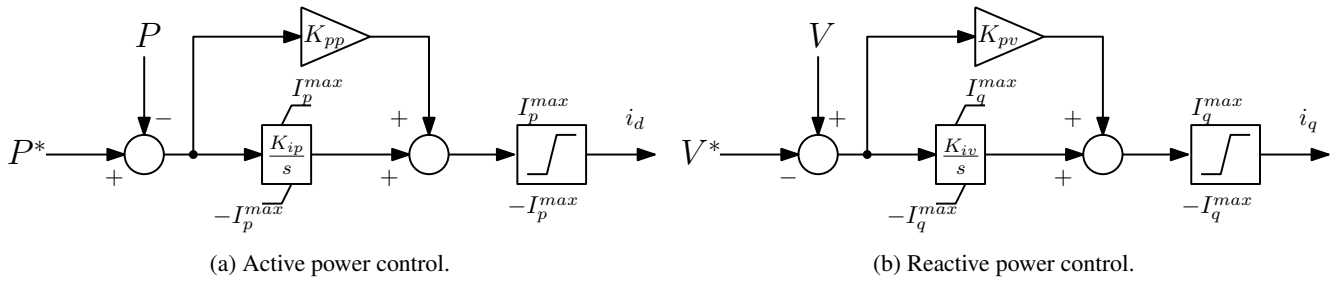
Figure 3.17: Active and reactive powers control of the grid-following converter [2].

The variables and parameters used in these block diagrams are the following :

- $P$ and $P^*$ are the per-unit active power injected into the AC grid and active power set-point, respectively ;

- $V$ and $V^*$ are the per-unit measured voltage and voltage set-point, respectively ;

- $K_{pp} = 0$ and $K_{ip} = 39$ are the gains of the PI control for the active power control ;

- $K_{pv} = 6.667$ and $K_{iv} = 0$ are the gains of the PI control for the reactive power control ;

- $I_p^{max}$ (resp. $I_q^{max}$) and $-I_p^{max}$ (resp. $-I_q^{max}$) are the maximum and minimum values that the $d$-axis (resp. $q$-axis) component of the current $i_d$ (resp. $i_q$) is allowed to take.

The grid-following converter thus injects some active power $P$ depending on the active power set-point $P^*$. A PI controller is designed so that the converter injects the right amount of active power into the grid depending on the $d$-component of its current $i_d$. The set-point value of the current is set by the means of the current controllers and its phasor is adjusted depending on the value of the estimated grid angle $\tilde{\delta}_g$. As can be seen in the diagram, the current is limited by $I_p^{max}$, in absolute values. For the reactive power control, the reasoning is similar but the $q$-axis component of the current $i_q$ is controlled depending on the voltage set-point that is set in the controller. The components of the current $\bar{I}$ are limited by the values of $I_p^{max}$ and $I_q^{max}$ such that the magnitude of this current is limited to 1 pu in the simulations. Finally, there is no measure of the grid frequency that influences the active power produced by the grid-following VSC in the active power control and thus no implementation of frequency response techniques.

### 3.3.4.2   Grid-forming converter

Grid-forming converters can operate according to several strategies [26]:

- Droop control ;

- Virtual Synchronous Machine (VSM) ;

- Matching approach ;

- Virtual Oscillator based Control (VOC) ;

- ICT/IoT based approach.

The first two approaches are detailed in SECTIONS 3.2.2.1 and 3.2.2.2[7], respectively. The VSM strategy could include the emulation of inertia or not and it is noteworthy that two issues are encountered. The first one concerns the fact that power converters are not able to deal with post-fault large over-currents as synchronous machine do. The second issue is regarding the implementation of the emulation of the synchronous machine itself. Indeed, it consists in numerically integrating higher order nonlinear dynamics based on AC-side measurements causing significant time delays in the controller loop of the grid-forming. Thus, this method does not take advantage of the fast-acting behaviour of inverters that can improve the system dynamics. The last three techniques are not explained in this report since they are not used in the chosen grid-forming converter model. However, explanations can be found in [26].

In order to simulate the behavior of a grid-forming converter, the model implemented in RAMSES, including the emulation of inertia with droop control, has been used and its block diagram is represented in FIGURE 3.18. This model is referenced as "GF MFR" in the simulations, where "GF" stands for grid-forming and "MFR" for Measured Frequency Reference since the grid frequency is estimated by the PLL.

---

[7]It is noteworthy that only voltage-source models can be used to emulate inertia with grid-forming inverters.
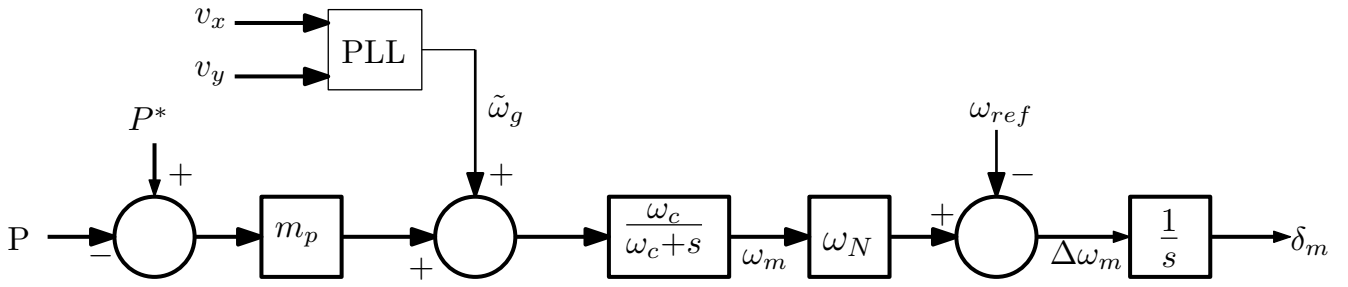
Figure 3.18: Block diagram of the operation of the grid-forming with measured frequency reference model [3].

The variables and parameters used in this model are the following :

- $P = v_x i_x + v_y i_y$ and $P^*$ are the per-unit active power injected into the AC grid and active power set-point, respectively ;

- $m_p$ is a per-unit parameter associated with the droop control ;

- $\omega_c$ is the cutoff frequency of the low-pass filter in [pu/s], which is associated with the inertial effect ;

- $\delta_m$ is the phase angle of the voltage $\bar{V}_m$ in [rad] and $\Delta\omega_m$ is its derivative in [rad/s].

The block diagram of the grid-forming converter can be translated as follows. First, the converter computes the difference between $P$ and $P^*$, in order to check whether the active power injected into the grid corresponds to the active power set-point. If not, it multiplies it by $m_p$ in order to translate this power difference into a frequency difference. Indeed, as explained hereafter, $m_p$ is directly linked to the frequency droop of the converter. Then, it adds this frequency difference to the estimated grid frequency $\tilde{\omega}_g$ and the sum is low-pass filtered, with a cut-off frequency of $\omega_c$, itself directly linked to the emulated inertia. The resulting frequency is multiplied by $\omega_N$, the nominal frequency, in order to go from a per-unit frequency to a frequency in radians. The converter model then subtract $\omega_{ref}$ from the previous result in order to get $\Delta\omega_m$, which is finally integrated to get the angle $\delta_m$, at which the converter imposes its voltage $\bar{V}_m$. It is important to note that the active power can be adjusted by this grid-forming converter model depending on the frequency deviations without any limitation in the current flowing in the converter and injected into the grid. The results obtained from the simulations have thus to be interpreted knowing that a current limiter should ideally be implemented in the model in order to obtain realistic results that could be applied to existing networks without compromising the converter operation.

The corresponding frequency droop $K$ and emulated inertia $H$ of the converter, similar to the physical parameters of a synchronous machine, are thus implemented in the controller and can be computed by the means of the following two relations :

$$2H = \frac{1}{m_p \omega_c} \tag{3.6}$$

$$K = \frac{1}{m_p} \tag{3.7}$$

The parameters of the grid-forming converter can be freely tuned in order to get the expected values for $K$ and $H$ of the implemented controller. Nevertheless, it is important to keep in mind that the energy source connected

to the converter needs to be able to cover the required amount of power varying with these two parameters. In other words, even if this model can take whatever values for the frequency droop and the emulated inertia, physical boundaries of the power source are still to be taken into account.

Also, the TSO could choose to either mimic the behaviour of a synchronous machine by choosing a certain value of inertia characterized by an under-damped response, or to tune the model characteristics so that the converter reacts to a fault with a damped or an over-damped response. Even if this would give rise to a less oscillatory response, the rate of change of power would be even larger within the time following a frequency dip or increase. There is thus a choice to make in order to obtain a trade-off between the damping response of the system and its physical capability to react to an event. Finally, the hardware limit of the converter is also a physical consideration to take into account while tuning the different parameters.

Nevertheless, a considerable advantage can be taken from this implementation. The manufacturer could choose to change the inertial characteristic of the converters and adjust it depending on the specific grid requirements. In the future, we could even consider to vary the damping and inertial characteristic of the grid-forming converters based on the varying needs of the system grid [12].

The last feature that is implemented in this model is the current limiter. The latter is required since converters are not able to withstand high currents flowing in them. Since for grid-forming converters the voltage is controlled in contrast to grid-following converters where the current is the controllable output, the current in the converter is not limited by a saturation block anymore but by the use of a virtual impedance, represented in red in FIGURE 3.19 [3]. The value of the virtual impedance $R_{VI} + j \cdot X_{VI}$ is computed depending on the value of the current $\bar{I}$ and becomes effective after a certain delay after the magnitude of the current $\bar{I}$ is greater than the allowed one $I_{max}$, set to 1 pu in the simulations, as for the grid-following converter.
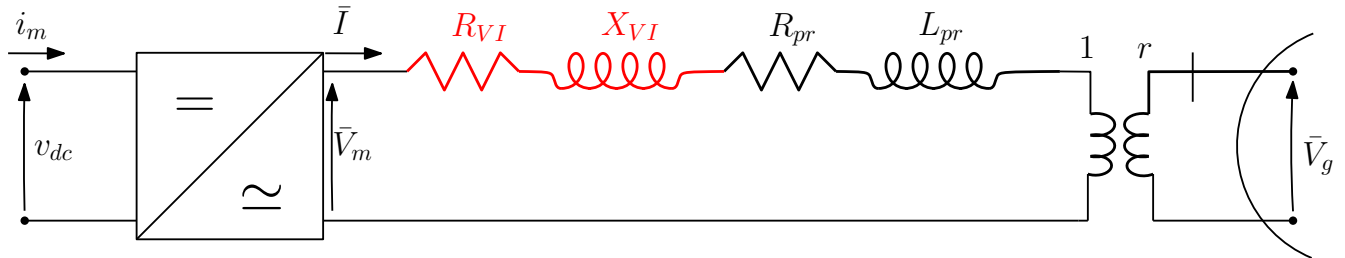


Figure 3.19: Phase reactor of the grid-forming converter with the virtual impedance [3].

The values of the resistance $R_{VI}$ and the reactance $X_{VI}$ of the virtual impedance are computed by the means of the following relations :

$$R_{VI} = K_{pVI}\Delta I \tag{3.8}$$

$$X_{VI} = \sigma_{X/R}R_{VI} \tag{3.9}$$

where $K_{pVI}$ equals 0.6716 $\Omega$/A, $\sigma_{X/R}$ equals 5 and $\Delta I$ is given by :

$$\Delta I = I - I_{max} \quad \text{if } I \geq I_{max} \tag{3.10}$$

$$\Delta I = 0 \qquad\qquad \text{if } I < I_{max} \tag{3.11}$$

It is important to note that the computation methods implemented in the model of the grid-forming converter with the virtual impedance are non-linear. Thus, when the current is greater than $I_{max}$, the Newton-Raphson method used in `RAMSES` for the computation of the network power flow does not implement linear computations anymore. Thus, the moment at which this change occurs is delayed by a certain amount of time, equal to 0.001 second in the simulations. The virtual impedance is thus activated after this delay, possibly bringing to a current peak in the simulations where the current exceeds 1 pu. This peak is thus not realistic but due to the phase reactor approximation in the model.

# Chapter 4

# Application to the Nordic network

In this chapter, the stability of the *Nordic network*, implemented in the software `RAMSES`, is studied with different changes compared to its initial configuration. The objective is to replace synchronous machines implanted in the original network by renewable energy sources together with or without additional technologies and obtain a final network topology that is safe and secure when potential faults arise. Each configuration can include different kinds of elements, especially including :

- Synchronous machines in the parts of the network that are not modified ;

- Grid-following and/or grid-forming converters, connected to renewable energy sources :

    - Grid-following converters are not capable to participate in the frequency regulation ;

    - Grid-forming converters are capable to participate in the frequency regulation, if it is required.

- Synchronous condensers ;

- VSC HVDC links, that are connected to the AC network through either grid-following converters at both sides or through a grid-following VSC at one side and a grid-forming VSC at the other one.

First of all, the tools that are used for the simulations `RAMSES` and `ARTERE` are presented in this chapter. Then a general overview of the initial configuration of the Nordic network and its topology is detailed and dynamic simulations after the occurrence of some faults are given and commented. The third section includes dynamic simulations of different configurations of the central part of the network. Finally the fourth part proposes dynamic results of a particular topology of the Nordic network where a HVDC link has been added to the original configuration. Both last sections focus on the frequency response of the network, its voltage control and discuss about several mix of various technologies that can replace the removed synchronous machines.

## 4.1   Simulation tools

`RAMSES`, standing for "*RApid Multithreaded Simulation of Electric power Systems*", is a software for dynamic time simulations of electric power systems in phasor mode and is the simulation tool that is used to run simulations on networks composed of synchronous machines, loads, transmission lines and synchronous condensers. Power flow computation by Newton method is performed using the software `ARTERE`, standing for the french sentence

"*Analyse des Réseaux de Transport de l'Energie électrique en Régime Etabli*".  It can be used to simulate contingencies while controlling voltages and is set up so that the slack bus compensates the active power generation after an imbalance occurs.

## 4.2   Presentation of the Nordic network

The one-line diagram of the Nordic network implemented in RAMSES is illustrated in FIGURE 4.1. Composed of 20 generators, the north part includes hydro power plants while both central and south parts are mainly composed of thermal generation. The upper left equiv. part of the network represents an external connection, mainly supplied by the equivalent synchronous machine $g20$, being connected to the slack bus of the whole system. Transmission lines are rated at 400 kV and some of them are equipped with series compensation. This transmission network is connected to regional systems operating at either 200 or 130 kV. The nominal frequency at which the network operates is 50 Hz and only the generators located in the north and equiv. areas participate in the frequency control. All thermal power plants are thus characterized by a constant mechanical torque and thermal power plants use speed governors with a droop coefficient of 8 % for the equiv. zone and 4 % for the rest of the machines to participate in the frequency regulation. Finally, Load Tap Changers (LTCs) are also placed in the system in order to restore distribution voltages and thus load power when a contingency occurs by adjusting the transformer ratio over 33 positions.  The per-unit system, the network data of the transmission lines, the transformers, the shunt compensation, the generators and the models used to represent any component of the network can be found in [33].

This system operates in two different operating points.  The first one, called "*operating point A*", is insecure since it does not respect the $n - 1$ criterion.  Modifications have then been carried out in order to get a secure "*operating point B*", where machines $g15$ and $g18$ have been divided into two identical ones with half nominal apparent power to make contingencies less severe and an additional synchronous machine $g16b$ has been placed exactly in the same way as $g16$, reducing power generated by equivalent generator $g20$. These changes have made the system more robust and secure whatever fault arises. Indeed, any generator outage can be stood by the system and lines faults are stood for 5 cycles, corresponding to 100 ms, which are cleared by tripping the corresponding line.  Finally, in general, the system operates such that the north part composed of hydro power plants supplies power to the central part through five transmission lines.

The Nordic network in *operation point B* has been chosen as "test network" for various reasons.  First, this network is ensured to be initially safe and secure, whatever the fault that arises. Studies can thus be focused only in the changes that are carried out in this network instead of focusing on the original topology of the network which takes a non-negligible amount of time to be built and studied deeply.  This way, using an already secure network allows to compare its operation to any other configuration with some changes that have been done, for different kinds of faults.  Thus, in any case where the changes unsecure the network after any of these faults, it can be directly concluded that these changes do not lead to the best configuration that can be applied to the Nordic network.  Moreover, as it represents the typical topology of any existing network in the Nordic part of Europe, implanting renewable energy sources is a possible situation that systems operators can be faced on, since the power potential of hydro and wind powers for instance is quite high in these regions.  Finally, since this network is composed of different types of power plants, interconnection, different voltage levels and other features, it can be taken as a generic case. The modification carried out on this network can thus be applied to any other network.
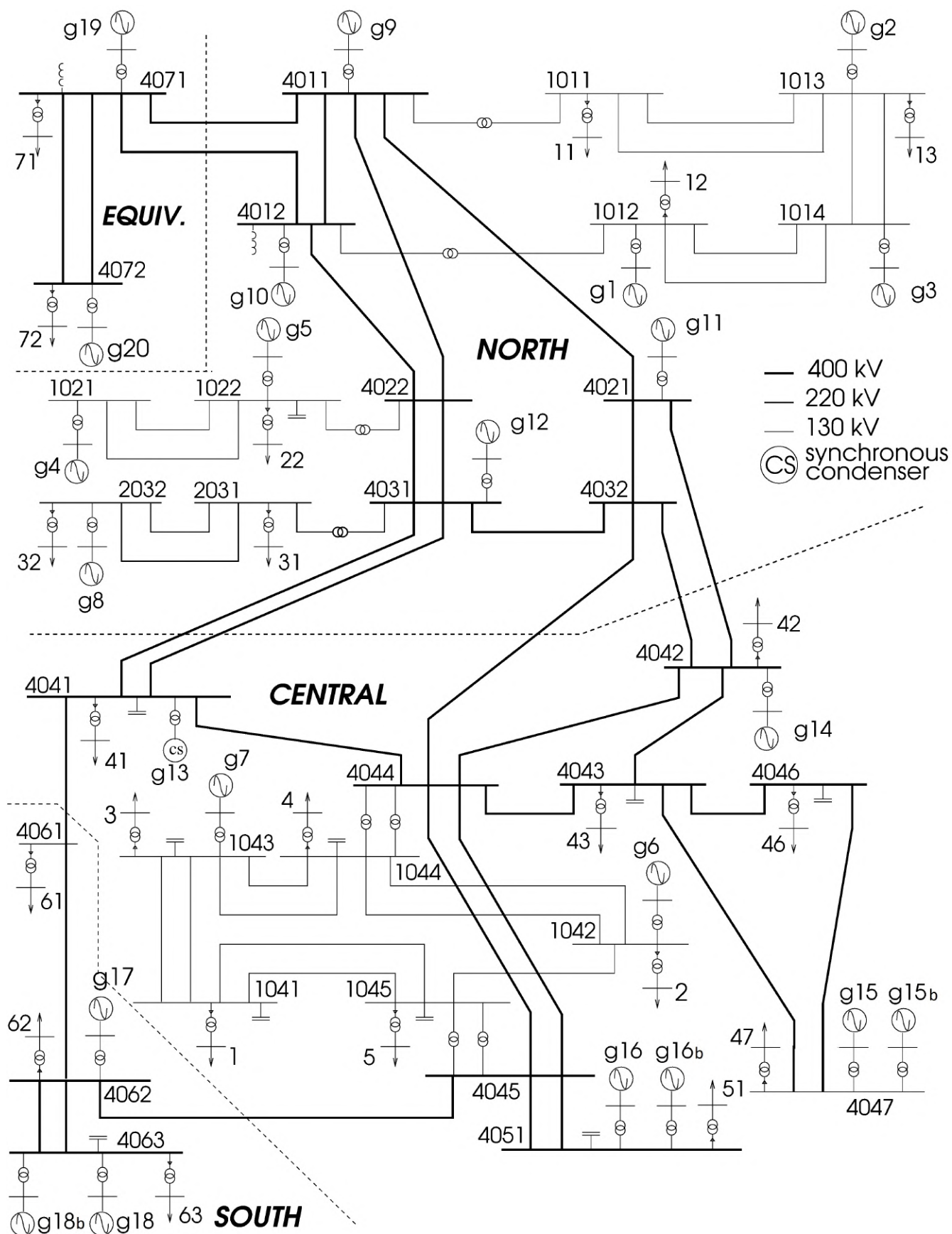
Figure 4.1: One-line diagram of the Nordic system in operation point B [33].

### 4.2.1 Dynamic simulations with the initial configuration of the Nordic network

This subsection is dedicated at presenting dynamic simulations carried out with the initial configuration of the Nordic network. Four different events that will be analysed at least once in the next sections of this chapter are considered :

- The loss of synchronous machine $g1$ or $g15$ after 1 second ;

- The tripping of line 4032-4044 after 1 second ;

- A short-circuit at bus 4032 after 1 second cleared 100 milliseconds later by the tripping of line 4032-4044.

FIGURE 4.2 represents the rotor speed of synchronous machine $g12$, representing the system frequency, after the loss of either $g1$ or $g15$ while FIGURE 4.3 shows the voltage at bus 1042, 1043, 4042, 4047 and 4051 after the tripping of line 4032-4044 or the short-circuit at bus 4032 cleared by the tripping of line 4032-4044. TABLE C.1 in APPENDIX C presents the numerical results of this simulation. For all simulation results presented in this report, the horizontal axis representing the time is adjusted for visibility reasons so that each plot illustrates the beginning of the graph until it reaches a steady-state value. In general, all simulations have been launched for either 300 or 400 seconds to ensure that the steady state is reached.
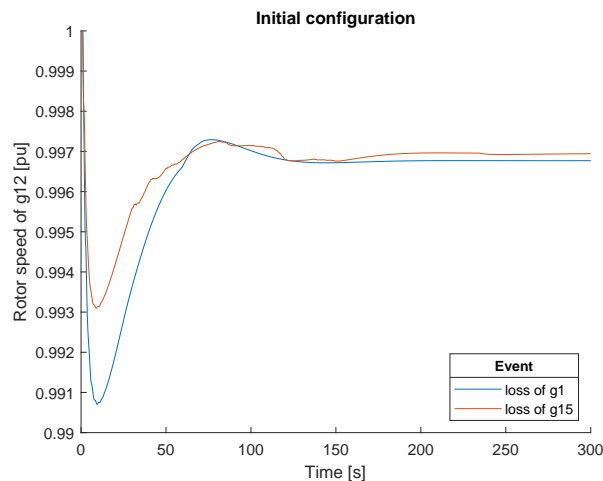


Figure 4.2: Rotor speed after the loss of $g1$ or $g15$, with the initial configuration of the Nordic network.
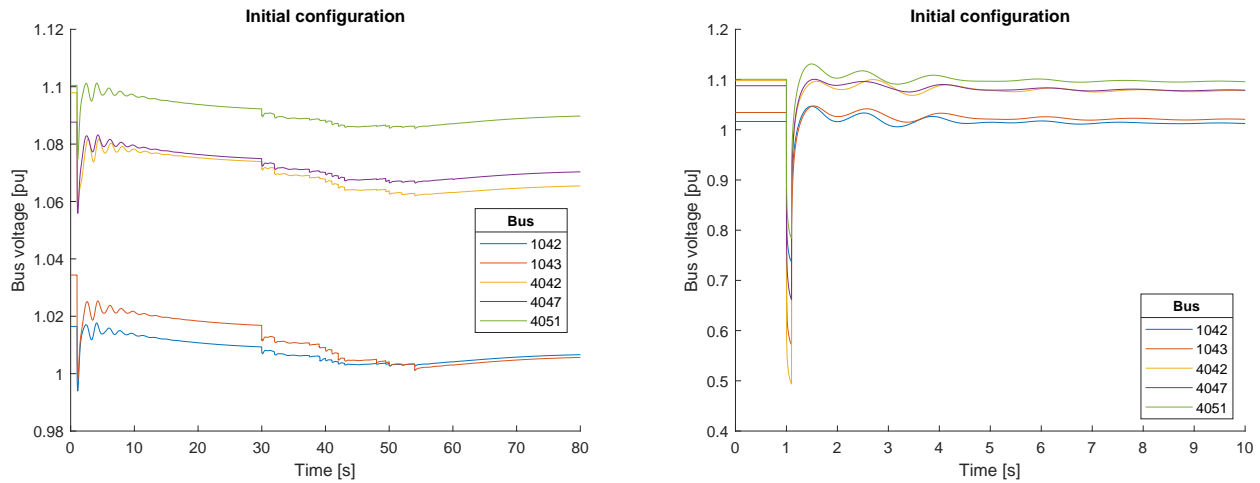
(a) Tripping of line 4032-4044.                    (b) Short-circuit at bus 4032 and tripping of line 4032-4044.

Figure 4.3: Bus voltages in the central part after the tripping of line 4032-4044 or the short-circuit at bus 4032 cleared by the tripping of line 4032-4044, with the initial configuration of the Nordic network.

It can be easily observed that the frequency decreases after the loss of each synchronous machine during the transient period, since the generated power does not match the consumed power by the loads anymore. Frequency reserves are thus activated and hydro power plants located in the north part of the network with a droop coefficient of 4 % produce an additional amount of power to restore the system frequency. This is why the frequency drop stops its course after 10 seconds to increase to a steady-state value of 0.9968 and 0.9969 pu for the loss of $g1$ and $g15$ respectively. The frequency drop during the transient period is deeper with the active power initially produced by the generator that is lost. Loosing 540 MW initially produced by $g15$ causes a voltage drop of 0.69 % and 0.93 % after the loss of $g1$ initially producing 600 MW. These deviations are computed compared to the nominal value of 1 pu.

The tripping of line 4032-4044 causes a voltage drop at each bus. The deviation from the initial value averages 2.92 % during the transient period. The voltage evolution after the transient period is characterized by a staircase curve, illustrating the activation of the LTCs for the voltage recovery in the whole network. On the other hand, bus voltages obtained after the short-circuit are characterised by deeper voltage drops. Indeed, the maximum transient deviations from the initial bus voltage range from 27.45 to 55.04 %, corresponding to minimum values of the voltage from 0.7372 to 0.4937 pu during the transient period. These are due to the short-circuit that affects the bus voltage in the central part and is cleared by the tripping of the line 4032-4044. At that moment, each bus voltage increases again to a value similar to the initial one.

For the four events, the frequency does not deviate from the nominal value by more than 5 % and the steady-state voltage of each bus is always located between 0.9 pu and 1.1 pu which is acceptable. This proves the stability of the initial configuration of the Nordic network. The goal of this work is to compare these dynamic simulations with the ones obtained with other configurations of the Nordic network to determine if renewable energy sources connected through converters can replace the synchronous machines initially placed in the network.

## 4.3 Replacement of synchronous machines in the central part with Voltage-Source Converters

Simulations in this section aim at illustrating the effect on the network dynamics of replacing synchronous generators with renewable energy sources connected to the grid through Voltage-Source Converters (VSCs). More especially, this is carried out by removing synchronous machines $g6$, $g7$, $g14$, $g15$, $g15b$, $g16$ and $g16b$ initially placed in the central part of the network and by replacing them with grid-following or grid-forming VSCs, as represented in FIGURE 4.4. The frequency response and the voltage control of the modified network is analysed in this section followed by a deeper analysis focusing on the effect of adding various technologies to the central part of the network, including each type of VSCs and synchronous condensers.
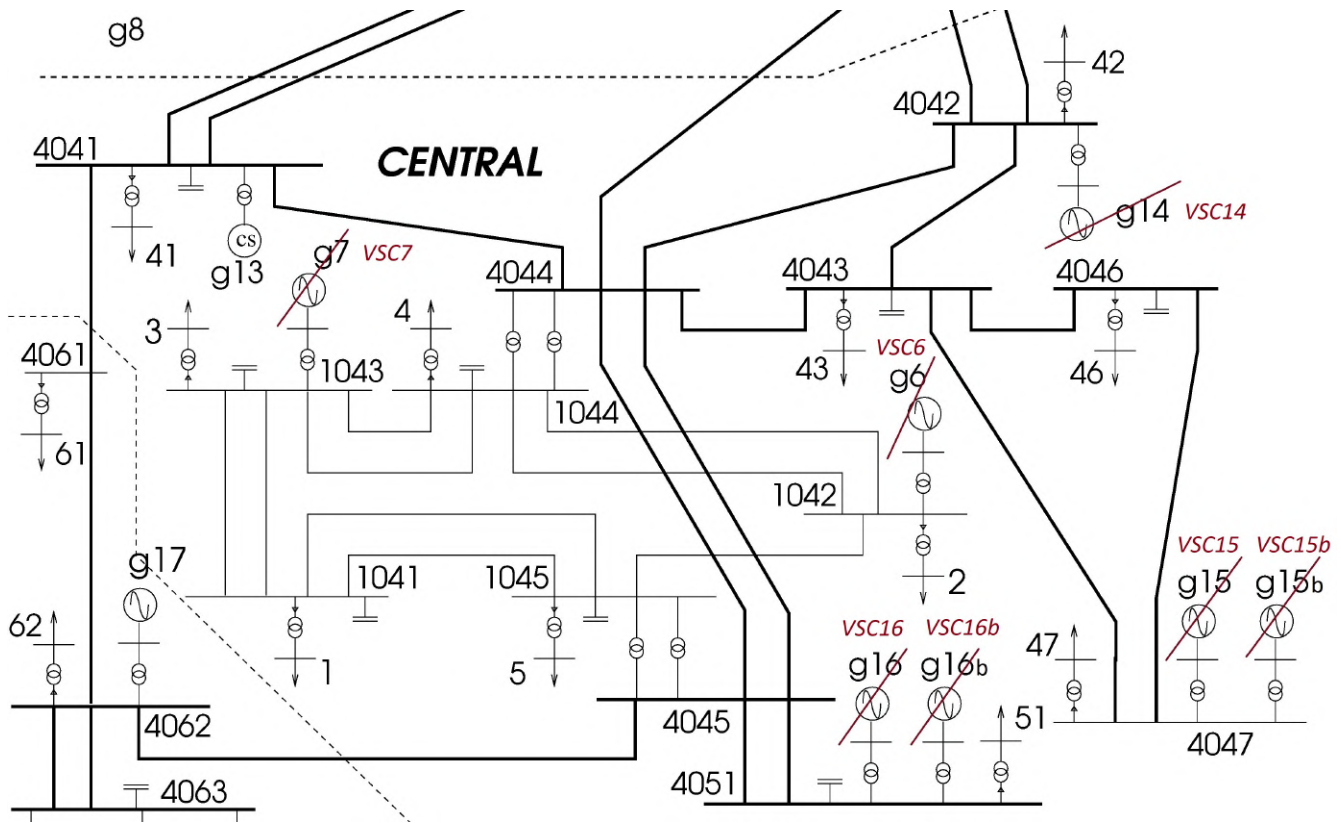


Figure 4.4: One-line diagram of the central part of the Nordic system where synchronous machines are replaced with VSCs.

The replacement of a synchronous machine with a VSC is achieved by disconnecting the synchronous machine with its step-up transformer and connecting the VSC at the bus to which this transformer was initially connected, as shown in FIGURE 4.5. In the simulations, a Voltage-Source Converter replacing synchronous machine $gx$ is called VSC$x$ in the figures and in the comments and the type of energy buffer, i.e. the RES connected to the network through the VSC, is ignored. It is assumed that the active power produced by each synchronous machine can be replaced with a renewable energy source producing the exact same amount of active power.
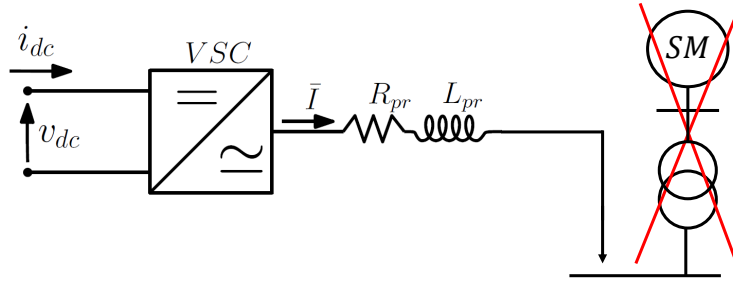
Figure 4.5: Illustration of the replacement of a synchronous machine with a Voltage-Source Converter.

It is initially assumed that no renewable energy source participates in the frequency control, as it is the case with synchronous machines in the central part of the initial configuration of the Nordic network. Then, as grid-forming converters can have a certain frequency droop to participate in the frequency response, these are studied with a 4 % droop, the same value as for hydro power plants located in the north part of the network. Both cases are studied considering the loss of generator $g1$ to analyse the frequency response of the modified network.

The goal of the second part is to study the voltage control of the central part network after a contingency. The fault considered in that specific case is the tripping of line 4032-4044, connecting the north part to the central one.

Finally, simulations where a short-circuit occurs at bus 4032 cleared by the tripping of line 4032-4044 are carried out where various mixes of grid-following converters, grid-forming converters and/or synchronous condensers are proposed. The purpose is to determine the best configuration of the central part of the network, especially focusing on the voltage control and the capability of the VSCs to withstand the fault.

TABLE 4.1 presents the nominal apparent power of the synchronous machine and the nominal active power of the turbine. In total, a capacity of 3510 MW and a total amount of dispatched active power of 3450 MW are replaced with VSCs.

Table 4.1: Data of synchronous machines in the central part of the Nordic network for operating point B [33].

| Synchronous machine | Nominal apparent power $S_{nom}$ [MVA] | Nominal active power $P_{nom}$ [MW] | Generated active power $P$ [MW] |
|---|---|---|---|
| $g6$ | 400 | 360 | 360 |
| $g7$ | 200 | 180 | 180 |
| $g14$ | 700 | 630 | 630 |
| $g15$ | 600 | 540 | 540 |
| $g15b$ | 600 | 540 | 540 |
| $g16$ | 700 | 630 | 600 |
| $g16b$ | 700 | 630 | 600 |
| **Total** | 3900 | 3510 | 3450 |

### 4.3.1 Frequency response

This section aims at studying the frequency response of the Nordic network while replacing the synchronous machines located in its central part with grid-following or grid-forming converters. For that purpose, the event that is considered is the loss of $g1$ after 1 second. This synchronous generator produces 600 MW and consumes 19.6 Mvar [33]. Thus, the central part of the network will not face important voltage changes which is the reason why these are not shown for this event. The changes will especially occur in the system frequency, directly related to the rotor speed of the synchronous generators that are left in the network, in the frequency estimated by the converters but also in their produced active power and the current flowing into them.

FIGURE 4.6a represents the rotor speed of generator $g12$ located in the north part of the network after the loss of $g1$, with three configurations : the initial configuration of the Nordic network where all synchronous machines are left and the configurations where the synchronous machines in the central part are replaced with grid-following or grid-forming converters. FIGURE 4.6b on the right side represents the frequency estimated by each grid-forming VSC. TABLES C.2 and C.3 in APPENDIX C present the numerical results of this simulations.
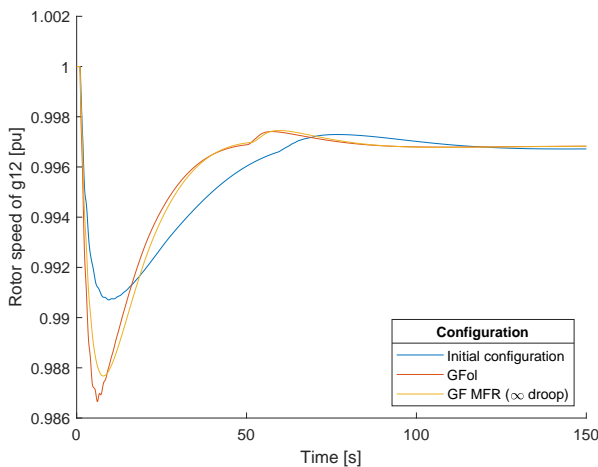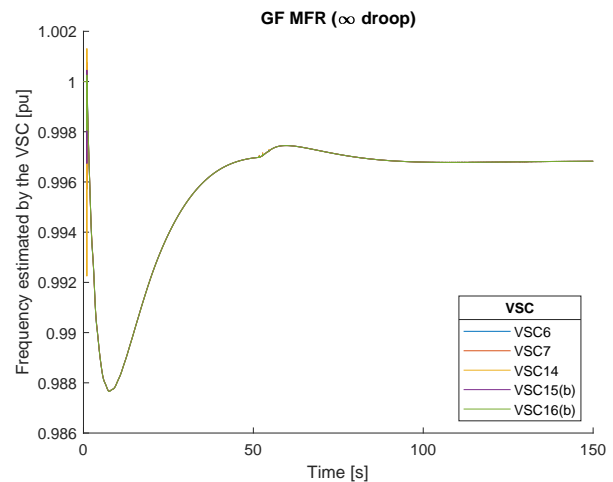


(a) Rotor speed of $g12$.

(b) Frequency estimated by each grid-forming VSC.

Figure 4.6: Rotor speed of $g12$ and frequency estimated by each VSC after the loss of $g1$, with the replacement of SMs in the central part with VSCs.

The figure on the left side gives information about the difference in the evolution of the frequency depending on the configuration of the central part of the network. In each configuration, the frequency drops after the loss of $g1$, due to the active power imbalance in the network. The frequency drop is more pronounced in the configurations where the synchronous machines are replaced with VSCs, in both grid-following and grid-forming mode. This is a direct consequence of the lack of inertia in the system due to the replacement of synchronous generators that inherently participate in the inertial response. The slope at which the frequency drops during the transient period is thus steeper and thus the frequency nadir is lower with the presence of VSCs. Indeed, with synchronous generators

in the central part, the frequency nadir reaches 0.9907 pu while with grid-following converters it reaches 0.9867 pu and 0.9877 pu with the grid-forming converters. The frequency drop stops it course because of frequency reserves that are activated in the north and equiv. parts of the system. Additional active power is thus produced by these synchronous generators equipped with a speed governor and make the frequency increase to a steady-state value of 0.9968 pu in the three configurations. Finally, the slope of the curve after the frequency drop is steeper with both types of VSCs. The synchronous machines are characterized by slower dynamics that affect the frequency recovery. At any time, the frequency does not reach values that are higher than 5 % greater than the nominal value of 1 pu.

Regarding the figure on the right side, the frequency estimated by each grid-forming converter is approximately the same for all VSCs, expect the small peak and drop occurring at the moment the fault is applied to the network. These come from a numerical error in the estimation of the frequency through the PLL. Apart from that, the curves are exactly the same as the rotor speed of $g12$ when grid-forming converters are used, corresponding to the yellow curve in FIGURE 4.6a.

FIGURES 4.7 and 4.8 represent the current flowing in each VSC after the loss of $g1$, when the central part of the network is either full of grid-following or grid-forming converters instead of synchronous machines. TABLE C.4 in APPENDIX C presents the numerical results of this simulation.
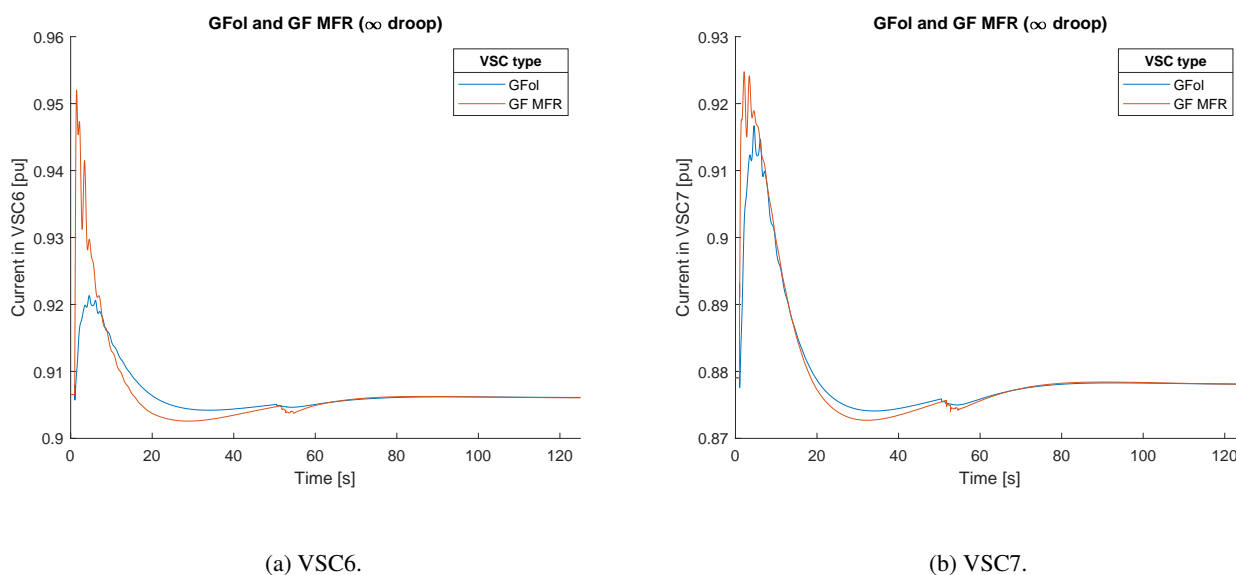


(a) VSC6.



(b) VSC7.

Figure 4.7: Current in each VSC (VSC6, VSC7) after the loss of $g1$, with the replacement of SMs in the central part with VSCs.
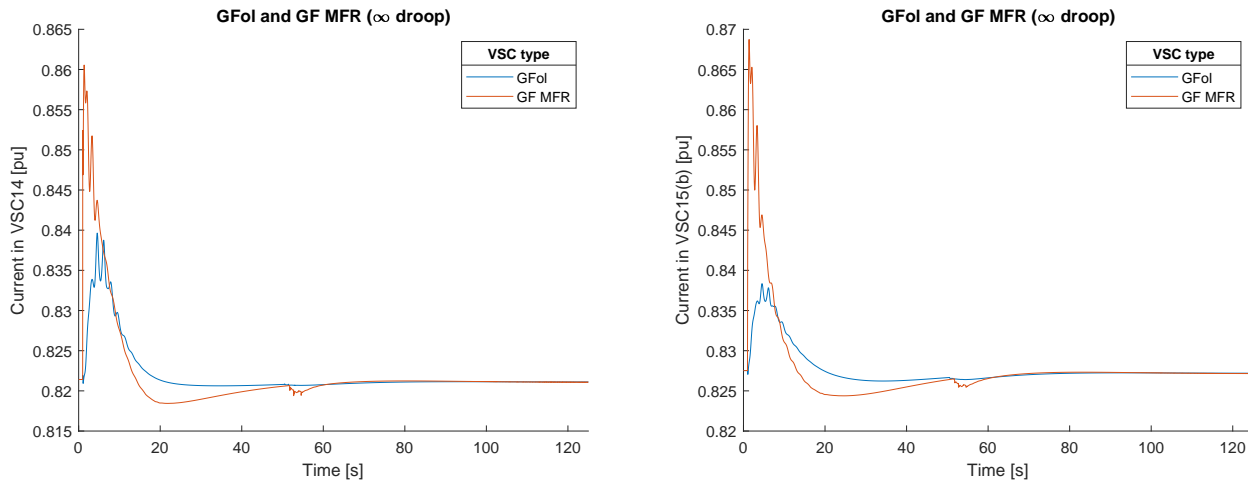
(a) VSC14.



(b) VSC15(b).
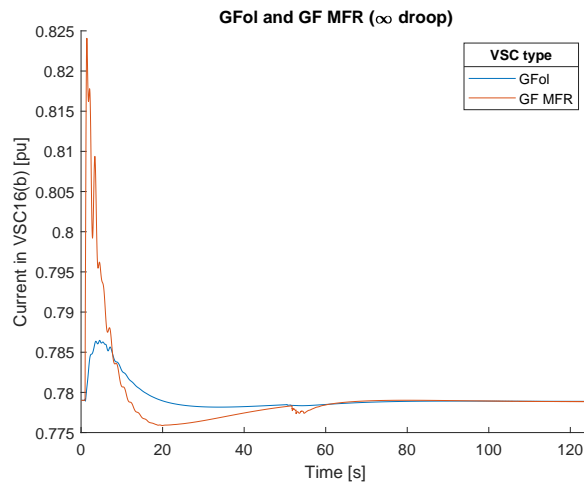


(c) VSC16(b).

Figure 4.8: Current in each VSC (VSC14, VSC15, VSC16) after the loss of $g1$, with the replacement of SMs in the central part with VSCs.

From these two curves, it can be noticed that the current always shows a peak after the occurrence of the fault in $g1$ that decreases afterwards to a steady-state value similar to the initial one. When grid-following converters are used, the change in the current is due to the variation of the bus voltage magnitude and in the active power. The latter is varying during the transient because of the time required for the frequency reserves to take place. With the grid-forming converters, the peak is always reached more rapidly and reaches higher values because of the changes in the bus phase. Nevertheless, these peaks never exceed the maximum value of 1.1 pu, leading to the safe operation of the VSCs. The highest current reached by the grid-following VSCs is 0.9213 pu and 0.9520 pu for the grid-forming VSCs, both by VSC6. These curves are thus acceptable.

Until now, all grid-forming VSCs implement an infinite frequency droop as the synchronous machines that they replace. The results that are discussed next focus on the comparison between this case and the one where grid-forming VSCs have a 4 % droop, allowing the RES connected behind to participate in the frequency control.

FIGURE 4.9a represents the rotor speed of generator $g12$, corresponding to the system frequency, and FIGURE 4.9b shows the frequency estimated by VSC14, after the loss of $g1$ and when synchronous machines in the central part of the network are replaced with grid-forming VSCs having either an infinite or a 4 % frequency droop. The graph representing the evolution of the current in the other VSCs are similar to the one of VSC14, except for the peak and the drop at the occurrence of the fault due to a computation error by the PLL, which is why they are not shown. TABLES C.2 and C.3 in APPENDIX C present the numerical results of this simulations.
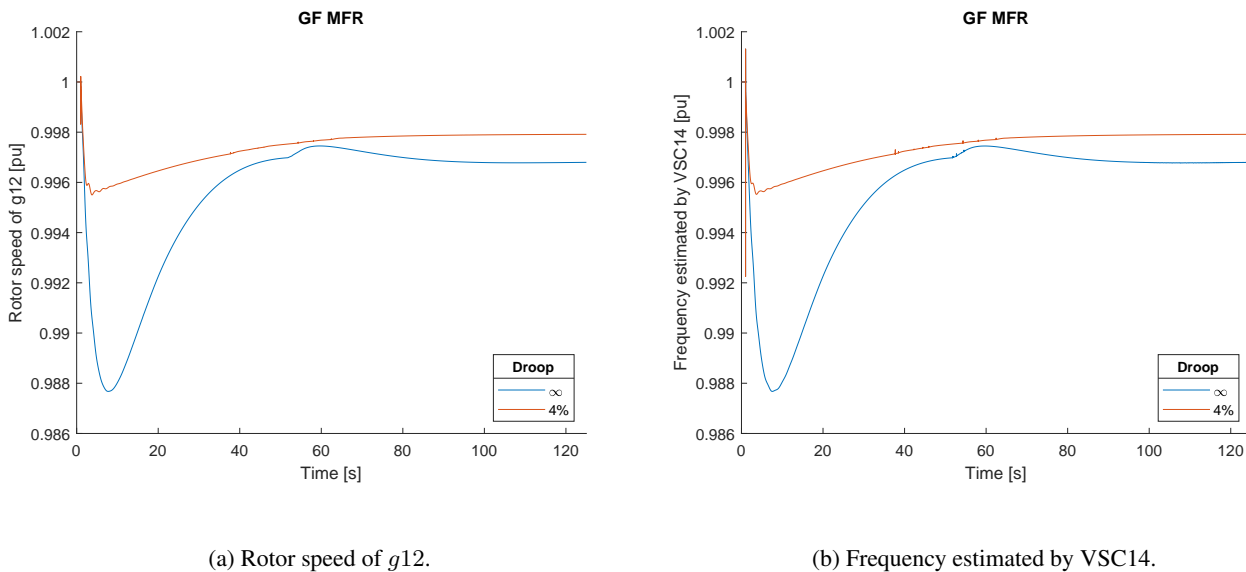


(a) Rotor speed of $g12$.                                      (b) Frequency estimated by VSC14.

Figure 4.9: Rotor speed of $g12$ and frequency estimated by VSC14 after the loss of $g1$, with the replacement of SMs in the central part with grid-forming converters, for different droops.

When comparing both graphs, it can be noticed that both are similar. Indeed, the frequency is well estimated by the PLL of each grid-forming converter, except for the peak and drop occurring at 1 second when $g1$ is lost. The frequency drop and its steady-state value are improved when choosing a 4 % droop instead of an infinite one. This makes sense since, with a finite droop, the RES connected to the grid through a converter participates in the frequency regulation and thus produces an additional amount of active power to compensate the loss the active power initially produced by $g1$. More generators participate in the frequency control and help the network to recover its frequency. This is directly reflected by a frequency drop that is less deep and a steady-state value closer to the nominal value of 1 pu. Numerically, the minimum value reached by the frequency is improved from 0.9877 pu to 0.9955 pu by choosing a finite droop of 4 % and the steady-state frequency is improved from 0.9968 pu to 0.9979 pu. Previously, it has been mentioned that the curve of the frequency obtained with VSCs was acceptable and since the one obtained with a droop of 4 % is even better, choosing to replace synchronous machines with grid-forming converters having this frequency droop is acceptable as well. This is justified by the fact that the frequency does not deviate from the nominal value by more than 5 %.

FIGURE 4.10 represents the evolution of the frequency estimated by VSC6 within 300 and 60 seconds, after the loss of $g1$ and with the replacement of synchronous machines in the central part of the network with grid-forming converters only. Those can have either an infinite or a 4 % frequency droop. If the droop of the VSC is set to 4 % instead of being infinite, it is listed in the legend of both graphs. TABLE C.5 in APPENDIX C presents the numerical results of this simulation.



(a) Within 300 seconds.      (b) Within 60 seconds.
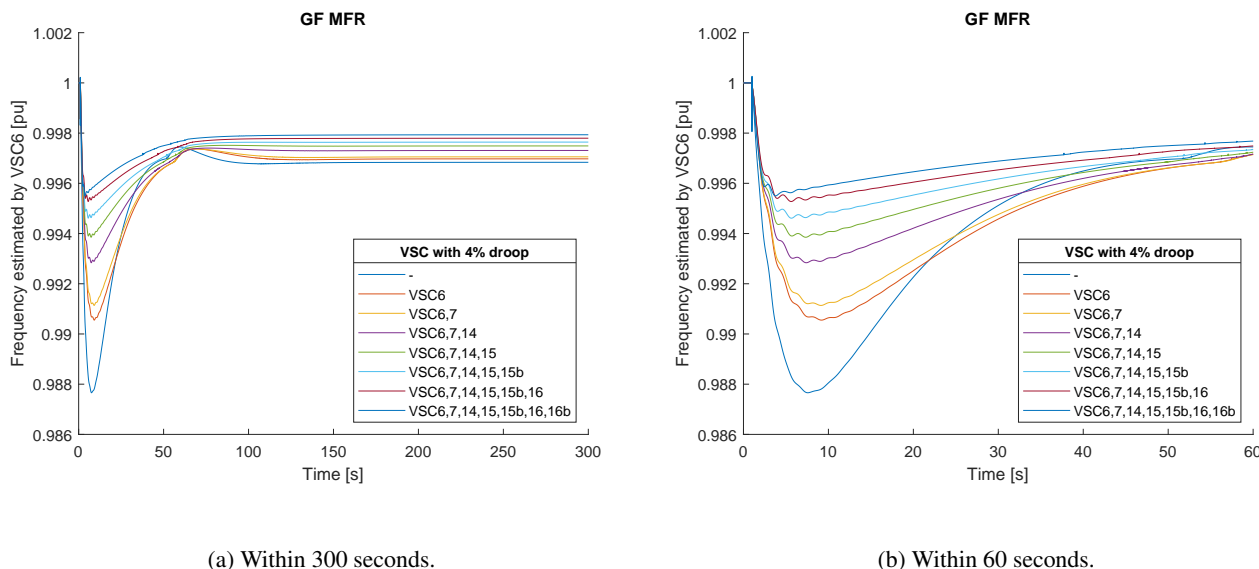
Figure 4.10: Frequency estimated by VSC6 after the loss of $g1$, with the replacement of SMs in the central part with grid-forming converters, for different droops.

The objective of showing such graphs is to illustrate the evolution of the system frequency estimated by the PLL of VSC6 in this case when more and more grid-forming converters have a finite droop of 4 %. As it can be seen in the figure, the more VSCs participating in the frequency response, the higher the nadir reached by the estimated frequency. As already mentioned, the frequency nadir goes from 0.9877 pu to 0.9955 pu when none to all grid-forming converters have a 4 % droop. Moreover, the inertial response of the system is improved as well since the RoCoF is lower, i.e. the slope at which the frequency decreases at the moment $g1$ is lost is less steep. The improvement is also visible in the steady-state frequency since the latter is greater when more VSCs have a 4 % droop, going from 0.9968 pu to 0.9979 pu. All these conclusions seem to be logical since the more VSCs participating in the frequency regulation, the more active power is generated after the power imbalance, which is reflected in the frequency evolution. Finally, by using more VSC with a 4 % droop instead of an infinite, the time at which the frequency drop is stopped is shorter as well as the time needed to recover the frequency.

FIGURE 4.11 represents the current flowing in each grid-forming converter replacing a synchronous machine initially placed in the central part of the network, after the loss of $g1$ and for different frequency droops. TABLE C.4 in APPENDIX C presents the numerical results of this simulation.
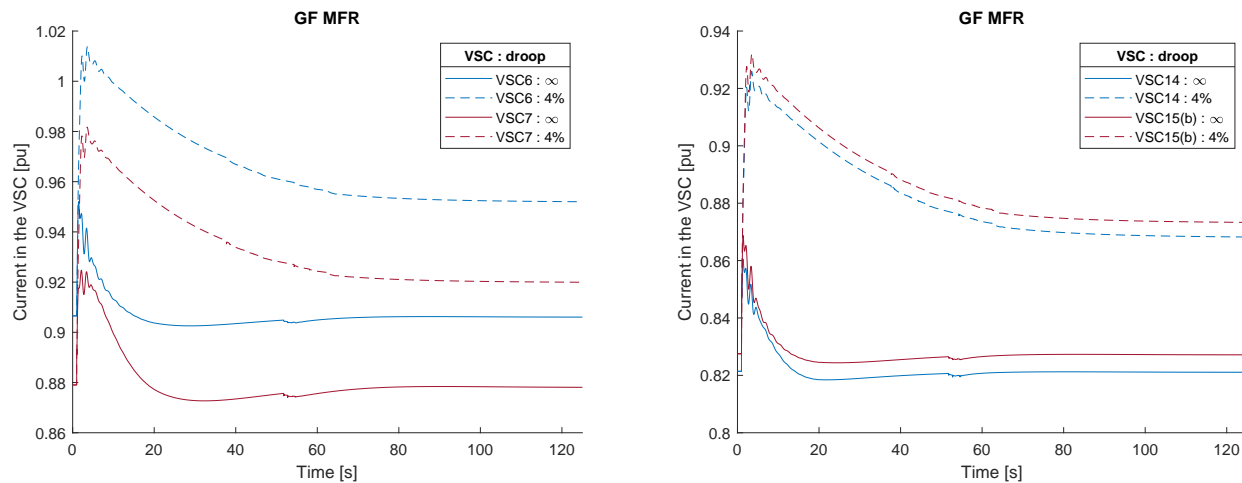


(a) VSC6 - VSC7.



(b) VSC14 - VSC15(b).
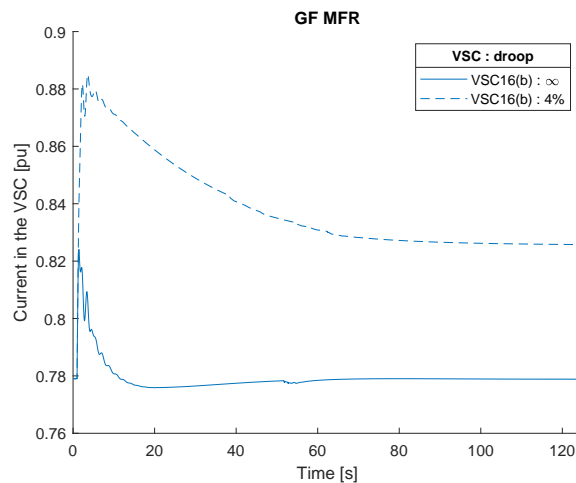


(c) VSC16(b).

Figure 4.11: Current in each VSC after the loss of $g1$, with the replacement of SMs in the central part with grid-forming converters, for different droops.

By modifying the frequency droop of the grid-forming VSCs from an infinite to a finite one, the current peak is higher as its steady-state value. It increases by 0.0617 pu on average for each VSC. This is logical since VSCs with a 4 % droop make the RES connected to it participate in the frequency regulation and thus increase its production of active power, whose increase is directly proportional to the produced current. Nevertheless, the current never

reaches a value higher than the limit set to 1.1 pu for the safe operation of the converters. Indeed, the maximum value reached by these currents range from 0.8851 to 1.0138 pu, allowing to use the configuration where grid-forming converters are used with a 4 % droop.

Finally, FIGURE 4.12 represents the evolution of the power produced by VSC6 after the loss of $g1$. Three configurations are considered : the one with grid-following converters and the ones with grid-forming converters having all an infinite or a 4 % frequency droop. The curves of the active power produced by VSC7, VSC14, VSC15(b) and VSC16(b) are not shown since they are quite similar to the one of VSC6, arbitrarily chosen. TABLE C.6 in APPENDIX C presents the numerical results of this simulation, for all VSCs.
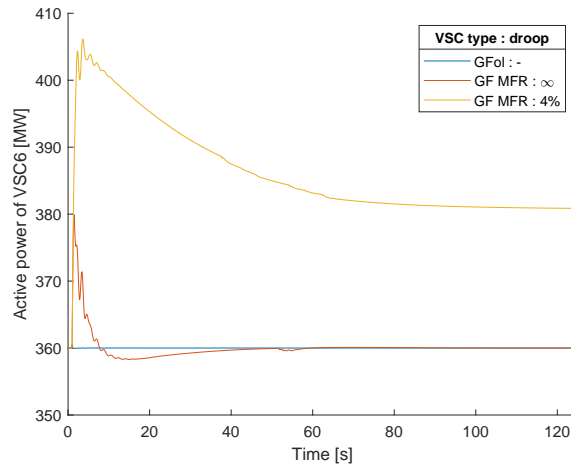


Figure 4.12: Produced active power of VSC6 after the loss of $g1$, with the replacement of SMs in the central part with VSCs, for different droops.

When replacing synchronous machines with grid-following converters, the produced power is kept almost constant during the whole time span following the contingency since this kind of converters has been implemented such that it does not participate in the frequency control. It is characterized by a fast dynamics and no inertia, causing a very small peak of produced active power. This peak is so small that it is not visible in the figures. Depending on the VSC that is considered, it is between 0.03 and 0.13 % higher than the active power initially produced by the VSC. However, this is not the case with grid-forming converters. When these have an infinite droop, the loss of $g1$ influences their transient behaviour during which they produce a peak of active power. This peak is due to the fact that grid-forming converters are characterized by an finite virtual inertia of 4.5 seconds, slowing the dynamics of the converter down and bringing to some active power oscillations before reaching a steady state. The increase is 5.27 % higher than the initial amount of active power on average. Then, the active power decreases to go back to its initial production. With a finite droop of 4 %, the peak of produced active power is way greater since it increases by 12.93 % on average compared to the active power that is initially generated. Moreover, the steady-state value is also greater than the initial production, which is due to the fact that the power initially generated by $g1$ and lost after 1 second needs to be compensated. Grid-forming converters thus participate well in the frequency response since their produced active power reaches a certain peak in the transient period and a steady-state value higher than the initial produced power.

### 4.3.1.1  Conclusions of the simulations

The dynamic simulations focusing on the loss of $g1$ led to several observations. First, it is noticeable that the frequency drop is deeper and the RoCoF is higher with VSCs compared to synchronous machines because of the lack of inertia. However, the frequency recovery is improved with VSCs, characterized by faster dynamics compared to synchronous machines. For both events, the frequency does not deviate from the nominal value by more than 5 %, making each configuration acceptable. The frequency estimated by the PLL is always similar to the system frequency except the first peak and drop due to incorrect numerical computation. When the RES is connected through a grid-forming converter, it participates in the frequency control with a frequency droop of 4 %. In this case, the general evolution of the frequency, including the RoCoF, the frequency drop and steady-state value, is improved since more power plants participate in the frequency regulation. The current in each VSC is always lower than 1.1 pu, confirming the validity of the studied configurations. It is the case even if it increases with VSCs having a finite frequency droop of 4 %. The shape of the current is a bit different between grid-following and grid-forming converters. Finally, the active power of the grid-following converters is quite constant with time after the loss of $g1$ since these converters are characterised by fast dynamics and no virtual inertia. With grid-forming converters, their slower dynamics and virtual inertia brings a peak in the produced active power, event when the droop is infinite. This peak and the steady-state active power both increase if the droop is set to 4 % since the RES participates in the frequency regulation.

### 4.3.2 Voltage control

The second part of this section focuses on the voltage control of the modified network, where grid-following or grid-forming converters are implanted in its central part. For that purpose, the event that is considered is the tripping of the line connecting bus 4032 to bus 4044, which links the north part to the central part, after 1 second. This is a crucial event in the initial configuration of the network in *operating point A* since it does not withstand this contingency, which is especially why it does not satisfy the $n-1$ criterion [33]. In these simulations, an infinite frequency droop has been considered for all grid-forming converters, since these simulations focus on voltage control only. This parameter is thus not specified in the title or in the legend of the presented figures anymore.

FIGURE 4.13 illustrates the bus voltages after the tripping of line 4032-4044 with the replacement of synchronous machines in the central part with either only grid-following or grid-forming converters. TABLE C.7 in APPENDIX C presents the numerical results of this simulation.
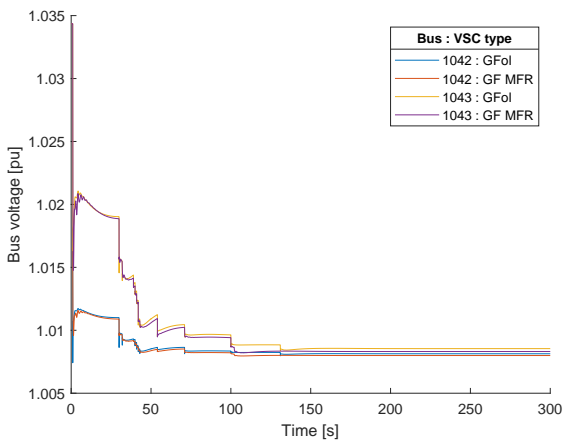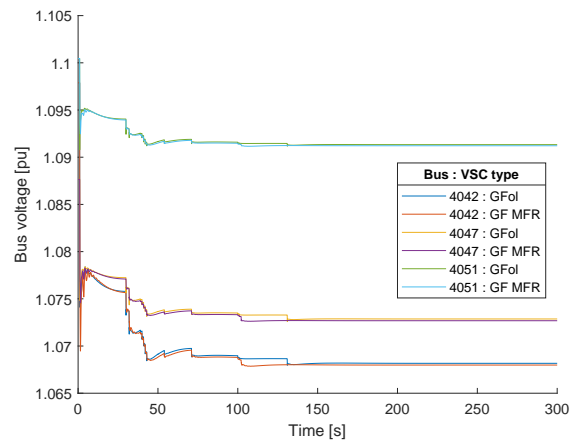


(a) Bus 1042 - 1043.
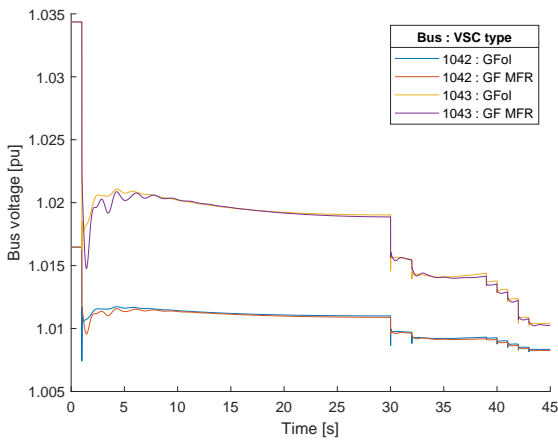
(b) Bus 4042 - 4047 - 4051.

(c) Bus 1042 - 1043 (zoom).
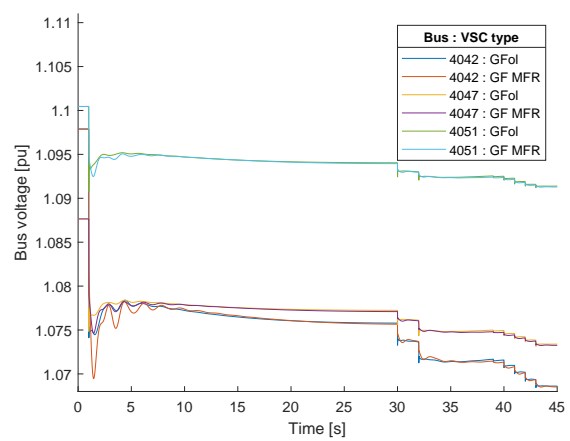
(d) Bus 4042 - 4047 - 4051 (zoom).

Figure 4.13: Bus voltages in the central part after the tripping of line 4032-4044, with the replacement of SMs in the central part with VSCs.

These figures illustrate a similar behaviour voltage evolution at any bus, for both types of converters, except for the insignificant oscillations occurring with grid-forming VSCs. Thus, in order to analyse in more details the evolution of the voltage at bus located in the central part, the behaviour of the voltage at two bus is studied. Bus 1042 is chosen because it is located at the centre of the central part of the Nordic network. It is analysed with bus 4042 as well since it is characterized by the most significant decrease in voltage after the tripping of the line.

First, the evolution of the voltage at bus 1042 is illustrated in FIGURE 4.14 when line 4032-4044 is tripped after 1 second, with the replacement of more and more synchronous machines with either grid-following or grid-forming VSCs. TABLE C.8 in APPENDIX C presents the numerical results of this simulation.
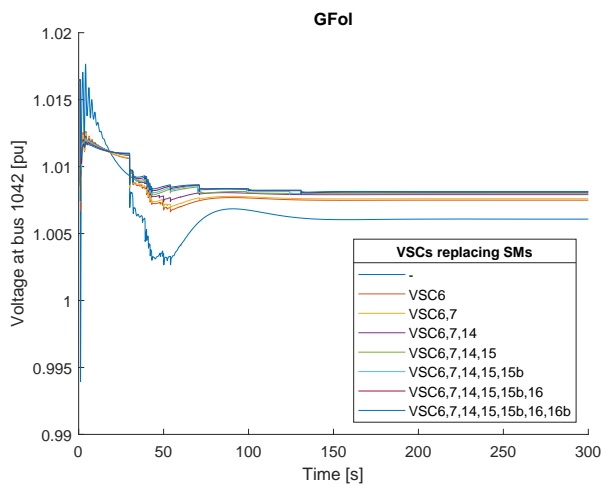


(a) Grid-following VSCs.
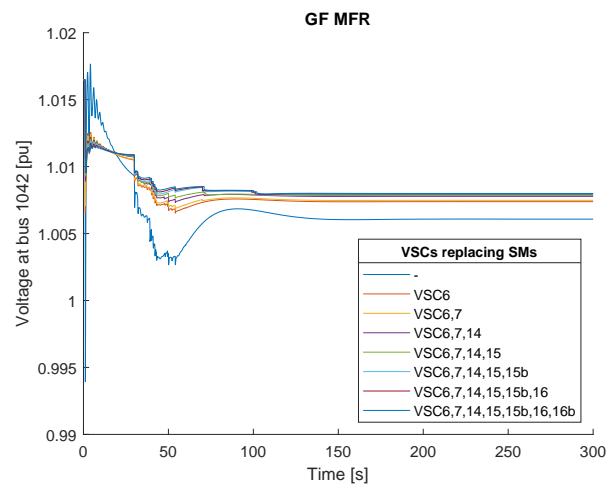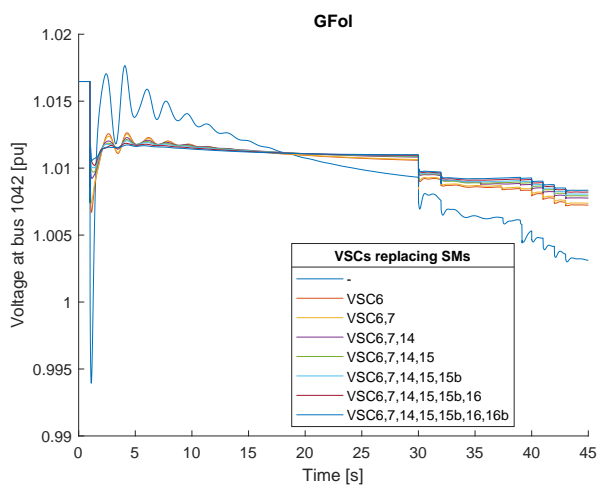
(b) Grid-forming VSCs.

(c) Grid-following VSCs (zoom).
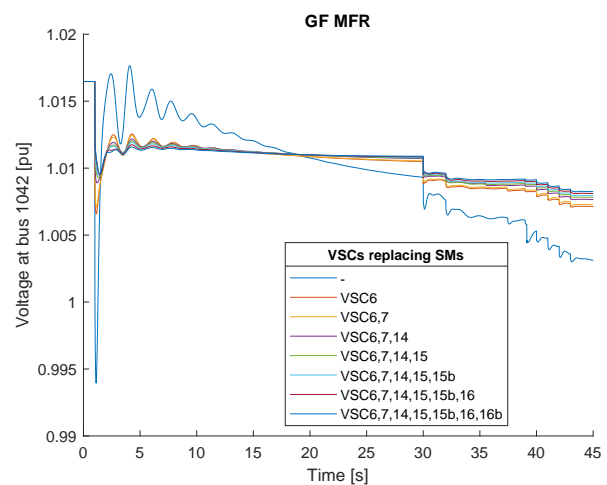
(d) Grid-forming VSCs (zoom).

Figure 4.14: Voltage at bus 1042 after the tripping of line 4032-4044, with the replacement of SMs in the central part with VSCs.

Then, similar figures are represented in FIGURE 4.15 for the voltage at bus 4042. TABLE C.9 in APPENDIX C presents the numerical results of this simulation.
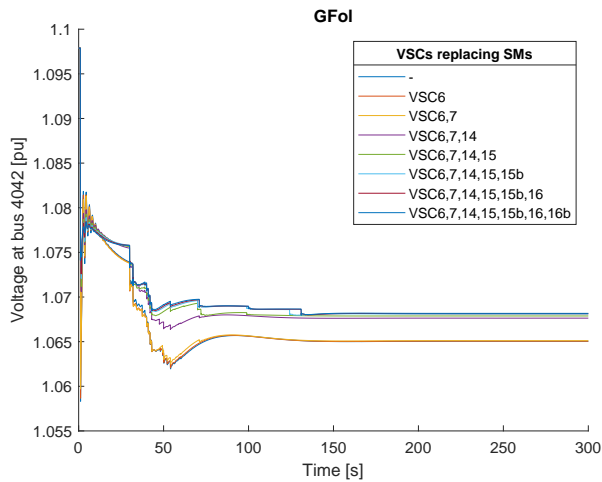


(a) Grid-following VSCs.
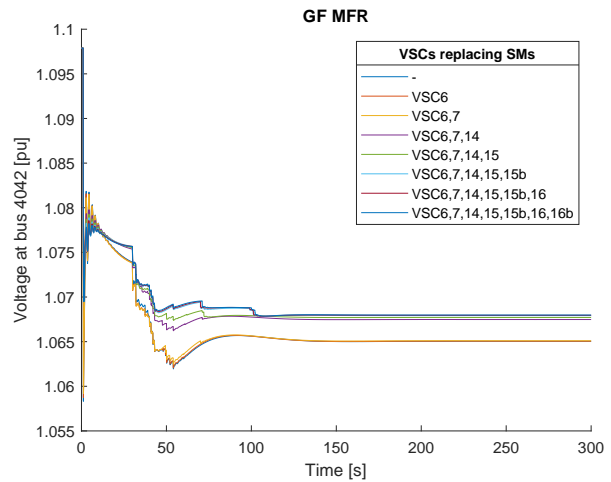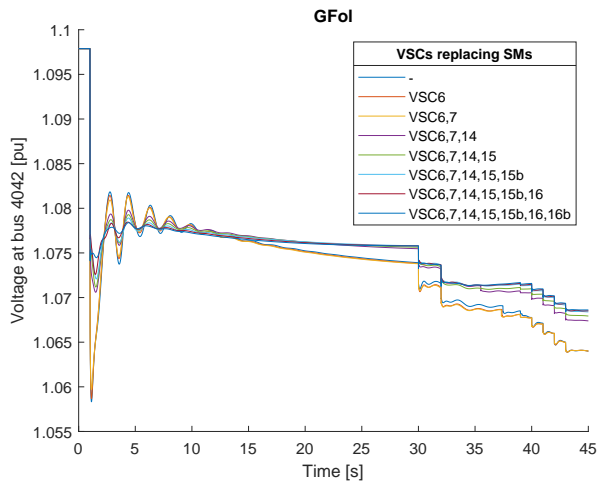
(b) Grid-forming VSCs.

(c) Grid-following VSCs (zoom).
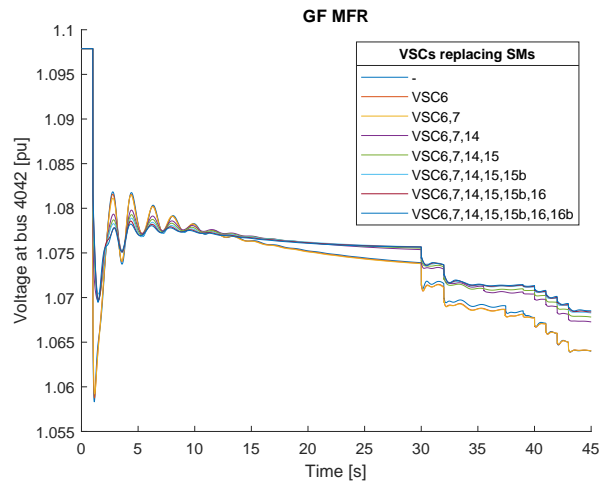
(d) Grid-forming VSCs (zoom).

Figure 4.15: Voltage at bus 4042 after the tripping of line 4032-4044, with the replacement of SMs in the central part with VSCs.

Regarding the evolution of the voltage at bus 1042, it can be noticed that this evolution is improved with the presence of VSCs, whatever their type, compared to the configuration where synchronous machines are the generators in the central part of the network. Indeed, the voltage drop just after the occurrence of the fault is less deep with VSCs and even more with a higher number of VSCs that replace the removed synchronous machines. With these machines, the maximum transient deviation from the initial voltage reaches 2.22 % while with only one VSC, it is equal to 0.97 % for the grid-forming and 0.96 % for the grid-following case. Also, voltage oscillations occurring with the initial configuration of the Nordic network are damped with the VSCs, again whatever their type. The higher number of VSCs are implanted in the network the lower the amplitude of theses oscillations since synchronous machines that bring these oscillations are removed from the central part of the network. Indeed, the rotor swings of the synchronous machines affect the voltage characteristics while the parameters of the VSCs are tuned such that no oscillation takes place after a contingency. Finally, even if the time to reach a steady-state voltage is approximately the same for any configuration, occurring after 130 seconds approximately, the steady-state voltage reached at bus 1042 is improved with the number of VSCs implanted in the network since it gets closer the initial value of 1.0165 pu. Indeed, even if this improvement is not significant it reaches 1.0061 pu with the initial configuration while it reaches 1.0081 pu an 1.0080 pu when all synchronous machines of the central part are replaced with grid-following and grid-forming converters, respectively.

On the other hand, the conclusions drawn for bus 1042 differ a bit from the ones related to bus 4042. First, it can be noticed that there is no significant change between the results obtained with the initial configuration of the central part, when $g6$ or $g6$ and $g7$ are replaced with VSCs, whatever their type. The voltage drop after the occurrence of the fault, the oscillations and the steady-state values are all similar for each of these configurations. Some improvements can be noticed when adding at least one VSC replacing $g14$, in addition to VSC6 and VSC7. The reason behind this is the following : the voltage that is represented is the one to which machine $g14$ is initially connected to. Thus, if no change occurs at this specific bus, its voltage characteristic is not affected by the changes occurring at the other bus located in the central part, because of the high electrical distance separating each other. In the specific case where $g14$ is replaced with VSC14, the voltage drop is improved by reaching a transient minimum value of 1.0697 pu and 1.0706 pu when the VSCs are implemented in grid-forming and grid-following modes, respectively, compared to 1.0583 pu when the central part is composed of synchronous machines only. Moreover, with the presence of at least VSC14, the oscillations following the voltage drop are more damped and the steady-state value is improved with the number of VSC implanted into the network. In conclusion, the configuration using the highest number of VSCs is the best configuration in terms of voltage control of the network after the tripping of line 4032-4044.

Finally, no significant difference can be highlighted regarding the type of VSC that is chosen instead of the removed synchronous machine, for both bus 1042 and 4042. For this particular event, there is thus no specific preference in choosing either grid-following or grid-forming converters.

The current flowing in each type of VSCs when these replace all synchronous machines in the central part of the network is shown in FIGURES 4.16 and 4.17. TABLE C.10 in APPENDIX C presents the numerical results of this simulation.
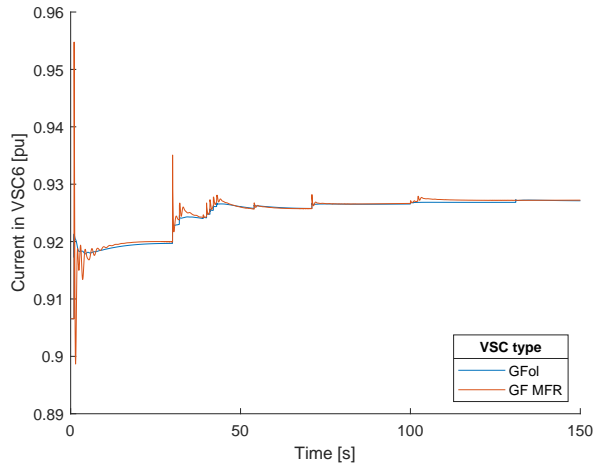


(a) VSC6.
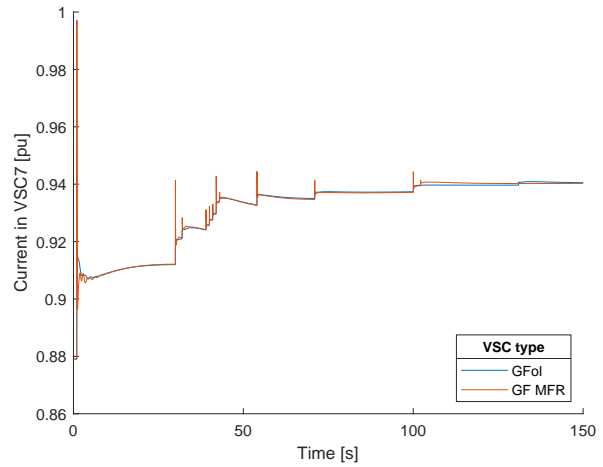


(b) VSC7.
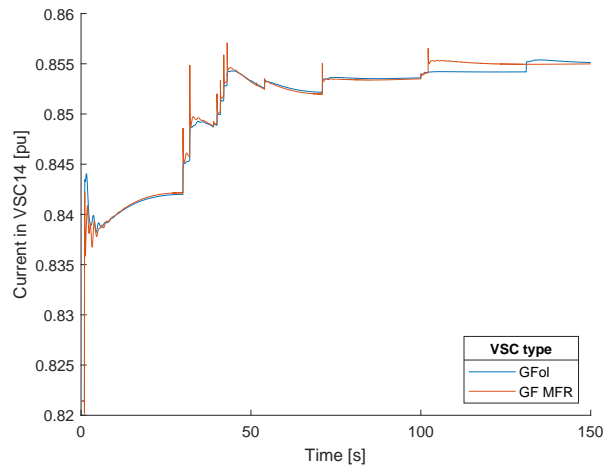


(c) VSC14.

Figure 4.16: Current in each VSC (VSC6, VSC7, VSC14) after the tripping of line 4032-4044, with the replacement of SMs in the central part with VSCs.

(a) VSC15(b).　　　　　　　　　　　　　　　　　　　(b) VSC16(b).
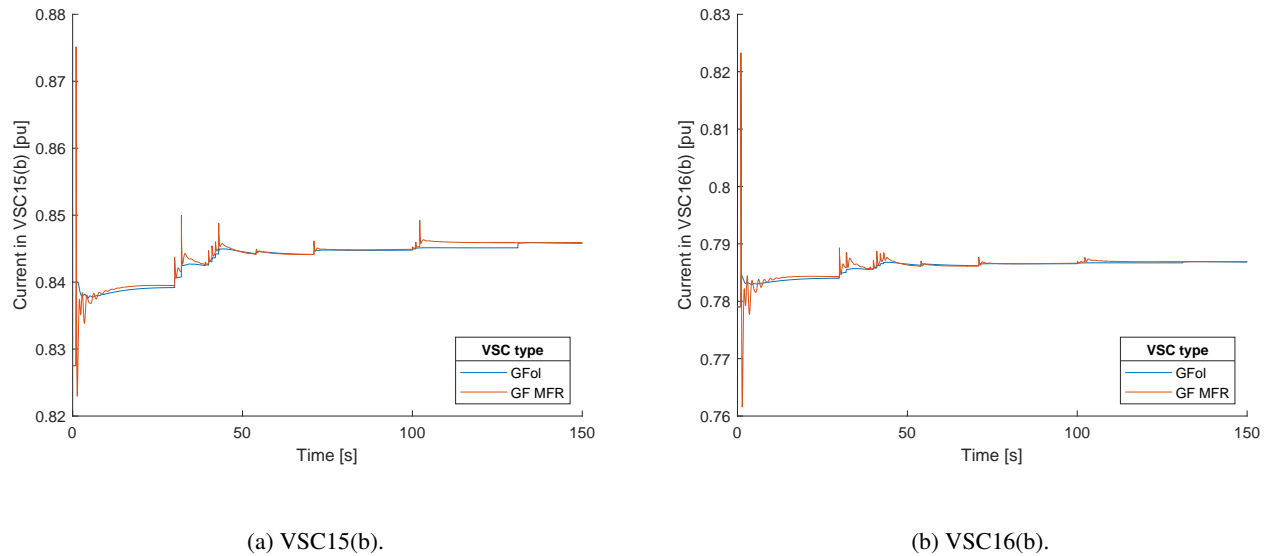
Figure 4.17: Current in each VSC (VSC15, VSC16) after the tripping of line 4032-4044, with the replacement of SMs in the central part with VSCs.

In general, more oscillations and higher amplitudes occur in the case of grid-forming converters compared to grid-following ones, as in the case where $g1$ is lost. Also, no current limiter is activated in this case for any type of VSCs since no curve exceeds the value of 1 pu. For the grid-forming converters, the maximum current reaches 0.9972 pu and 0.9409 pu for the grid-following VSCs, reached in both cases by VSC7.

### 4.3.2.1   Conclusions of the simulations

The tripping of line 4032-4044 illustrates several effects on the voltage control in the central part. The main effect that is quite noticeable is the stability of the VSCs. Indeed, both types of converters show similar results where the voltage is better supported with VSCs replacing synchronous machines initially producing power in the central part of the network. The voltage drop is less deep, the support is permanently improved helping the voltage stabilise to steady-state voltages closer to their initial values, and the oscillations coming from the rotor swings of the synchronous machine disappear as soon as more VSCs are placed in the network. Finally, the changes in the evolution of the voltages are more pronounced when the VSCs that replace the synchronous machines are close to the bus voltage that his been illustrated. Regarding the current, as it is always lower than the limit of 1.1 pu guaranteeing the safe operation of the converters, it allows use of configurations where synchronous machines in the central part are all replaced with either grid-following or grid-forming converters.

### 4.3.3   Mix of various technologies

This third section is dedicated to the comparison between different configurations of the central part of the Nordic network. The objective is thus to find the best configuration using grid-following converters, grid-forming converters and/or synchronous condensers but more importantly to determine why it is the best by explaining the effect of each technology added to the modified network. In order to analyse each mix that can be made in the central part of the network, the critical event that is considered is a short-circuit occurring after 1 second at bus 4032 cleared 100 milliseconds later by the tripping of line 4032-4044. As for the study of the voltage control, the grid-forming converters that are used in the following simulations implement an infinite droop, which is why it is never mentioned in the figures.

The first result that is shown is the instability of the configuration with only grid-following converters in the central part of the Nordic network. FIGURES 4.18 and 4.19 show the evolution of each bus voltage located in the central part, to which synchronous machines replaced with grid-following converters are connected to in the initial configuration, after a short-circuit at bus 4032 followed by the tripping of line 4032-4044. TABLE C.11 in APPENDIX C presents the numerical results of this simulation.
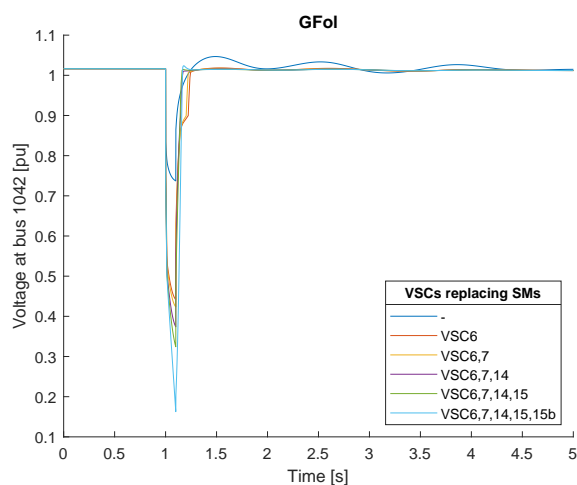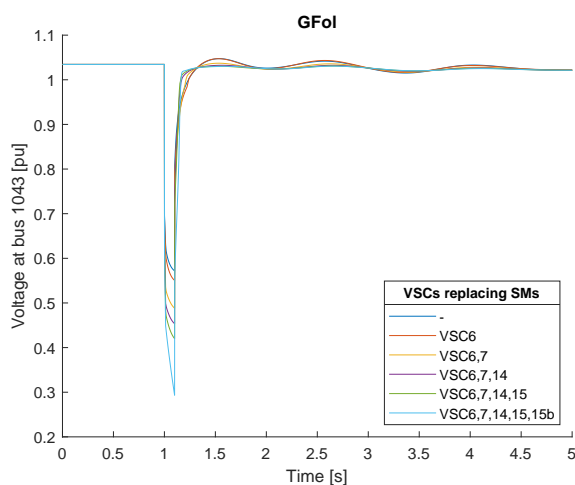


(a) Bus 1042.                                                     (b) Bus 1043.

Figure 4.18: Voltage at bus 1042 and 1043 after a short-circuit at bus 4032 and the tripping of line 4032-4044, with the replacement of SMs in the central part with grid-following converters.

(a) Bus 4042.



(b) Bus 4047.



(c) Bus 4051.

Figure 4.19: Voltage at bus 4042, 4047 and 4051 after a short-circuit at bus 4032 and the tripping of line 4032-4044, with the replacement of SMs in the central part with grid-following converters.

First of all, it can be directly noticed that the behaviour of each bus is similar. In each case, there is a huge voltage drop after 1 second due to the short-circuit occurring at bus 4032 cleared by the tripping of line 4032-4044. For each bus, the voltage drops even more when more grid-following converters are connected to the network, reaching values until 0.1627, 0.2933, 0.2246, 0.1856 and 0.6640 pu bus 1042, 1043, 4042, 4047 and 4051 respectively when VSCs replace synchronous machines $g6$, $g7$, $g14$, $g15$ and $g15b$. When an additional grid-following converter replaces synchronous machine $g16$ or $g16b$, the software is not able to simulate the behaviour of the network anymore since too low voltages are reached. This illustrates well the consequences of a low inertia network where the RES connected to the grid through grid-following converters do not have a sufficient short-circuit power to

withstand this kind of faults. It is thus necessary to find another configuration than this one implying only grid-following converters, since this configuration of the network is unsecure.

The current flowing in each grid-following VSC after the fault is shown in FIGURE 4.20. The legend presents the grid-following VSCs that replace the synchronous machines in the central part of the network. TABLE C.12 in APPENDIX C presents the numerical results of this simulation.



(a) VSC6.

(b) VSC7.

(c) VSC14.

(d) VSC15(b).
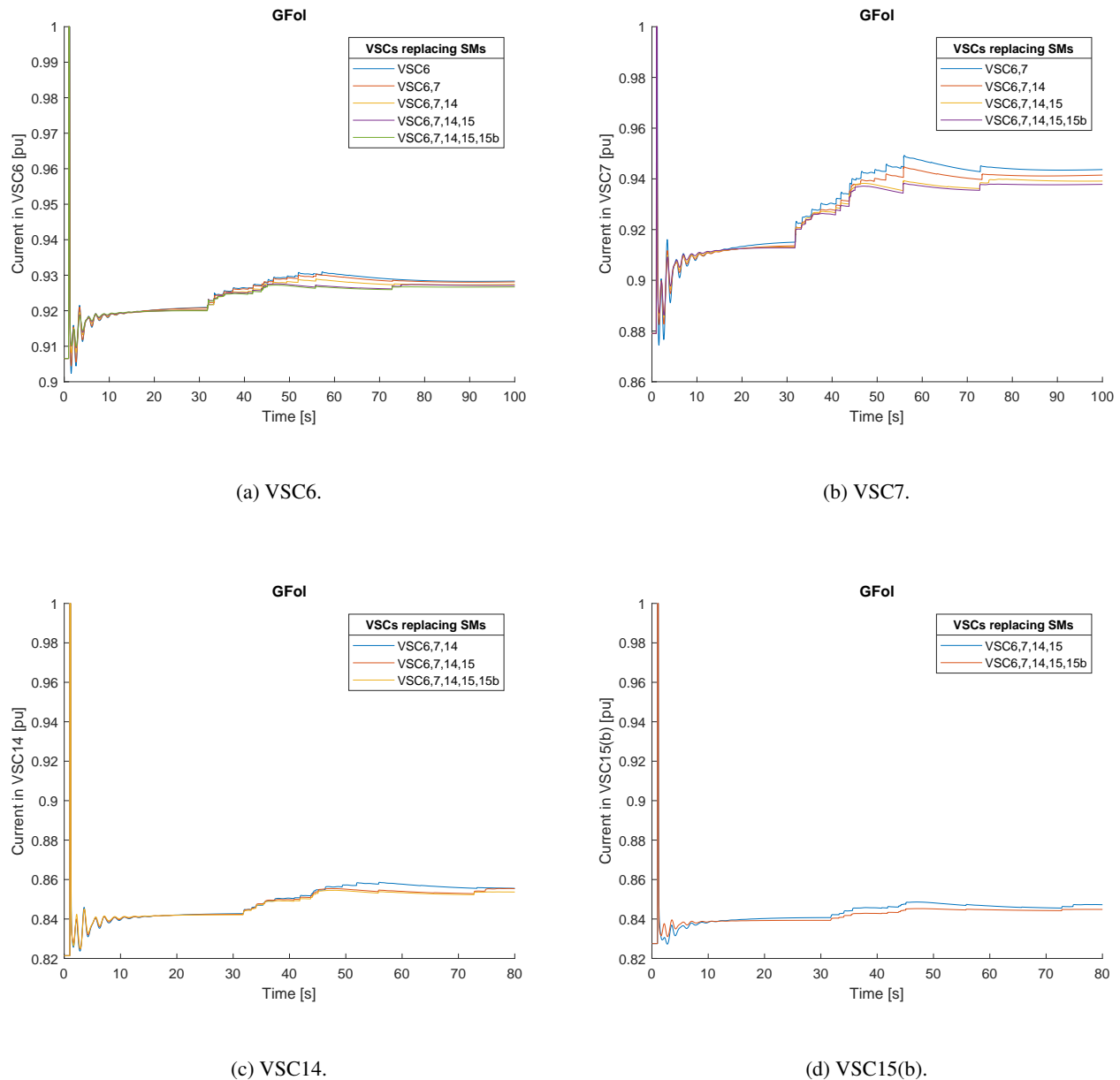
Figure 4.20: Current in each grid-following VSC after a short-circuit at bus 4032 and the tripping of line 4032-4044, with the replacement of SMs in the central part with grid-following converters.

The main comment that can be made is that the current limiter makes the current remain lower than or equal to 1 pu in all configurations. This limits the capability of the grid-following converters to withstand the short-circuit

and is the reason why this configuration does not give rise to acceptable results. The converter is not able to produce a high enough current during the transient period bringing to an unstable situation after the short-circuit.

This configuration implying only grid-following converters thus needs to be modified to obtain better results. For that purpose, synchronous condensers can be used since these machines provide as much short-circuit power as synchronous machines and help in the voltage stability by the means of the amount of reactive power that they produce. FIGURES 4.21 and 4.22 presents the voltage at bus 1042, 1043, 4042, 4047 and 4051 with the configuration implying only grid-following in the central part in addition to more and more synchronous condensers placed in this part of the network. TABLE C.13 in APPENDIX C presents the numerical results of this simulation. All synchronous condensers are rated at 300 MVA, as it is the case for $g13$, and are connected to bus where removed synchronous machines had their step-up transformer connected to. If one synchronous condenser is connected to the same bus to which a removed synchronous machine $gx$ is initially connected to, this synchronous condenser is named SC$x$.
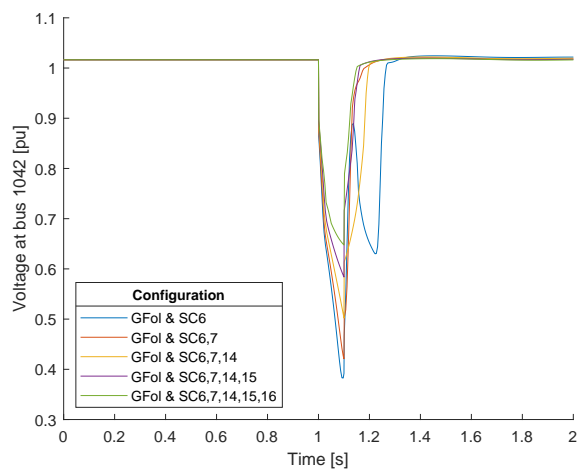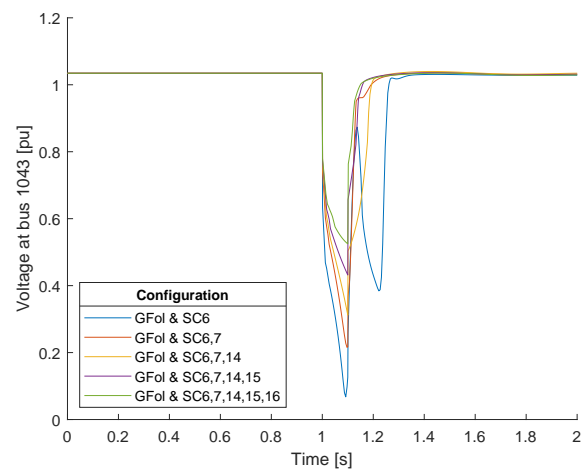


(a) Bus 1042.                                                                 (b) Bus 1043.

Figure 4.21: Voltage at bus 1042 and 1043 after a short-circuit at bus 4032 and the tripping of line 4032-4044, with the replacement of SMs in the central part with grid-following converters and synchronous condensers.
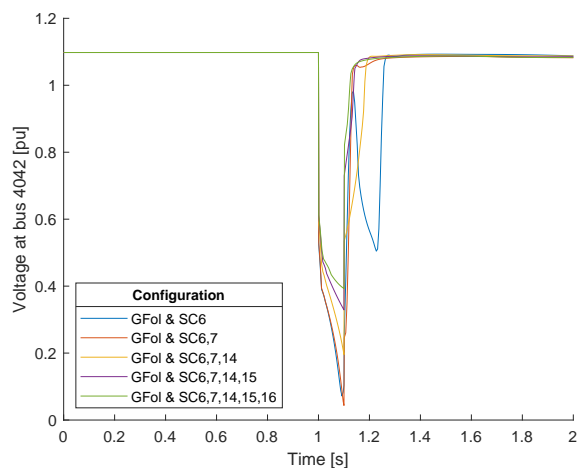
(a) Bus 4042.
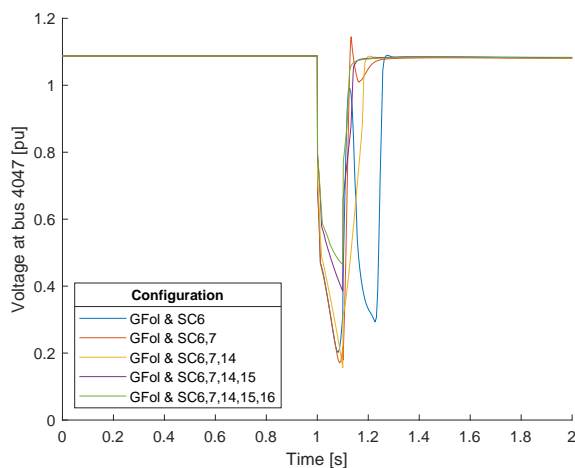


(b) Bus 4047.
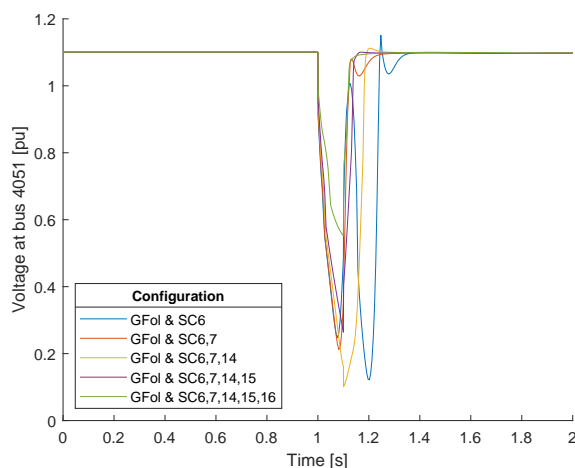


(c) Bus 4051.

Figure 4.22: Voltage at bus 4042, 4047 and 4051 after a short-circuit at bus 4032 and the tripping of line 4032-4044, with the replacement of SMs in the central part with grid-following converters and synchronous condensers.

The presented figures illustrate the effect of adding more and more synchronous condensers in the central part of the network. The voltage drop at each bus after the occurrence of the fault is less deep when adding more and more synchronous condensers by the means of their short-circuit power and voltage control capabilities. This effect is even more pronounced if the added synchronous condenser is connected to the bus whose voltage evolution is illustrated. For instance, when looking at FIGURE 4.22a, it can be noticed that the voltage drop reaches 0.0718 pu with SC6 and 0.0435 pu with SC6 and SC7, while it increases to 0.1957 pu with SC6, SC7 and SC14, the latter being connected to bus 4042. Also, it can be noticed that a second voltage drop arises at each bus voltage when only SC6 added to the network in addition to the grid-following VSCs. This effect is not admissible in power

networks since the fault should be cleared after the tripping of line 4032-4044. Adding at least one synchronous condenser SC7 allows to get rid of this second voltage drop and makes the configuration acceptable. Finally, the steady-state value increases a little bit with the number of synchronous condensers added to the network but all values are between 0.9 and 1.1 pu, which is acceptable.

FIGURE 4.23 shows the current flowing in the grid-following converter VSC7 when the central part is composed only of those in terms of active power generation and with more and more synchronous condensers. Only the current in this VSC is shown since all VSCs are characterized by a similar current evolution. TABLE C.14 in APPENDIX C presents the numerical results of this simulation, for all VSCs.



(a) Within 100 seconds

(b) Within 2 seconds.

Figure 4.23: Current in grid-following VSC7 after a short-circuit at bus 4032 and the tripping of line 4032-4044, with the replacement of SMs in the central part with grid-following converters and synchronous condensers.

This figure illustrates also the effect of adding synchronous condensers to the network. The current flowing in each converter is limited to 1 pu by its current limiter but this peak lasts during a less amount of time when more synchronous condensers are placed in the central part of the network. Also, in the long term, the current is always reduced when more synchronous condensers are placed in the network, especially if the synchronous condenser is connected to the same bus as the one to which the VSC is connected. Indeed, synchronous condensers, as synchronous machines, have the capability to withstand very high transient currents and provide short-circuit power to the network after a fault.

FIGURES 4.24 and 4.25b show the reactive power produced by each synchronous condenser in the configurations where grid-following VSCs in addition to more and more synchronous condensers are replacing synchronous machines in the central part of the network. TABLE C.15 in APPENDIX C presents the numerical results of this simulation.



(a) SC6.

(b) SC7.
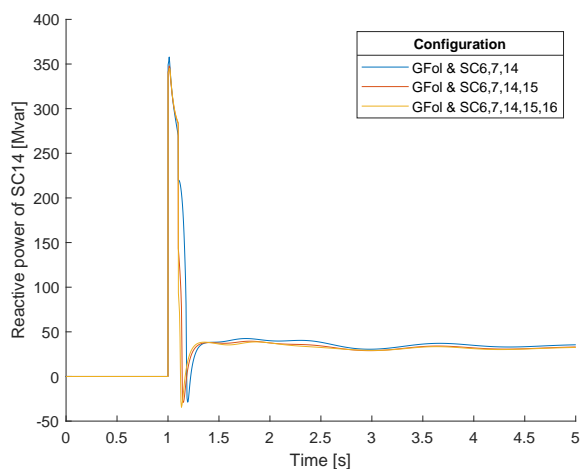


(c) SC14.

Figure 4.24: Produced reactive power by synchronous condensers (SC6, SC7, SC14) after a short-circuit at bus 4032 and the tripping of line 4032-4044, with the replacement of SMs in the central part with grid-following VSCs and synchronous condensers.

(a) SC15.                                          (b) SC16.
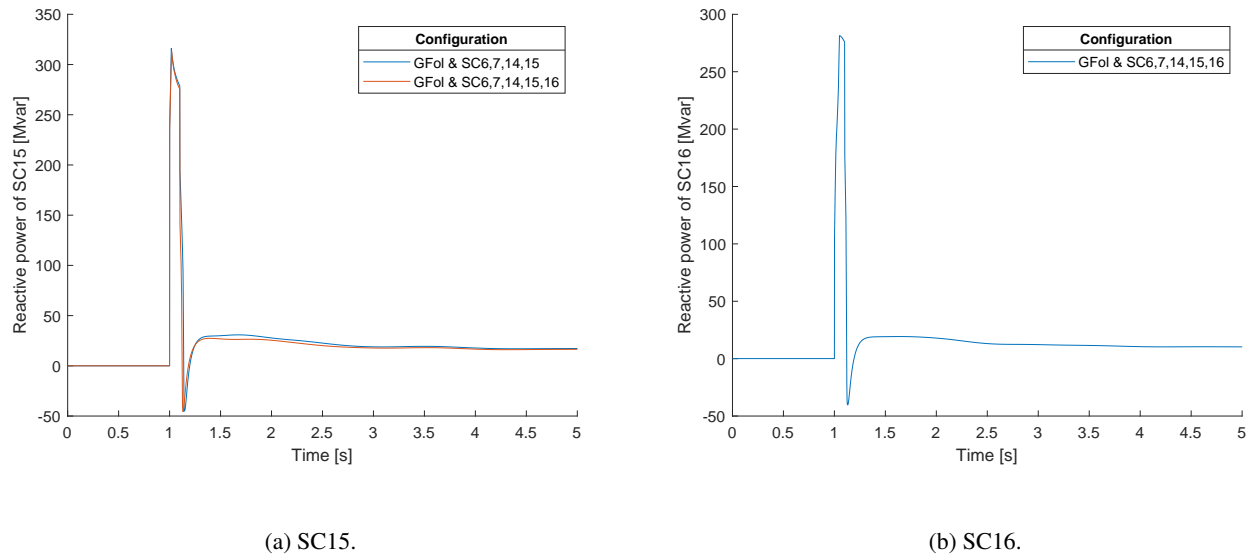
Figure 4.25: Produced reactive power by synchronous condensers (SC15, SC16) after a short-circuit at bus 4032 and the tripping of line 4032-4044, with the replacement of SMs in the central part with grid-following VSCs and synchronous condensers.

There are several conclusions that can be drawn from the presented figures. First, it can be noticed that for a single synchronous condenser, i.e. by looking at only one figure at a time, the amount of reactive power produced by each synchronous condenser is reduced with the number of synchronous condensers that increases. This totally makes sense since there are more synchronous condensers to produce reactive power to stabilize the voltage. Also, the total amount of produced reactive power increases with the number of synchronous condensers which directly causes more stable voltages in the central part of the network, which has been already concluded from FIGURES 4.21 and 4.22. Finally, in each configuration, the peak of produced reactive power of each synchronous condenser ranges from 218.39 Mvar by SC6 to 357.83 Mvar by SC14, which can be concluded that each synchronous condenser plays a role in the voltage support after the occurrence of the short-circuit.

Since the configuration with only grid-following VSCs replacing synchronous machines in the central part does not make the Nordic network secure, different configurations are compared such that the effect and the need of each technology can be highlighted. These are the following :

- The initial configuration, where the central part of the network is composed of synchronous machines only as power generators ;

- Only grid-forming converters replacing synchronous machines in the central part ;

- Grid-following converters replacing synchronous machines $g7$, $g15b$, $g16$ and $g16b$ with grid-forming converters replacing synchronous machines $g6$, $g14$ and $g15$[1] ;

- Grid-following converters with synchronous condensers, all rated at 300 MVA, replacing synchronous machines in the central part ;

- Grid-forming converters with synchronous condensers, all rated at 300 MVA, replacing synchronous machines in the central part.

FIGURES 4.26 and 4.26 illustrate the evolution of the voltage at bus 1042, 1043, 4042, 4047 and 4051 in all aforementioned configurations. TABLE C.16 in APPENDIX C presents the numerical results of this simulation.
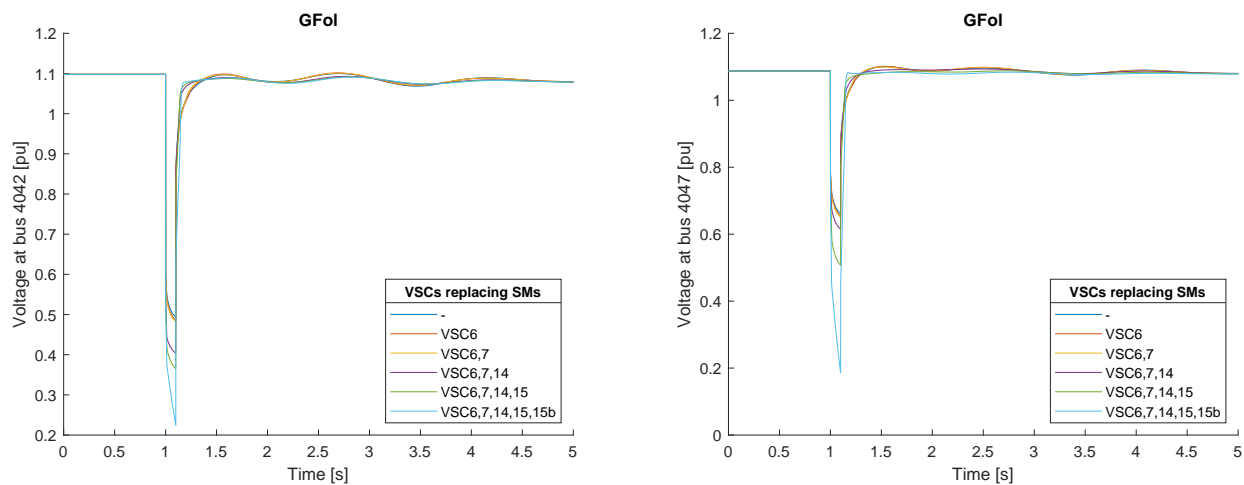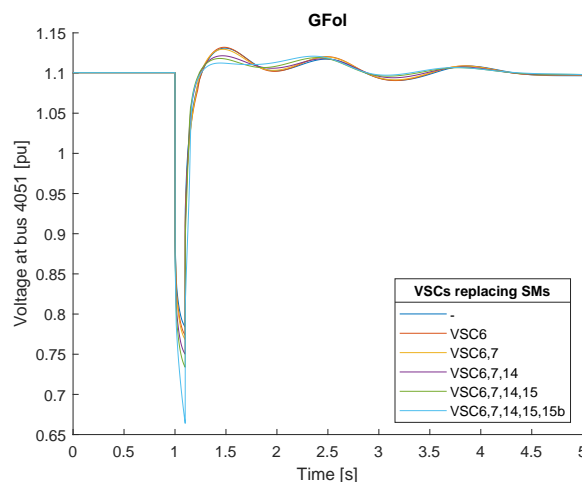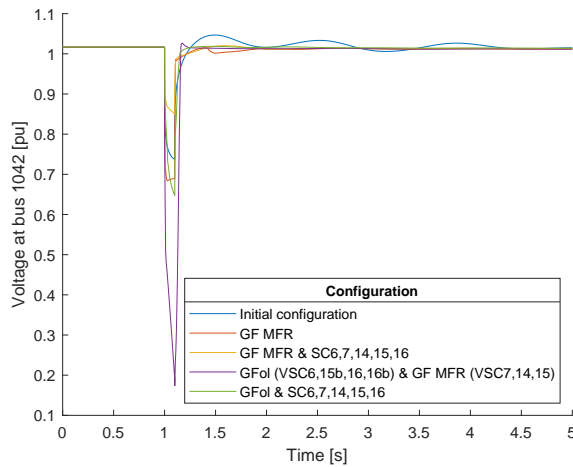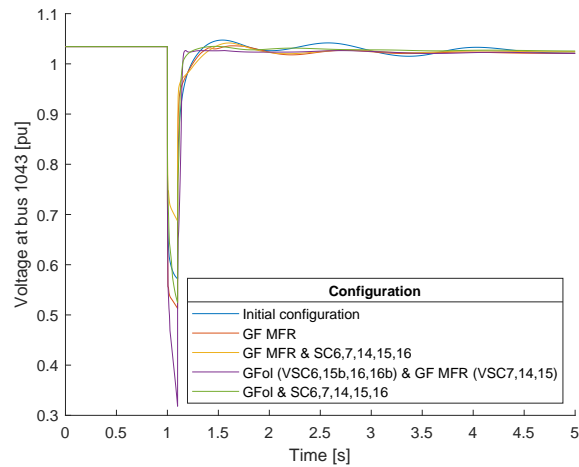


(a) Bus 1042.

(b) Bus 1043.

Figure 4.26: Voltage at bus 1042 and 1043 after a short-circuit at bus 4032 and the tripping of line 4032-4044, with the replacement of SMs in the central part with various technologies.

---

[1]The synchronous machines replaced with the grid-forming VSCs are the ones whose bus voltage reaches the deepest value during the transient period (see FIGURE 4.3b) Moreover, placing grid-forming converters as equally as possible across the whole system is motivated in SECTION 3.3.3.
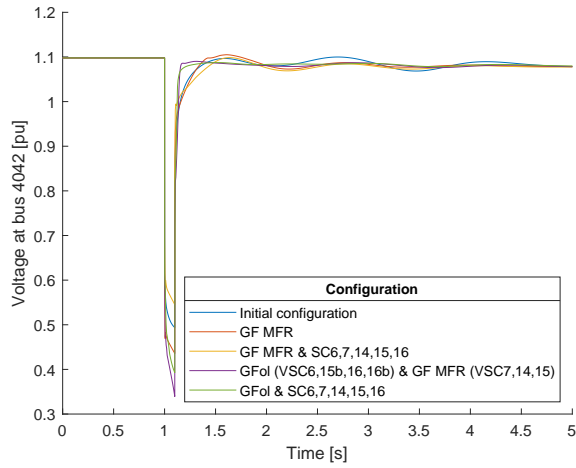
(a) Bus 4042.
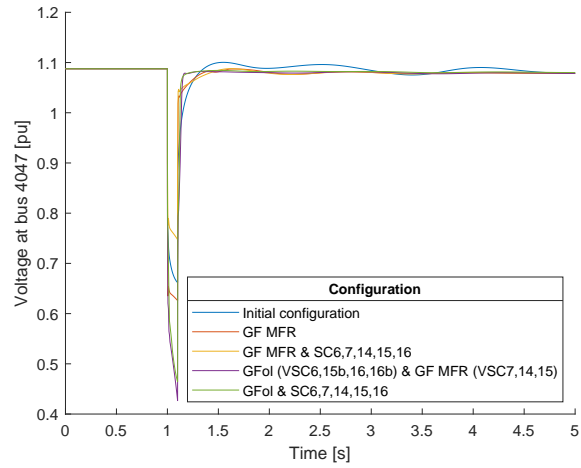


(b) Bus 4047.
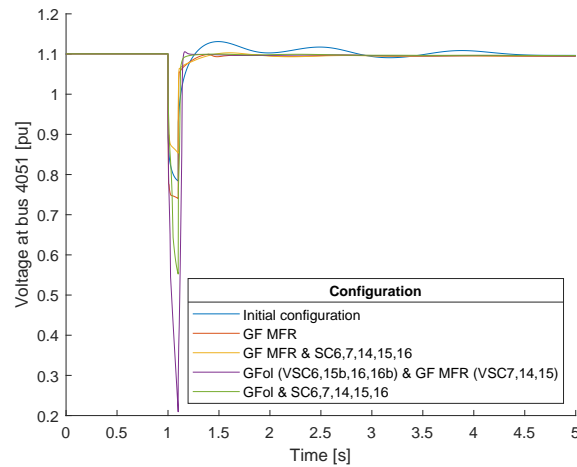


(c) Bus 4051.

Figure 4.27: Voltage at bus 4042, 4047 and 4051 after a short-circuit at bus 4032 and the tripping of line 4032-4044, with the replacement of SMs in the central part with various technologies.

Several conclusions can be drawn from the evolution of each bus voltage represented in these figures. First of all, it can be noticed that all buses have a similar behaviour : at the occurrence of the short-circuit, the voltage drops and the fault is then cleared by the tripping of line 4032-4044. At that moment, the voltage increases to stabilize to a steady state. The clearing of the short-circuit is clearly visible since each voltage reaches a steady-state value between 0.9 and 1.1 pu, which is acceptable. Also, it can be noticed that the voltage oscillations present especially at bus 1042 and 4051 in the initial configuration are damped in any other configuration, whatever the type of converter that is used, mixed or not with any other technology.

When comparing the different configurations, the same conclusions can be drawn from all bus voltages. Indeed, the best configuration based on this simulation is always the one where grid-forming converters are used together with synchronous condensers placed at each bus. This conclusion makes sense since grid-forming converters impose the voltage as they act as voltage sources and synchronous condensers have a short-circuit capacity allowing them produce reactive power to stabilize the voltage.

Then, the second best configuration is always the initial one, where synchronous machines are used as power generators in the central part of the network. Their short-circuit power helps in the voltage support after the occurrence of the short-circuit.

The third best configuration is the one where all of these machines are replaced with grid-forming converters followed by the configuration where grid-following are used together with synchronous condensers. These synchronous condensers help to provide short-circuit power after the fault and allows to use the grid-following converters while it is not the case when these are used standalone in the central part of the network. Thanks to their voltage-source topology, using grid-forming converters only allows to obtain similar results without the need of adding synchronous condensers. However, the results obtained with these two configurations are not as good as those obtained with the initial configuration.

The worst configuration for every bus giving rise to the deepest voltage drop is the one where grid-following converters are placed instead of synchronous machines $g6$, $g15b$, $g16$ and $g16b$ while synchronous machines $g7$, $g14$ and $g15$ are replaced with grid-forming converters. In that specific case, the grid-forming converters connected to bus 1043, 4042 and 4047 help in the voltage stability since thanks to them it is possible to obtain some results. Indeed, without these grid-forming converters, the configuration with only grid-following converters is unstable. However, the presence of these grid-forming converters do not lead to quite good results in terms of bus voltages, even at those where these converters are connected to. All buses taken together, the voltage drops reach values ranging from 0.4267 pu to 0.1734 pu in this configuration after the occurrence of the short-circuit.

In conclusion, different configurations can be chosen in this specific case where a short-circuit occurs in the network. The one implying grid-forming converters together with synchronous condensers gives even better results than those obtained with the initial configuration. However, a trade-off between the importance of the improvement and the economic investment for implanting that amount of synchronous condensers in the network has to be considered. On the other hand, results implying either only grid-forming converters, grid-following converters in addition to synchronous condensers or a mix of grid-following and grid-forming converters are a bit worst compared to those obtained with the initial configuration.

FIGURE 4.28 shows the current in each VSC after the short-circuit at bus 4032 cleared by the tripping of line 4032-4044, with the replacement of synchronous machines in the central part with grid-forming converters, without and with synchronous condensers, and the replacement with grid-following converters and synchronous condensers. TABLES C.17 and C.14 in APPENDIX C present the numerical results of these simulations.
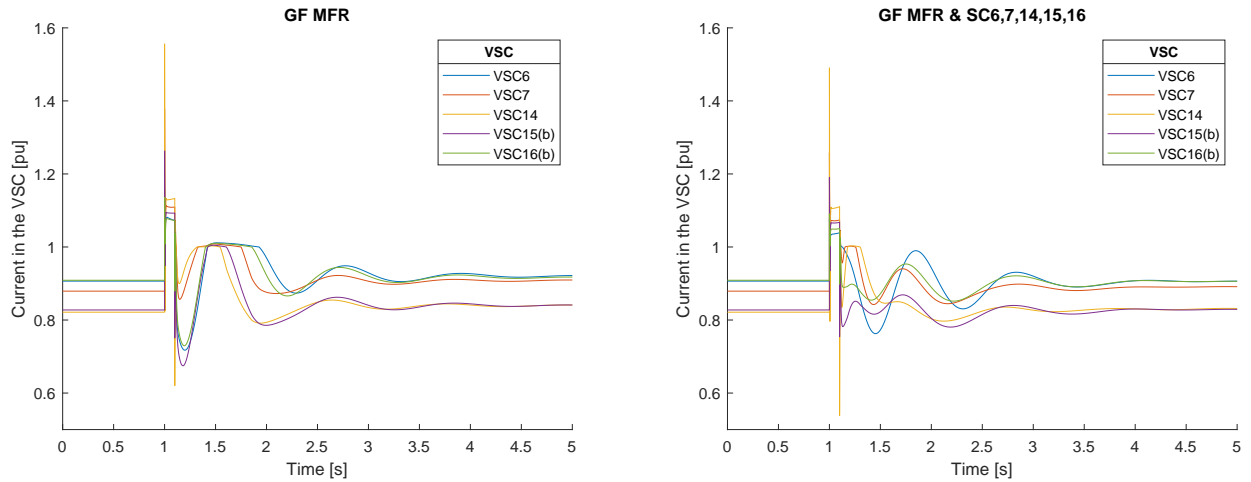


(a) Grid-forming VSCs.



(b) Grid-forming VSCs with SC6, 7, 14, 15 16.
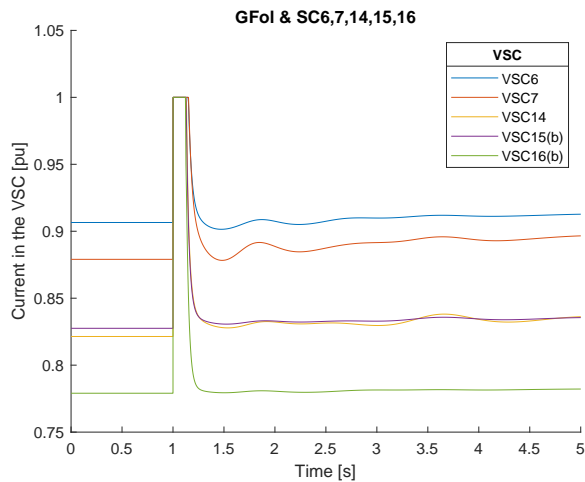


(c) Grid-following VSCs with SC6, 7, 14, 15 16.

Figure 4.28: Current in the VSCs after a short-circuit at bus 4032 and the tripping of line 4032-4044, with the replacement of SMs in the central part with grid-forming VSCs and with both types of VSCs with synchronous condensers.

First, it is important to note that the simulations need to be carried out with the presence of a current limiter in the model of the grid-forming converters. Without this limiter, the current reaches peak values between 1.2177 and

2.7737 pu for the configuration where only grid-forming converters are used and between 1.1480 and 2.5998 pu for the same configuration but to which synchronous condensers have been added in the central part of the network, in parallel to the grid-forming converters. A current limiter is thus more than required here for the protection of the converters after such a fault occurring in the network.

By comparing graphs represented in FIGURES 4.28a and 4.28b where grid-forming VSCs are used without and with synchronous condensers respectively, no major change can be noticed. In both cases, a peak occurs for each VSC, especially for VSC14 electrically close to the bus where the short-circuit occurs, whose bus voltage is the one that is characterized the deepest voltage drop. These peaks are though a bit reduced with the presence of synchronous condensers, since these machine provide short-circuit power, but not enough to allow to use the configuration with grid-forming converters without any current limiter. As explained in SECTION 3.3.4.2, this peak is due to the delay implemented in the phase reactor model and is not realistic. FIGURE 4.28c, illustrating the current in the grid-following VSCs used with synchronous condensers placed in parallel to them, show the presence of the current limiter since the curves reach a peak at 1 pu during the transient period.

FIGURE 4.29 shows the current in each VSC after the short-circuit at bus 4032 cleared by the tripping of line 4032-4044, with the replacement of synchronous machines in the central part with grid-following converters replacing synchronous machines $g6$, $g15b$, $g16$ and $g16b$ and grid-forming converters replacing $g7$, $g14$ and $g15$. TABLE C.17 in APPENDIX C presents the numerical results of this simulation.
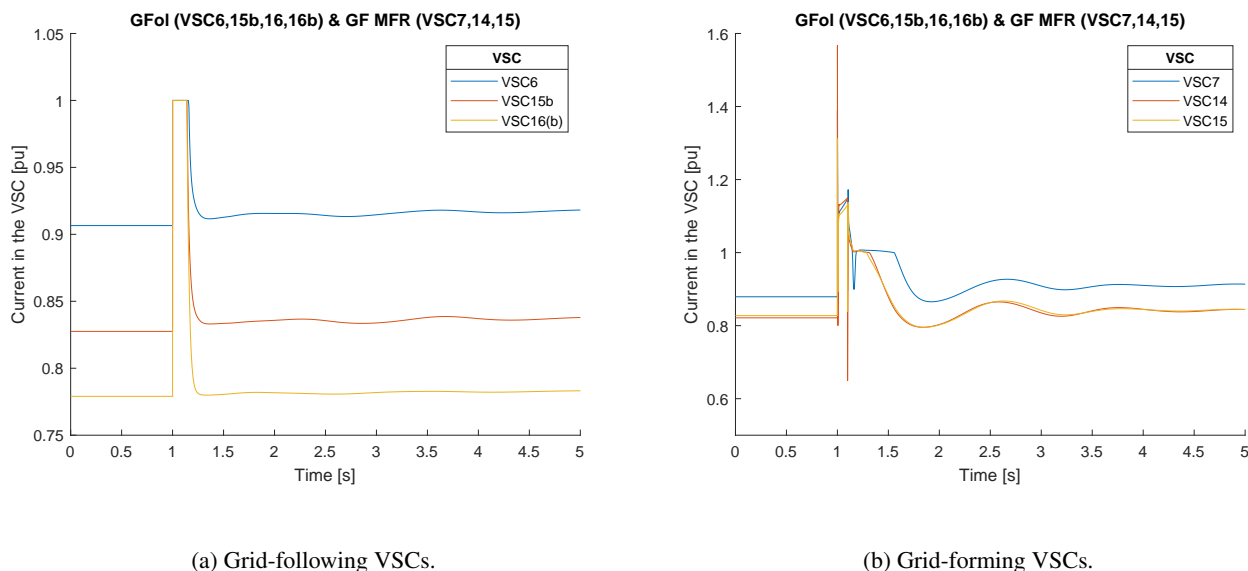


(a) Grid-following VSCs.                              (b) Grid-forming VSCs.
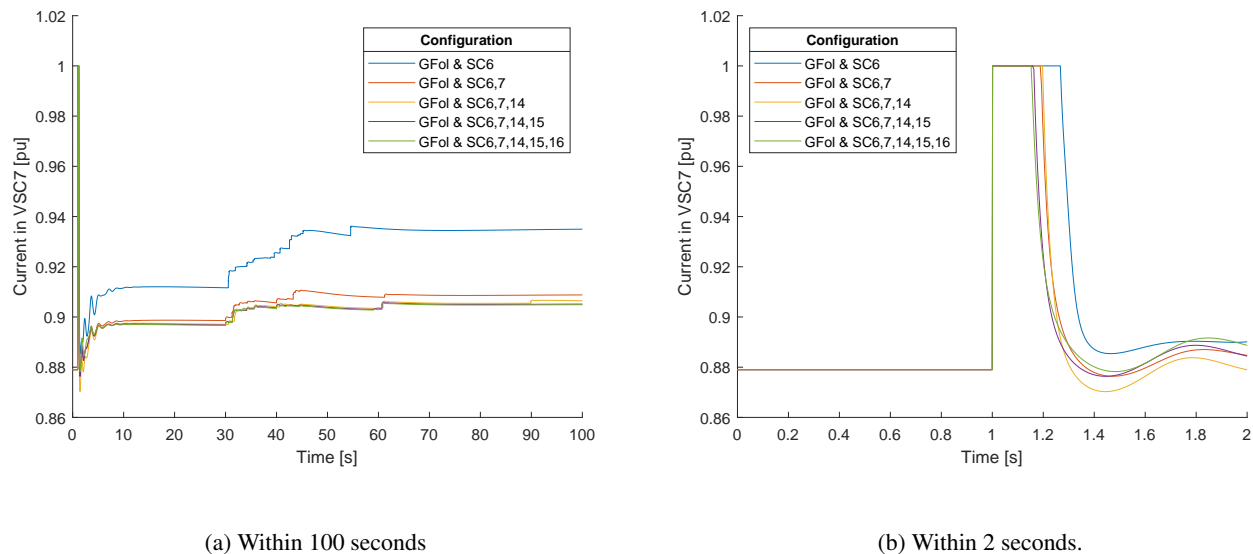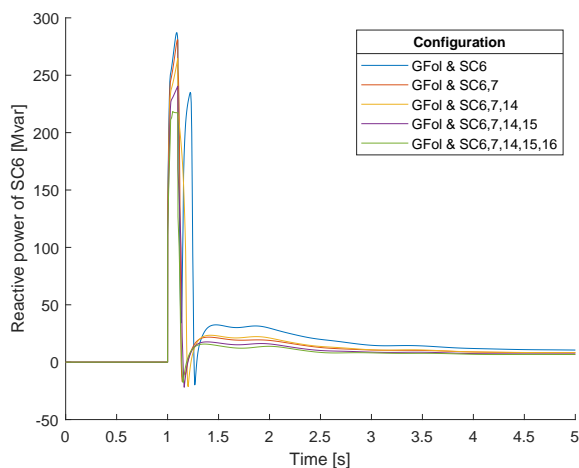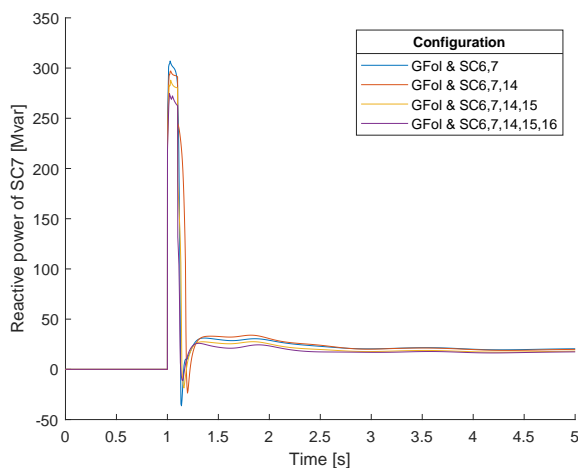
Figure 4.29: Current in the VSCs after a short-circuit at bus 4032 and the tripping of line 4032-4044, with the replacement of SMs in the central part with grid-following and grid-forming VSCs.

As for the previous graphs, FIGURE 4.29a representing the current in the grid-following converters shows that it is limited by the current limiter implemented in its model and set to 1 pu. Regarding FIGURE 4.29b representing the current in grid-forming converters VSC7, VSC14 and VSC15. The peak reached by each current shows that the current limiter is required. By the means of the virtual impedance, the current is limited to 1 pu, except for the

first non-realistic peak where it reaches 1.3884, 1.5674 and 1.3117 pu for VSC7, VSC14 and VSC15 respectively because of the delay required for the grid-forming converter to activate the virtual impedance and due to the phasor approximation.

FIGURE 4.30 shows the reactive power produced by synchronous condensers after the short-circuit at bus 4032 cleared by the tripping of line 4032-4044, with the replacement of synchronous machines in the central part with either grid-following or grid-forming converters in addition to synchronous condensers. TABLE C.15 and C.18 in APPENDIX C present the numerical results of each respective simulation.
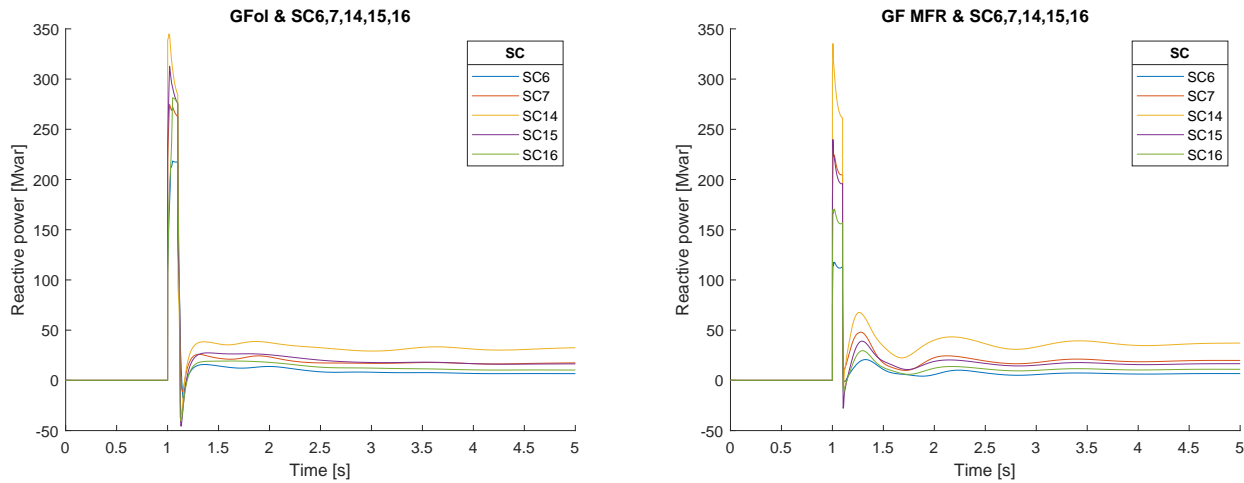


(a) Grid-following VSCs with SC6,7,14,15,16.

(b) Grid-forming VSCs with SC6,7,14,15,16.

Figure 4.30: Produced reactive power by synchronous condensers after a short-circuit at bus 4032 and the tripping of line 4032-4044, with the replacement of SMs in the central part with both types of VSCs with synchronous condensers.

In the configuration using grid-following converters together with synchronous condensers, their reactive power production increases during the transient period, ranging from 218.39 to 345 Mvar, in order to maintain a stable enough voltage and then decrease to a finite steady-state value. Regarding FIGURE 4.30b where the reactive power produced by each synchronous condenser used with grid-forming VSCs is illustrated, one can notice that the produced reactive power is way lower compared to the same configuration with the grid-following VSCs. Indeed, except for SC14 that produces 335.33 Mvar, the others produce between 117.70 to 239.78 Mvar during the transient period following the short-circuit. This result makes sense since grid-forming converters impose the voltage and thus the voltage control is improved compared to grid-following converters.

### 4.3.3.1 Conclusions of the simulations

This section aims at determining the role of each technology when placed in the central part of the network. For that purpose, various configurations are studied and the voltage at buses located in the central part of the network gives information about each configuration, helping decide which one to choose.

First, it is shown that the short-circuit occurring at bus 4032 is crucial for the configuration where only grid-following converters replace synchronous machines in the central part. Graphs of the voltage at bus in the central part of the network show that the more grid-following VSCs are penetrated the deeper the voltage drop. At the moment either $g16$ or $g16b$ is replaced with a grid-following VSC, the drop is so huge that the network does not withstand the short-circuit even if it is cleared 100 milliseconds later by the tripping of line 4032-4044. This illustrates the instability of grid-following VSC operating standalone in a part of the network and it shows that these converters do not have enough short-circuit power to withstand the fault, especially because their current is limited to 1 pu. However when adding two or more synchronous condensers to this configuration, short-circuit power provided by these machines help in the voltage stability. The more the synchronous condensers, the less deep the voltage drop at each bus of the central part. It can be seen that increasing the number of synchronous condensers added to the network will reduce the current produced by the VSCs during the whole time span. During the transient period, these machines will produce a huge amount of reactive power, helping to withstand the short-circuit.

Then, several configurations have been analysed more in-depth. The best results in terms of voltage are obtained by the configuration where grid-forming converters are used with synchronous condensers. Grid-forming converters act as a voltage source and are more fitted to support voltage compared to grid-following converters. Moreover, the presence of the synchronous condensers helps provide short-circuit power to withstand the short-circuit. Then, the second best configuration is the initial one, where synchronous machines help in the network stability through their short-circuit power capability. The third and fourth configurations are the ones where either grid-forming converters or grid-following with synchronous condensers are used. Similar results are obtained with both of them. Finally, the worst configuration mixes grid-following and grid-forming converters. The grid-forming converters allows to withstand the short-circuit but the configuration leads to the deepest voltage drop at every bus. The virtual impedance limiting the current produced by each grid-forming converter limits its capacity to support the voltage in the central part of the network after the occurrence of the short-circuit.

This study also shows the current of each converter. Because of the short-circuit, this current is high during the transient but limited by the saturation block for the grid-following converters and by the virtual impedance for the grid-forming converters. This is a direct consequence of the limit in the voltage support and the short-circuit capacity of these two converters. The grid-following converters all have a peak of 1 pu during the transient and the grid-forming converters have a higher one due to the delay of the virtual impedance and the phasor approximation. Adding synchronous condensers has a visible effect on the evolution of the current : it decreases when synchronous condensers are added to the network, as they provide short-circuit power that helps the converters withstand the short-circuit. A huge peak of reactive power is produced by these machines during the transient period, then decreasing to a finite steady-state value. However, this peak and the steady-state value decrease for all synchronous condensers when they are used with grid-forming converters compared to grid-following ones, due to the general mode of operation of the grid-forming converters that are more suited for voltage support.

## 4.4   HVDC connection between the equiv. and central parts

The next configuration analyzed in this chapter concerns the initial Nordic network to which a VSC HVDC link is added. As illustrated in FIGURE 4.31, this link is connected through a grid-following VSC to bus 4071 located in the equiv. part while the other side of the link is connected to bus 4045 in the central part. The VSC connecting the HVDC link to this bus can be chosen to be either a grid-following or a grid-forming converter. The following situation is studied : synchronous machines $g6$, $g7$, $g16$ and $g16b$ are removed from the network, which causes a lack of 1740 MW initially produced in the central part, from TABLE 4.1. This amount of power is thus instead transferred via this HVDC link from the equiv. part, especially coming from the interconnection represented by synchronous machine $g20$.


This section presents the general theory and the motivation of using HVDC links followed by the description of the model used in the simulations. The rest of the section is dedicated the study of the stability of this configuration of the network. Dynamic simulations using both types of VSC HVDC links focusing on the frequency response, the voltage control and finally the comparison of different mixes using various technologies are analysed, as for the previous section.
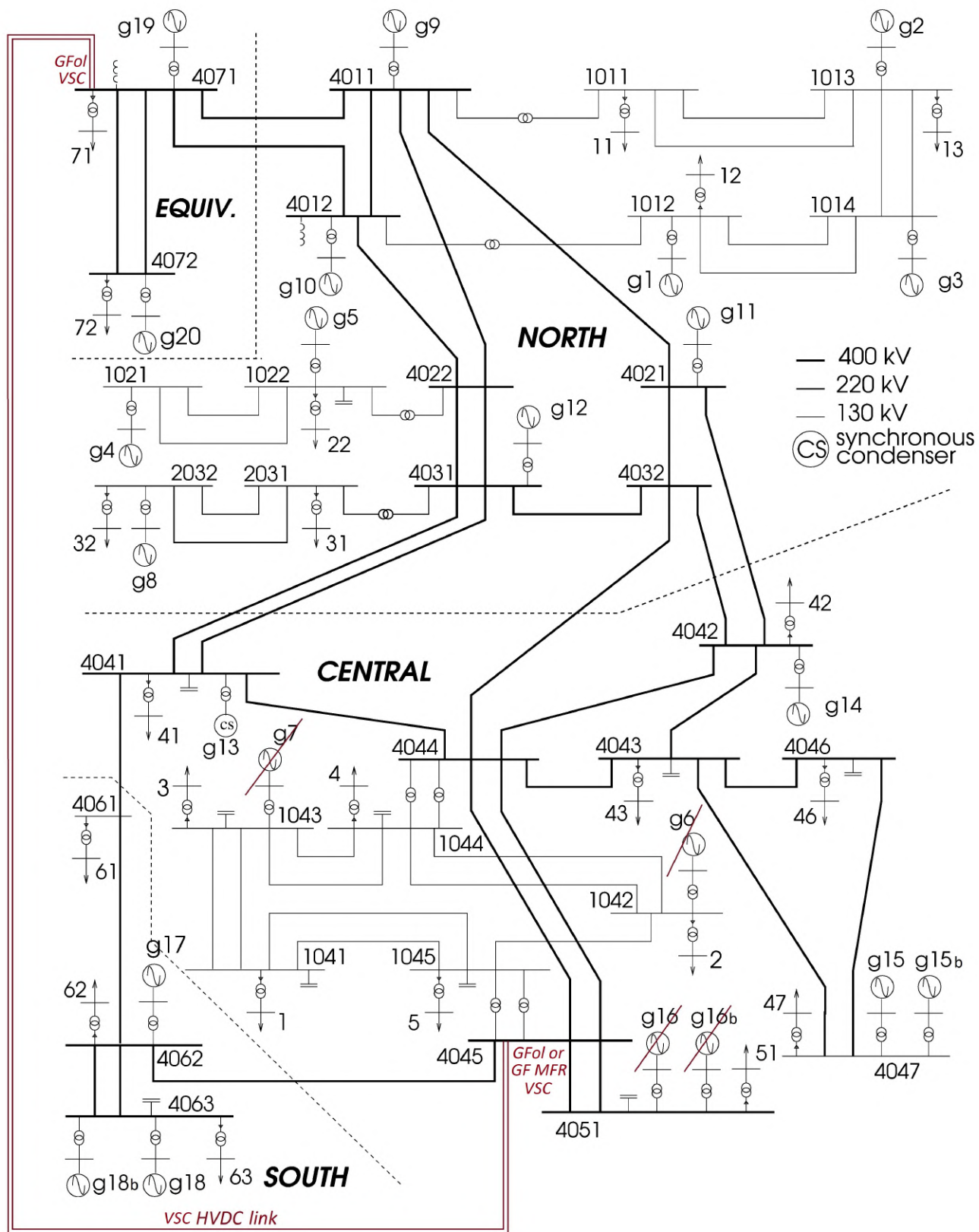
Figure 4.31: One-line diagram of the Nordic system with the HVDC link between the equiv. and central parts.

### 4.4.1 HVDC links

In this section, the study is based on active power transmitted from an interconnection to the central part of the Nordic network through a HVDC link. This technology is more and more used nowadays and is a significant substitute of HVAC links especially for long distances. This change is due for different reasons : the transmission losses are reduced, the operational costs are lower and the controllability as well as the security between AC grids with different system frequencies are improved since huge voltage deviations and power swings are not transmitted across the link. Moreover, after a certain distance, so-called the breakeven distance, the total cost including the total capital cost with the loss evaluation is lower compared to HVAC technologies, as represented in FIGURE 4.32. This distance is typically around 600 to 800 km for overhead lines and 40 to 120 km for submarine cables. Thus, HVDC links are especially connected to power plants whose resources are located far away from load centers like hydro power or remote coal plants. They are used for asynchronous interconnections or to interconnect different regions far away from each others through long submarine cables [34].
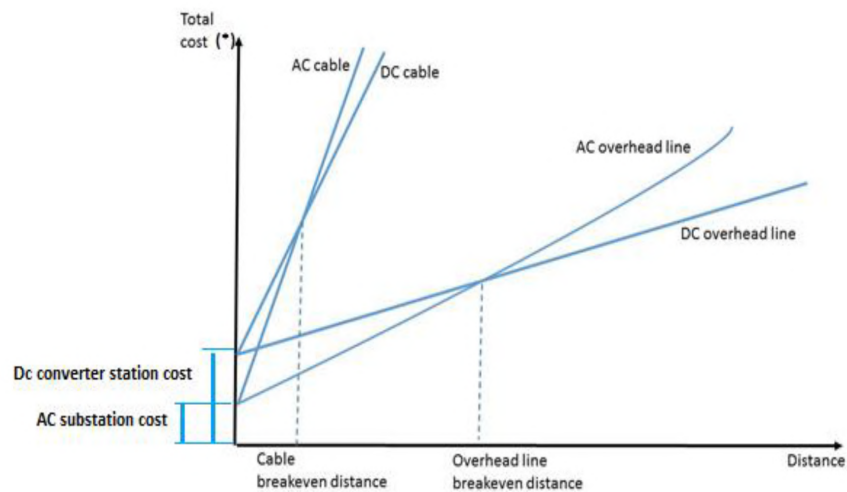


Figure 4.32: Total cost as a function of distance, for HVAC and HVDC links [34].

Two different HVDC technologies can be implemented in a transmission network. The first one uses Line-Commutated Current source converters, so-called LCCs, while the other uses self-commutated Voltage-Source Converters, or VSCs. A representation of both types of HVDC links is shown in FIGURE 4.33. The first type corresponds to the conventional HVDC transmission that is used with thyristor valves and requires a synchronous voltage source, thus a strong enough AC grid, to operate. On the other hand, VSC HVDC topologies have lots of benefits for the system performance. They are able to control active and reactive powers independently from each other while LCC HVDC always consume reactive power. Thus, VSC HVDC links offer a voltage support and a control capability which allows to place those anywhere in the AC network. Also, these HVDC links permit a black-start operation and less filters are needed compared to LCC HVDC links [32, 34]. TABLE 4.2 summarizes the characteristics of each type of HVDC links. This work makes use of a VSC HVDC link only because of the aforementioned advantages of these links and since it allows to compare the operation of grid-following and grid-forming converters as in the previous section.
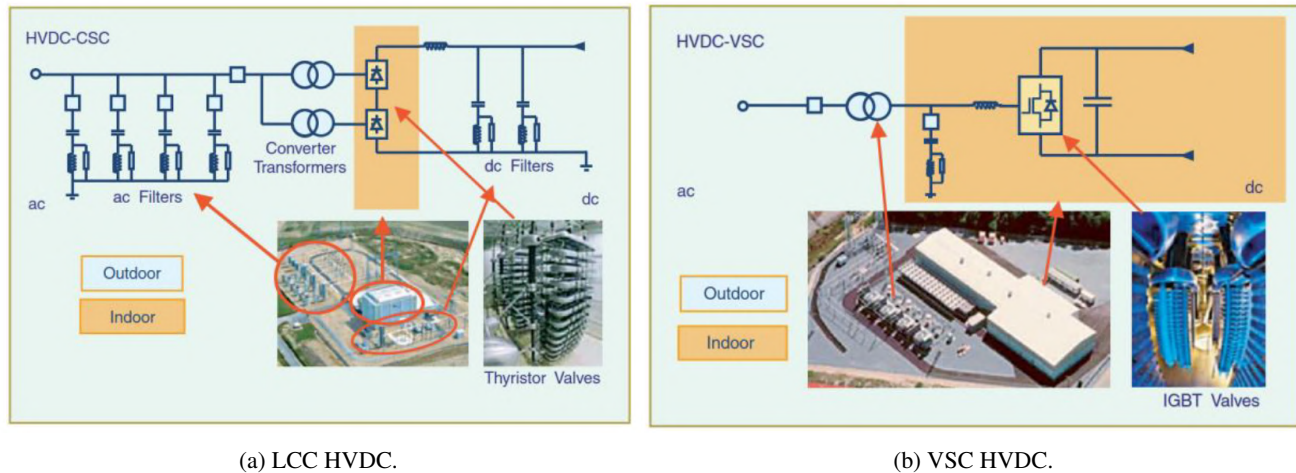
(a) LCC HVDC.                                                    (b) VSC HVDC.

Figure 4.33: Conventional LCC HVDC with current source converter and HVDC with voltage sourced converters (VSC) [34].

Table 4.2: Comparison of Line Commutated Converters (LCC) and Voltage-Source Converters (VSC) HVDC technologies [32].

|  | Line Commutated Converters | Voltage-Source Converters |
|---|---|---|
| Power rating | Large | Lower (but fast growing technology) |
| Harmonic filters | Large | Less filters needed |
| AC grid | Requires strong enough AC grid | Can operate with a weak AC grid |
| Cable insulation | Paper impregnated with oil | XPLE (plastic) |
| Power control | Active power | Active and reactive powers |
|  | Always consumes reactive power |  |
| Used as off-shore terminal to collect wind power | No | Yes |
| Price | Cheaper | More expensive (but fast growing technology) |
| Black-start capability | No | Yes |
| Commutation losses | Less losses but possible failure | More losses |

In general, the control of the HVDC link is divided in each side : one side of the link controls the voltage while the other side controls the power transferred through this link. In case of LCC technology, the rectifier side controls the current or the power and the inverter side controls the voltage [32]. However, in case of VSC-based HVDC links, both ends can either control the voltage or the power.

### 4.4.2 Modelling of the VSC HVDC link

The model of the VSC HVDC link implemented in RAMSES is represented in FIGURE 4.34.
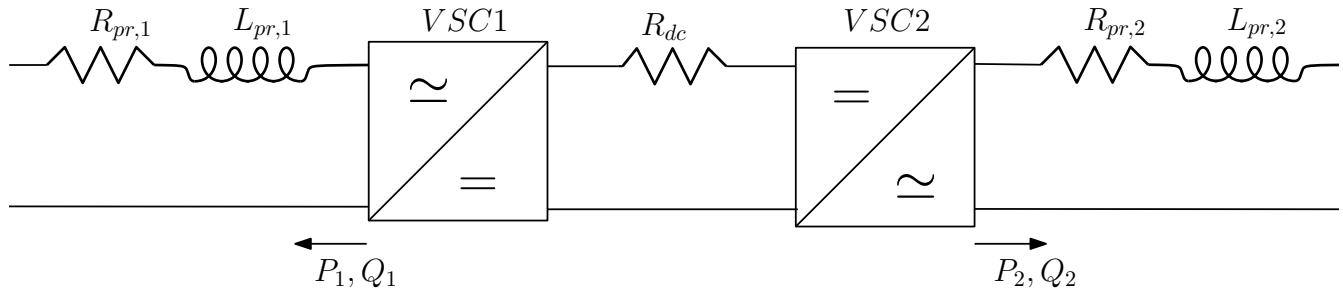


Figure 4.34: Model of the VSC HVDC link.

The HVDC link between the two converters VSC1 and VSC2 is rated at 525 kV, corresponding to the base voltage. The base power corresponds to the nominal apparent power of each VSC, set to 2100 MVA. The grid-following VSC connected to the equiv. part controls the voltage while in the central part the grid-following or the grid-forming VSC controls the active power transferred in this part. Joule losses in the HVDC link are represented by the resistance $R_{dc}$ equal to 0.011 $\Omega$/km [21]. The link is assumed to be 500 km long, giving rise to a total resistance of 5.5 $\Omega$. The nominal power transferred from the equiv. part to the central one is set to 2000 MW and the power loss in the link is due to the resistance $R_{dc}$ but also to losses in both converters characterized by a phase reactor resistance $R_{pr}$ and inductance $L_{pr}$ in the VSC model, equal to 0.005 and 0.15 pu respectively, as for the model of both types of VSCs. Finally, the current is limited through the same means as the ones described in SEC-TION 3.3.4 and the grid-forming converter VSC HVDC link can be characterized by a finite droop. Nevertheless, the droop is always infinite in the simulations. In the future figures, the grid-following VSC HVDC link is the one referenced to "GFol link" and "GF MFR link" stands for the VSC HVDC link that uses a grid-forming VSC at one side and a grid-following at the other. This link is mentioned as the "grid-forming VSC HVDC link" in the comments of the simulations for the sake of simplicity, even though a grid-following VSC is used in the equiv. part.

TABLE 4.3 gives the set-point active and reactive powers of the VSCs at both sides of the HVDC link after hav-ing removed synchronous machines $g6$, $g7$, $g16$ and $g16b$. Taken together, these machines are initially producing 1740 MW that are transferred through the link and corresponds thus the active power set-point of the VSC con-nected to bus 4045 in the central part of the network. This power comes from $g20$ that produces thus 3209.72 MW compared to 1374.88 MW in the initial load flow of the Nordic network [33]. The active power set-point of the VSC connected in the equiv. part at bus 4071 is set to 1785 MW. The power lost in the HVDC link and in the VSCs is thus equal to 45 MW in total. Finally, since the technology used is a VSC HVDC link, the reactive power can be controlled [32] : the VSC connected to bus 4045 produces 50.44 Mvar while 253.85 Mvar are produced by the VSC connected to bus 4071.

| VSC of the HVDC link | Active power $P$ [MW] | Reactive power $Q$ [Mvar] |
|---|---|---|
| VSC connected to bus 4071 | -1785 | 253.85 |
| VSC connected to bus 4045 | 1740 | 50.44 |

Table 4.3: Set-point active and reactive powers of the VSCs at each side of the VSC HVDC link.

### 4.4.3   Frequency response

As for the study focusing on the modification of the configuration of the central part of the network, the first analysis that is carried out in this section concerns the frequency response of the network. For that purpose, the fault that is considered is the loss of generator $g15$ after 1 second, whose nominal produced active and reactive powers are respectively equal to 540 MW and 85.87 Mvar. This generator is chosen since it is located in the central part of the network, more precisely connected to bus 4047, and is the one that generates the more active power in this zone of the network. It is important to mention that the simulations carried out in this section are the ones obtained when the LTCs initially present in the network are removed. This choice is made because the focus here concerns the frequency response and the LTCs affect it considerably. The effect of the LTCs is detailed in the next section focusing on the voltage control.

FIGURE 4.35 illustrates the rotor speed of $g12$ and the frequency estimated by the VSCs of the HVDC link, after the loss of $g15$ and with both types of HVDC links. TABLES C.19 and C.20 in APPENDIX C present the numerical results of this simulation.
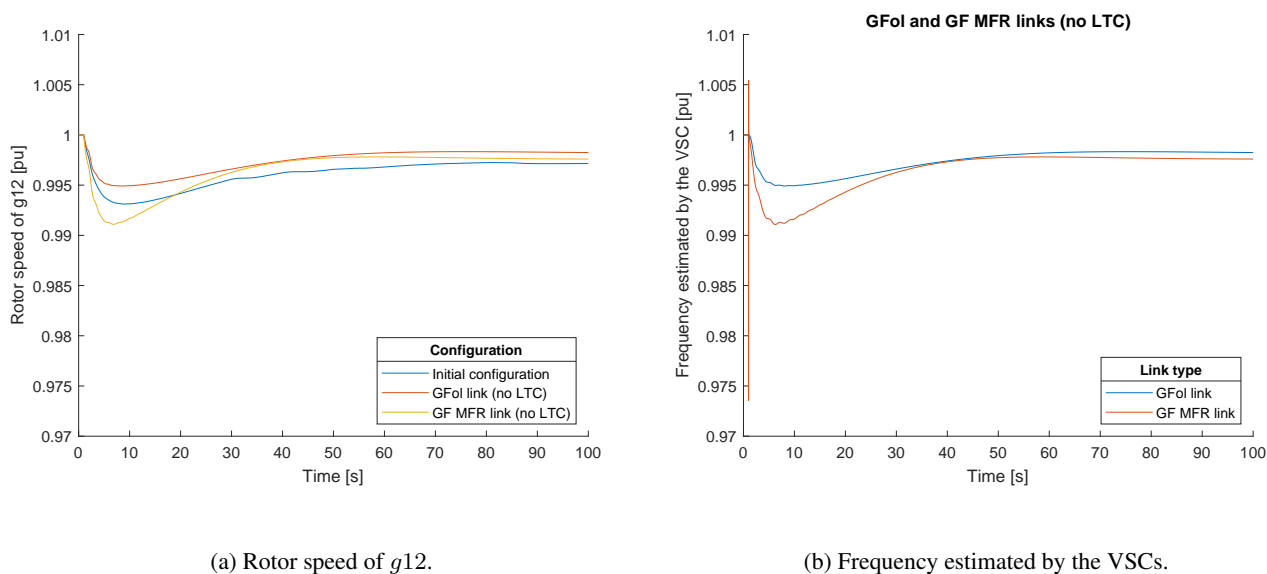


(a) Rotor speed of $g12$.                                 (b) Frequency estimated by the VSCs.

Figure 4.35: Rotor speed of $g12$ and frequency estimated by the VSCs after the loss of $g15$, with both types of HVDC links.

By looking at the figure representing the rotor speed of $g12$, illustrating the system frequency, it can be noticed that the curve obtained with both types of VSC HVDC links differs from the one obtained with the initial configuration. In the configuration where the grid-following VSC HVDC link is used, the frequency nadir reaches 0.9949 pu compared to 0.9931 pu with the initial configuration. This increase in the frequency nadir comes from the fact that the voltage support is worse with the grid-following converters. Thus, the bus voltages are characterized by deeper voltage drops and the loads consume less active power since it is directly proportional to $\frac{V}{V_0}$, where $V$ and $V_0$ are respectively the current and the initial voltages at the bus of concern [33]. This helps in the frequency response of the whole network and improves the frequency nadir. On the other hand, with the grid-forming VSC

HVDC link, the voltage is better supported in the central part since the grid-forming VSC controls it and the active power consumption by the loads is not varying after the loss of $g15$. The frequency nadir thus reaches the value of 0.9911 pu, which is worse compared to the one obtained with the initial configuration. This shows that the grid-forming VSC HVDC link has a harmful effect on the frequency response of the whole network. Nevertheless, even if this configuration is the worst in terms of frequency drop, it does not reach a value lower than 0.95 pu. It can be concluded that the two configurations are thus acceptable since the frequency deviation does not exceed 5 % compared to the nominal value.

As it has already been shown in the previous section, the frequency estimated by the VSCs of the HVDC link shown in FIGURE 4.35b corresponds well to the rotor speed of $g12$, expect for the first computation by the PLL of the grid-forming VSC at the occurrence of the fault.

Then, FIGURE 4.36 shows the current in each VSC of the HVDC link after the loss of generator $g15$, with both types of HVDC links. TABLE C.21 in APPENDIX C presents the numerical results of this simulation.



(a) Grid-following VSC HVDC link.　　　　　　　　(b) Grid-forming VSC HVDC link.
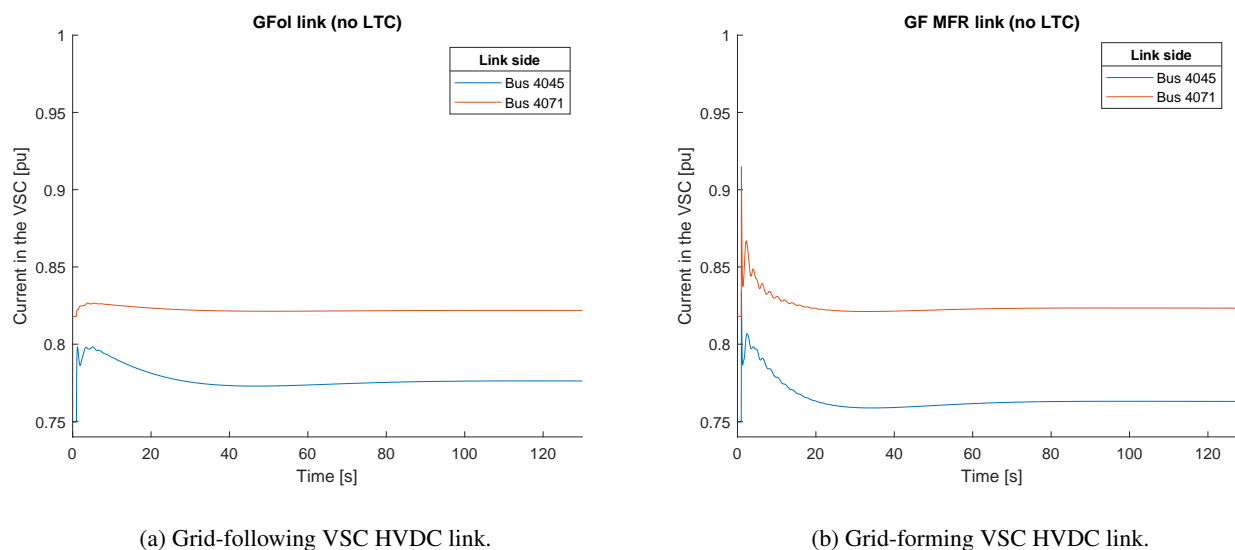
Figure 4.36: Current in the VSCs after the loss of $g15$, with both types of HVDC links and without the LTCs.

FIGURE 4.36a represents the current in each grid-following VSC connected either to bus 4045 or bus 4071, when the grid-following HVDC link is used. Both currents are characterized by a similar behaviour and by acceptable values since their peak reaches 0.7983 and 0.8266 pu for the VSC connected to bus 4045 and 4071 respectively. For the other VSC HVDC link type, whose current in the VSCs is represented in FIGURE 4.36b, both currents have the same behaviour as they both reach a peak value at the moment the fault occurs and then decrease to a steady-state value. Their value is always lower than 1 pu which allows to use the HVDC link without the activation of the current limiter. Indeed, the peak of the current in the VSC connected to bus 4045, i.e. in the grid-forming converter, reaches 0.9148 pu while in the grid-following VSC connected to bus 4071 it reaches 0.8343 pu.

### 4.4.3.1   Conclusions of the simulations

In conclusion, the frequency response varies a bit depending on the configuration that is considered. Compared to the initial configuration including LTCs, the frequency nadir is higher with the grid-following VSC HVDC link and lower with the grid-forming one. This is a direct consequence of the voltage support that is improved with the grid-forming VSC connected to bus 4045. Indeed, the voltage being better supported is closer to its initial value, less considerably affecting the consumption of the loads compared to the grid-following VSC usage. The loads consume less of the active power that helps in the frequency response after the loss of $g15$. The frequency is approximated by the VSCs through the PLL, showing a peak and drop at the moment the fault occurs due to a computation error. Regarding the currents, each VSC is characterized by a current that increases during the transient period to stabilize afterwards to a value close to the initial one. The frequency does not deviate from the nominal value by more than 5 % and the current in the VSCs is always lower than 1.1 pu making both configurations acceptable.

### 4.4.4 Voltage control

The voltage control of the network including the HVDC link is studied in this section. By consistency, the tripping of line 4032-4044 is the event considered for this study, as it is the case in the previous section.

FIGURE 4.37 illustrates the evolution of the voltage at bus 1042, 1043, 4042, 4047 and 4051 within 350 and 60 seconds with both types of HVDC links after the tripping of line 4032-4044. TABLE C.22 in APPENDIX C presents the numerical results of this simulation.
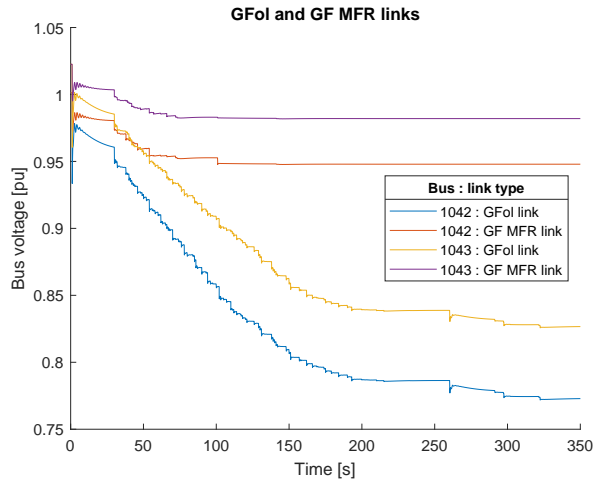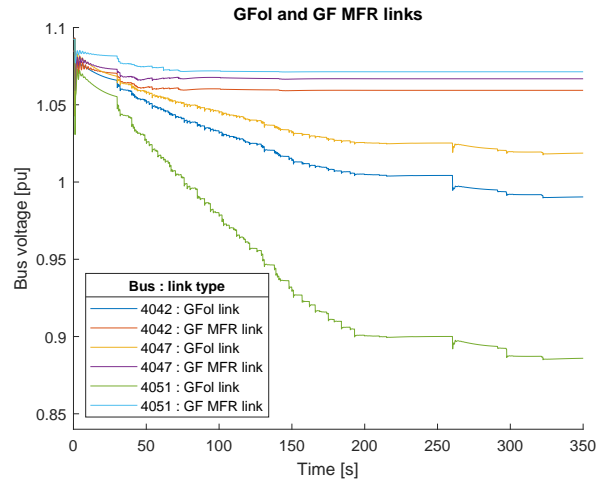


(a) Bus 1042 - 1043.
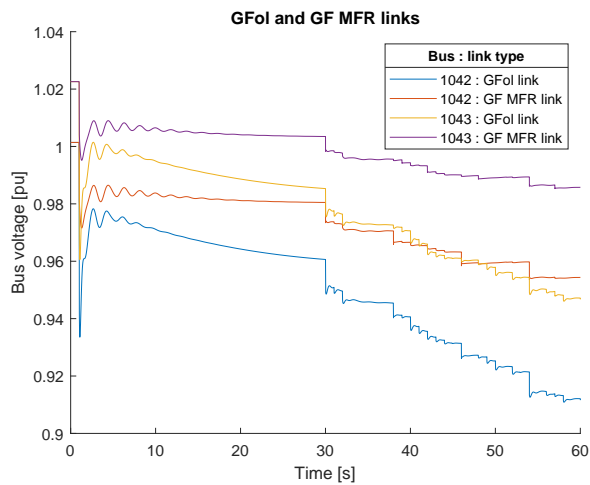
(b) Bus 4042 - 4047 - 4051.

(c) Bus 1042 - 1043 (zoom).
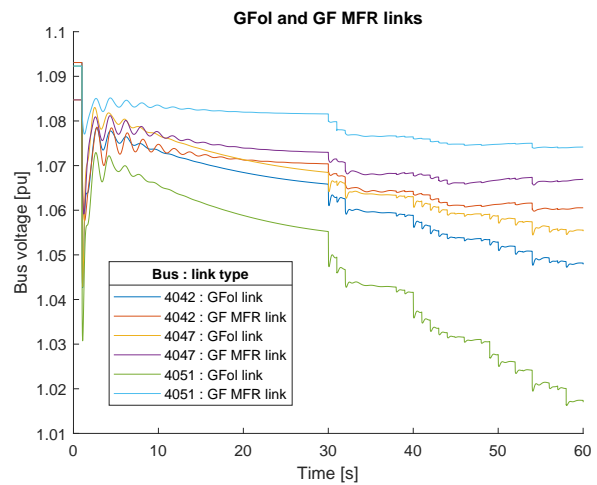
(d) Bus 4042 - 4047 - 4051 (zoom).

Figure 4.37: Bus voltages in the central part after the tripping of line 4032-4044, with both types of HVDC links.

From a general point of view, each voltage bus is subjected to the same behaviour after the occurrence of the fault. Indeed, each curve is characterized by a first voltage drop within the first 5 seconds. Then, the voltage stabilizes for the grid-forming VSC HVDC link and decreases for the grid-following VSC HVDC link within 30 seconds to finally decrease again to reach a steady-state value. However, some differences can be noticed depending on the type of VSC HVDC link that is chosen.

First, there are some improvements in terms of voltage drop when using the grid-forming VSC HVDC link. Indeed, with this HVDC link, the voltage decreases by values from 1.40 % to 3.24 %, depending on the bus, compared to the initial voltage. With the grid-following VSC HVDC link, these voltage drops are more pronounced since the difference ranges between 3.86 % and 6.78 %. This is due to the topology of grid-forming converters that impose the voltage and thus fit better to voltage issues compare to grid-following.

Second, the steady-state voltage reached by each bus is way better with the grid-forming VSC HVDC link. In fact, when using a connection through a grid-forming converter at bus 4045, the steady-state voltage reached by each bus ranges between 0.9479 pu and 1.0714 pu, depending on the bus, which are acceptable values since these are well between 0.9 and 1.1 pu. However, if this grid-forming converter is replaced with a grid-following one, these voltages become smaller and reach values between 0.7730 pu and 1.0188 pu. This is especially due to the huge decrease between 30 and 325 seconds caused by the activation of the LTC, giving rise to a staircase curve, which is not acceptable. When the synchronous machines $g6$, $g7$, $g16$ and $g16b$ are removed from the network, the reactive power that they produce is lost. The rest of the network as well as the HVDC link have to compensate this loss. In the case of the grid-forming VSC HVDC, the voltage is better supported compared to the grid-following VSC HVDC, the voltage drop during the transient period is thus less deep and less LTCs are activated. With the grid-following VSC HVDC link, the voltage support is not enough which activates the LTCs that change their tap to withstand the fault but make the network collapse. Thus, in order to use the grid-following VSC HVDC link, the configuration of the network should be revised to make it stable in terms of voltage. These curves illustrate well the effect, and in this particular case the need, of choosing a grid-forming topology rather than a grid-following one for converters.

Finally, with the grid-forming VSC HVDC link, voltage stabilizes much faster to a steady-state value compared to the grid-following HVDC link, that reaches a steady-state value only after 350 seconds compared to 100 seconds with a grid-forming converter connected to bus 4045.

Since it can be noticed that the instability of the grid-following VSC HVDC link is due to the presence of the Load Tap Changers initially placed in the network, FIGURE 4.38 shows the same bus voltages after the same fault but with a configuration where the network do not include Load Tap Changers anymore. TABLE C.23 in APPENDIX C presents the numerical results of this simulation.



(a) Bus 1042 - 1043.                                                                  (b) Bus 4042 - 4047 - 4051.
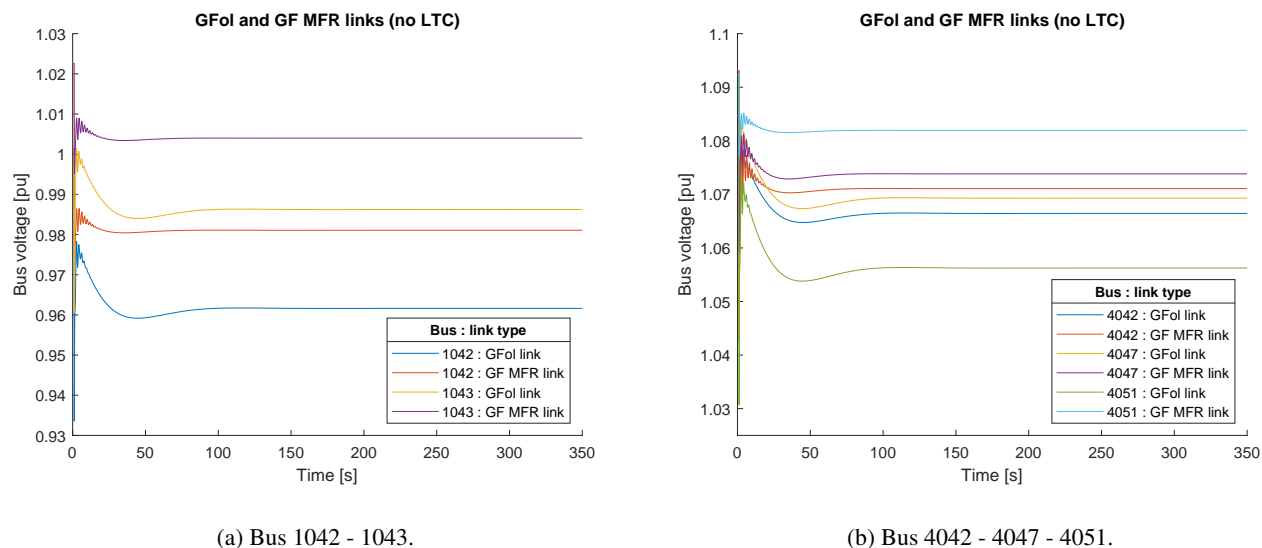
Figure 4.38: Bus voltages in the central part after the tripping of line 4032-4044, with both types of HVDC links and without the LTCs.

These figures confirm the conclusion drawn in the previous comments where it is stated that the LTCs is the reason why the network collapses after the tripping of line 4032-4044. When comparing this case with the previous one where the LTCs are not removed from the network, the transient voltage behaviour is not influenced by the removal of the LTCs. However, after 30 seconds, the voltage is not affected by the activation of the LTCs anymore and stabilizes more rapidly to a steady-state value which is higher than in the configuration with the LTCs. Indeed, with the grid-forming VSC HVDC link, the steady-state values range from 0.9811 to 1.0819 pu instead of ranging from 0.9479 to 1.0714 pu with the LTCs. With the grid-following VSC HVDC link, the improvement is clearly visible since the network does not collapse anymore. The steady-state values range from 0.9616 to 1.0693 pu compared to 0.7730 and 1.0188 pu, respectively, with the LTCs.

Thus, to counteract the voltage instability with the configuration including the grid-following VSC HVDC link and the LTCs, some measures should be taken in practice. First, the loss of the reactive power coming from the removed synchronous machines can be compensated by adding series compensation, switched shunt capacitors, Static Var Compensators (SVCs) or synchronous condensers. If these components are not added to the network, some changes should be done in the operation of the LTCs themselves. A signal could be sent to the LTCs to stop their activation and freeze the power network to avoid its collapse or the set-points of the LTCs should be modified to prevent them from changing their taps after the voltage drop and perform a selective power cut [31].

FIGURES 4.39 illustrates the evolution of the current in each VSC at both sides of the HVDC link after the tripping of line 4032-4044 with and without the LTCs. TABLES C.24 and C.25 in APPENDIX C presents the numerical results of this simulation.
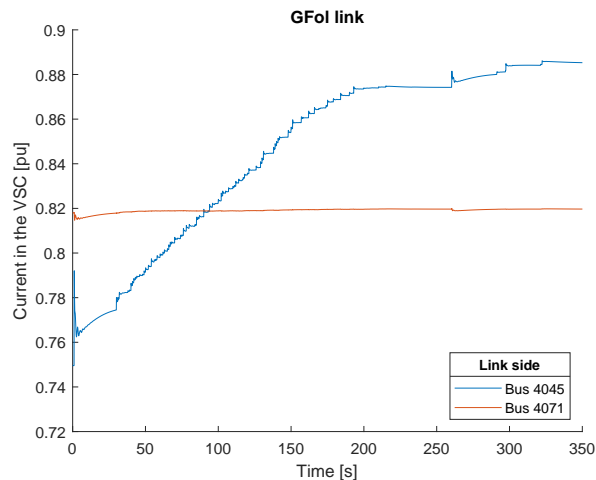


(a) Grid-following VSC HVDC link.
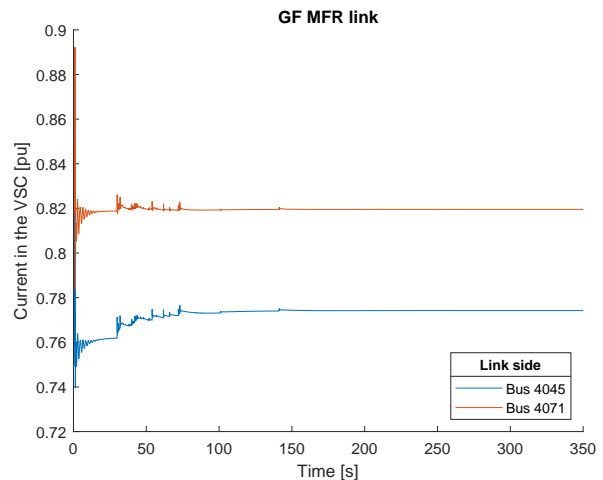
(b) Grid-forming VSC HVDC link.
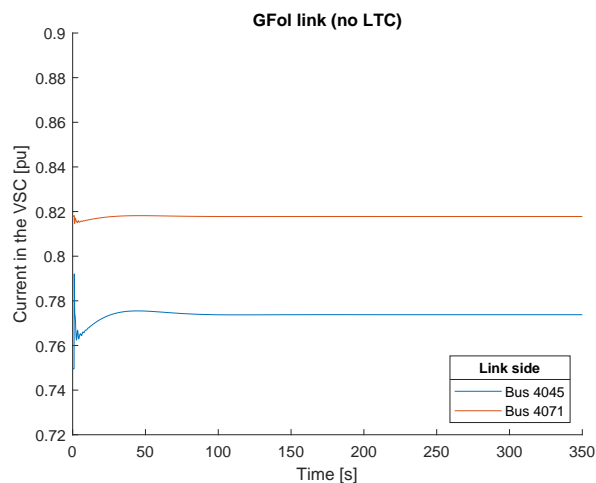
(c) Grid-following VSC HVDC link.
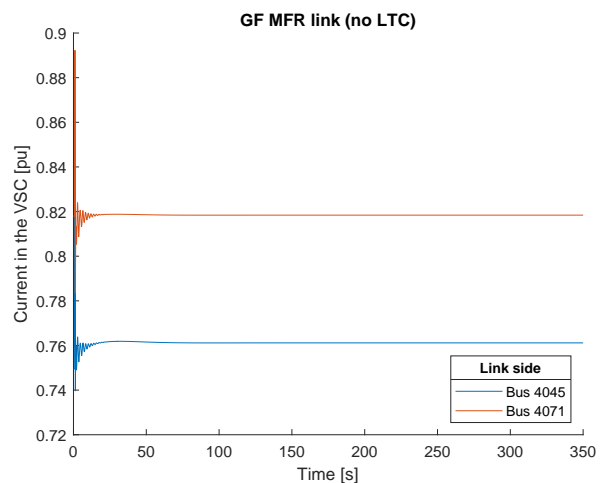
(d) Grid-forming VSC HVDC link.

Figure 4.39: Current in the VSCs after the tripping of line 4032-4044, with both types of HVDC links with and without the LTCs.

With the grid-forming VSC HVDC link, no huge change occurs while disconnecting the LTCs from the network. The current reaches a peak of 0.8210 and 0.8922 pu in the VSC connected to bus 4045 and bus 4071 respectively, during the transient period where the voltage drops, to finally stabilize to a steady state. On the other hand, with the grid-following VSC HVDC link and the LTCs, the current in the VSC connected in the central part to bus 4045 increases to 0.8852 pu in the same time the voltage decreases because of the control in reactive power that directly depends on the bus voltage and controls the $q$-axis component of the current. Without the LTCs, this increase does

not occur and the evolution of the current in both VSC is way more stable. In all cases, the current limiter is not activated since the values are lower than 1 pu.

#### 4.4.4.1 Conclusions of the simulations

With the grid-forming VSC HVDC link, the results obtained in this voltage control study are quite satisfactory. The tripping of the line gives rise to a voltage drop during the transient period and then the curve stabilizes to a steady state. The transient behaviour is worse using the grid-following VSC HVDC link. This shows that the grid-forming topology is more suited for voltage issues and helps the network to withstand the fault. On the other hand, the configuration with the grid-following VSCs at both ends of the VSC HVDC link gives rise to a deeper voltage drop during the transient that activates the LTCs during a longer period of time during which the network collapses. The steady-state is thus affected and some bus voltages reach unacceptable steady-state values out of the 0.9 and 1.1 pu range.

The LTCs removal highly improves the results. Without these LTCs, the steady-state values reached by the voltage with both HVDC links are higher and the use of the grid-following VSC HVDC does not lead to a network collapse anymore. This shows that in practice either compensation measures should be taken or the operation of the LTCs should be modified to prevent the network from collapsing if they are kept in the network.

The effect of the LTCs is also visible in the evolution of the current. More especially, for the grid-following VSC connected to bus 4045, the current increases at the same pace as the voltage decreases to produce reactive power but not enough to survive the fault. One gets rid of this effect by removing the LTCs since a flatter curve is obtained during the whole time span. In all configurations, the limit of 1.1 pu is not exceeded by any VSC.

### 4.4.5 Mix of various technologies

The objective of this last section of this chapter is to perform an analysis similar to the one performed in SEC-TION 4.3.3 where different configurations of the Nordic network are studied. For that purpose, the same event as the one considered in that section is chosen for the simulations, i.e. the short-circuit at bus 4032 cleared by the tripping of line 4032-4044. The configurations including the HVDC link and studied in this section are the following :

- The initial configuration, where the central part of the network is composed of synchronous machines only as power generators ;

- The configuration where only the grid-following or the grid-forming VSC HVDC link is used ;

- The two aforementioned configurations with synchronous condensers, all rated at 300 MVA, replacing synchronous machines $g6$, $g7$ and $g16$ ;

- The configuration where the grid-following VSC HVDC link is used together with grid-forming converters replacing synchronous machines $g6$, $g7$, $g16$ and $g16b$.

For the last configuration, the active power transferred through the grid-following VSC HVDC link and the reactive power produced at each side of it as well as the active and reactive powers produced by each grid-forming VSC replacing synchronous machines $g6$, $g7$, $g16$ and $g16b$ are presented in TABLE 4.4. Half of the active power initially produced by these synchronous machines is produced by the VSC replacing each of them and the rest of the power comes from the equiv. part, transferred in the central part by the means of the HVDC link. In this case, the power loss through the HVDC link is equal to 10 MW.

| VSC | Active power $P$ [MW] | Reactive power $Q$ [Mvar] |
|---|---|---|
| VSC connected to bus 4071 (HVDC link) | -880 | 52.71 |
| VSC connected to bus 4045 (HVDC link) | 870 | -54.31 |
| VSC6 | 180 | 129.97 |
| VSC7 | 90 | 47.87 |
| VSC16 | 300 | 32.58 |
| VSC16b | 300 | 32.58 |

Table 4.4: Set-point active and reactive power of the VSC at each side of the grid-following VSC HVDC link and of the grid-forming VSCs in the central part.

It is important to note that since an analysis of the effect of adding more synchronous condensers has been carried out in the previous section, it is not studied in this one. Thus, the configurations including synchronous condensers are always composed of SC6, SC7 and SC16 replacing respectively synchronous machines $g6$, $g7$ and $g16$. Synchronous machine $g16b$ being connected to the same bus as $g16$, no synchronous condenser replaces it.

FIGURES 4.40 and 4.41 illustrate the evolution of the voltage at bus 1042 within 350 seconds and the voltage at bus 1042, 1043, 4042, 4047 and 4051 within 5 seconds in all aforementioned configurations after the short-circuit at bus 4032 cleared by the tripping of line 4032-4044. TABLE C.26 in APPENDIX C presents the numerical results of this simulation.
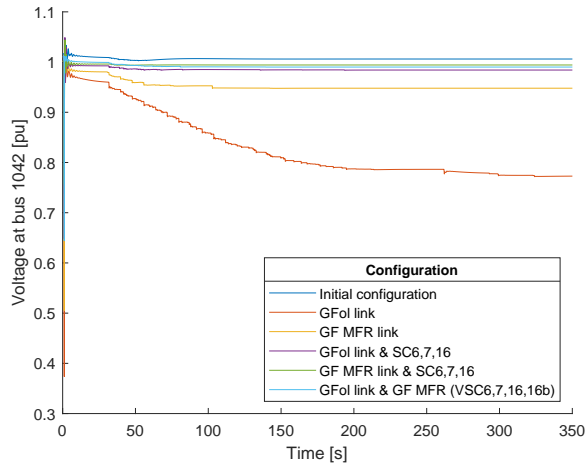


(a) Within 350 seconds.
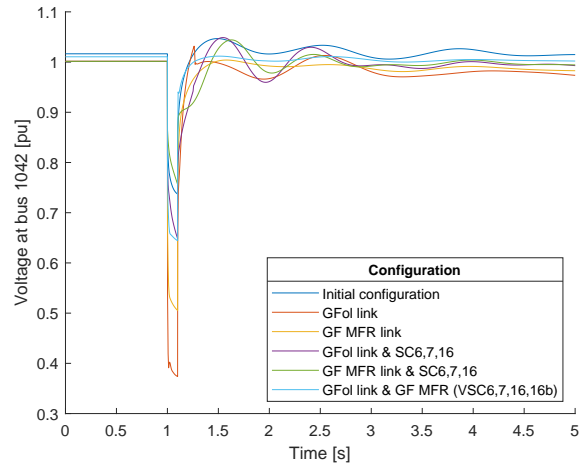
(b) Within 5 seconds.
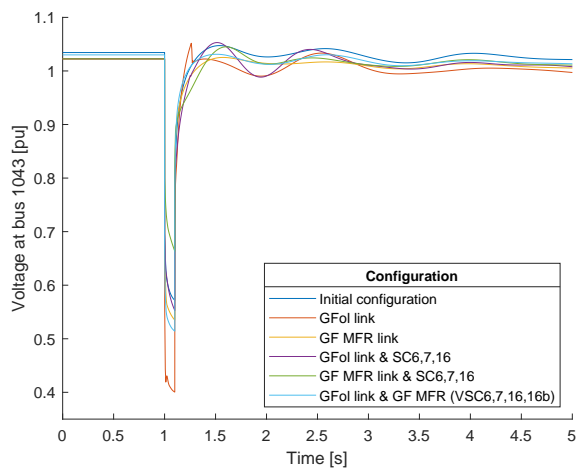


(c) Bus 1043.
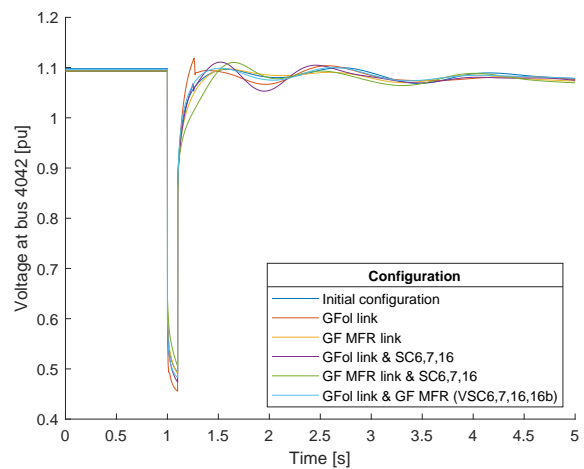
(d) Bus 4042.

Figure 4.40: Voltage at bus 1042, 1043 and 4042 after a short-circuit at bus 4032 and the tripping of line 4032-4044, with both types of HVDC links and various technologies.
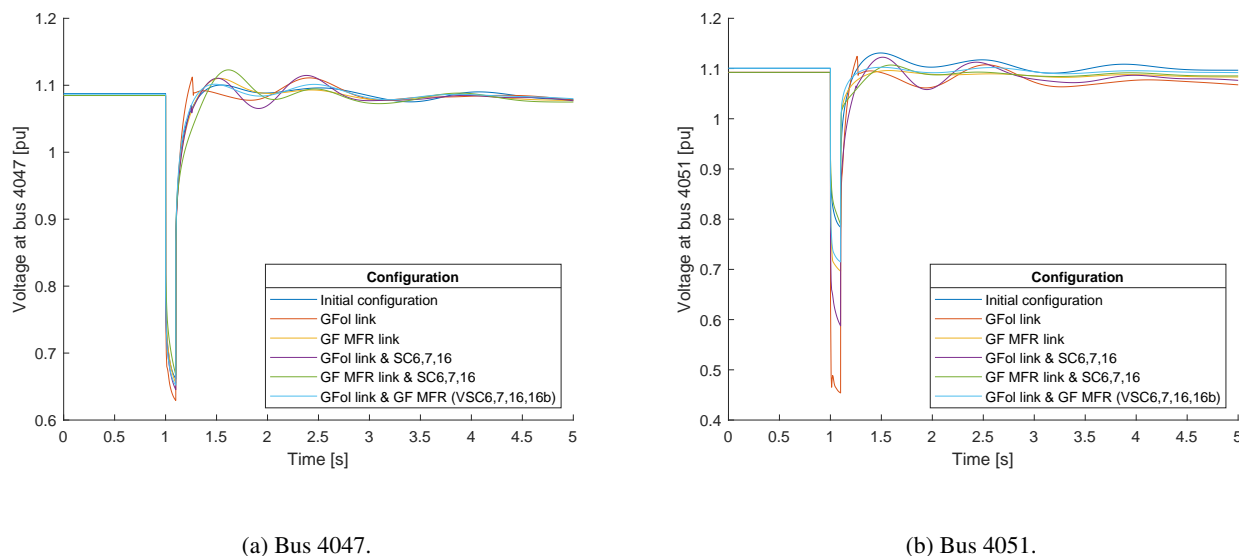
(a) Bus 4047.



(b) Bus 4051.

Figure 4.41: Voltage at bus 1043, 4042, 4047 and 4051 after a short-circuit at bus 4032 and the tripping of line 4032-4044, with both types of HVDC links and various technologies.

These figures give information about the voltage control of each configuration. First, it can be seen that the best configuration in terms of voltage stability is the one where the grid-forming VSC HVDC link is used together with three synchronous condensers, for all bus. This configuration leads to the less deep voltage drop after the short-circuit and is similar to the one studied in the previous chapter where the central part of the network is composed of a grid-forming VSC and synchronous condenser replacing a synchronous machine initially placed there. The grid-forming VSC connected at bus 4045 imposes the voltage at this bus and supports it with the help of synchronous condensers added to the network and the synchronous machines left in the central part. The second best configuration is the initial configuration. Synchronous machines placed in the central part of the network help in the voltage stability by providing short-circuit power. However, this configuration is not that much comparable in terms of the value the voltage drop reaches since the load flow is different from the three others, which leads to different initial voltages.

Second, the three next best configurations are the following ones : the one where only the grid-forming VSC HVDC link is used and the ones where the grid-following VSC HVDC link is used either with the synchronous condensers or the grid-forming VSCs. For buses 1042 and 1043, this is the configuration with the grid-following VSC HVDC link and the synchronous condensers that is the best among the three. This is caused by the presence of the synchronous condenser connected at these bus that produce reactive power and provide short-circuit power to help in the voltage support. Then, for buses 4042 and 4047, this is the configuration with only the grid-forming VSC HVDC that gives rise to a less deep voltage drop. Finally, the configuration mixing the grid-following VSC HVDC link with the grid-forming VSC gives rise to a less deep voltage drop at bus 4051. Again, the load flow of this configuration is based on a different load flow compared to the others. Comparing the exact value reached by the voltage during the transient as well as the steady-state value of each bus is thus not very relevant.

Finally, the worst configuration is the one that is composed of the grid-following VSC HVDC only.  As for the bus voltages shown in the previous analysis focusing in the voltage control, and more especially in the voltage stability in this particular case, the LTCs placed in the network are activated after 30 seconds to stabilise the voltage but a cascade effect occurs and causes a collapse of the power network.  This effect is eliminated by either changing the type of the VSC connected to bus 4045, i.e. using the grid-forming VSC HVDC link, or by using synchronous condensers or grid-forming VSCs connected to some bus in the central part of the network.  This way, the voltage is better supported and this cascade effect caused by the LTCs does not occur.  As explained in the previous analysis, this effect can also be cleared in practice by modifying the operation of the LTCs themselves.

FIGURE 4.42 shows the current in each VSC after the short-circuit at bus 4032 followed by the tripping of line 4032-4044, in the configuration where the grid-following VSC HVDC link is used with grid-forming converters replacing $g6$, $g7$, $g16$ and $g16b$. TABLE C.27 in APPENDIX C presents the numerical results of this simulation.
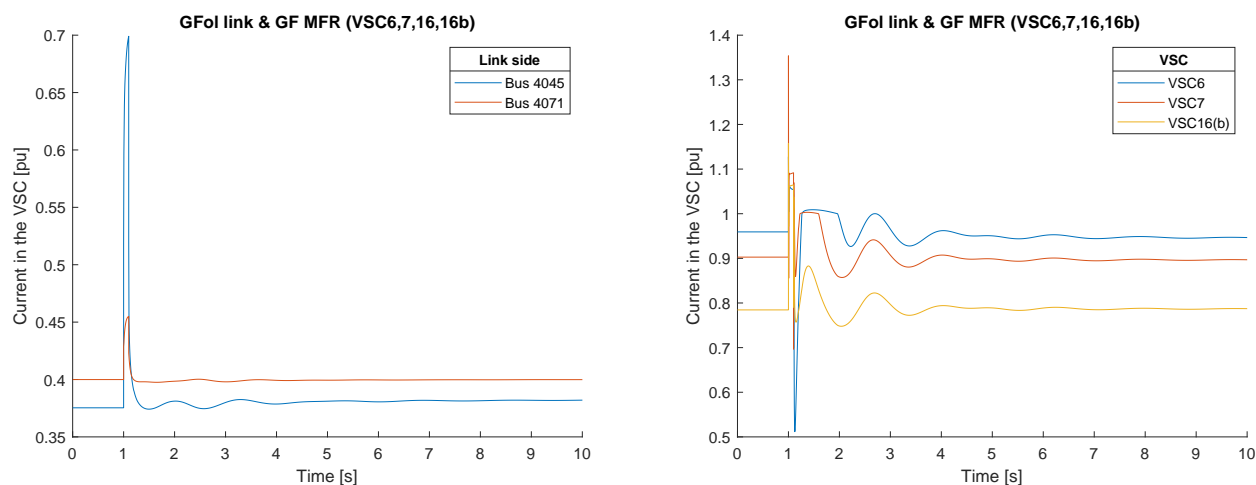


(a) Grid-following VSC HVDC link.                        (b) Grid-forming VSCs.

Figure 4.42: Current in the VSCs at both sides of the VSC HVDC link and grid-forming VSC6,7,16, 16b after a short-circuit at bus 4032 and the tripping of line 4032-4044, with the grid-following HVDC link and the grid-forming converters VSCs.

The current in the VSCs at both sides of the HVDC link is characterized by a certain peak due to the short-circuit and then decreases to a steady-state value similar to the initial one after the tripping of line 4032-4044. The peak is more pronounced in the VSC connected to bus 4045 since it is closer to the short-circuit than the VSC connected in the equiv. part to bus 4071. For both VSCs, the current is always smaller than 1 pu which is not the case for the grid-forming VSCs whose current limiter is thus triggered. This causes a peak due to the delay before the virtual impedance is activated that has no physical meaning. After this peak, the current is limited to 1.1 pu and decreases to a steady-state value similar to the initial one by the means of the tripping of line 4032-4044 that clears the short-circuit.

FIGURE 4.43 shows the current in each VSC connected at both sides of the HVDC link after the short-circuit at bus 4032 and the tripping of line 4032-4044. The upper graphs show the results without the addition of synchronous condenser while the lower graphs are the ones obtained with the configuration of the network where synchronous condensers are placed instead of synchronous machines $g6$, $g7$ and $g16$. TABLE C.27 in APPENDIX C presents the numerical results of this simulation.
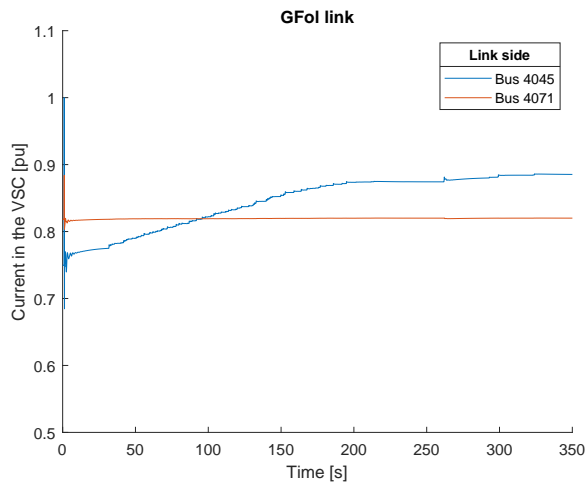


(a) Grid-following VSC HVDC link.
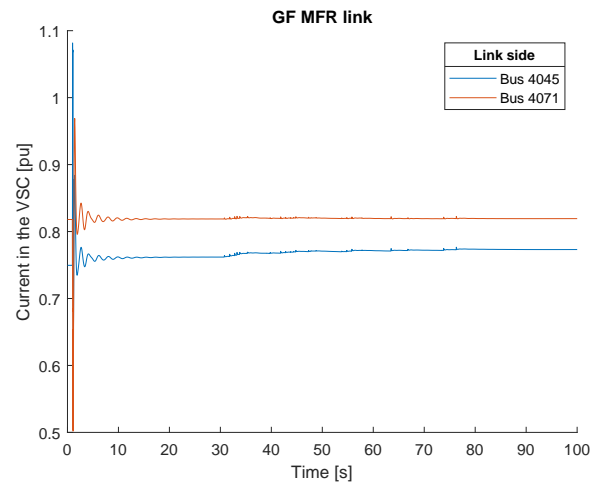
(b) Grid-forming VSC HVDC link.
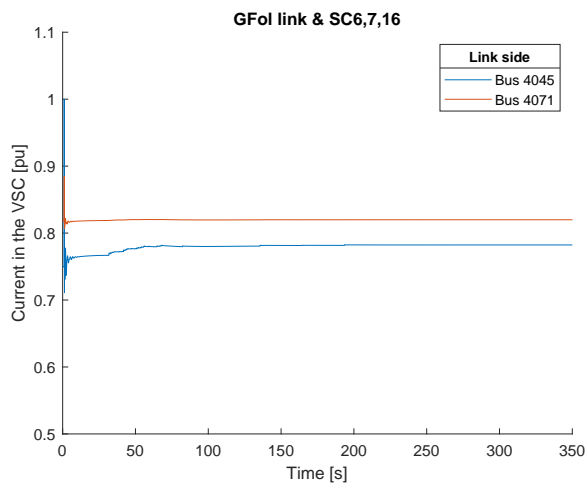
(c) Grid-following VSC HVDC link with SC6,7,16.
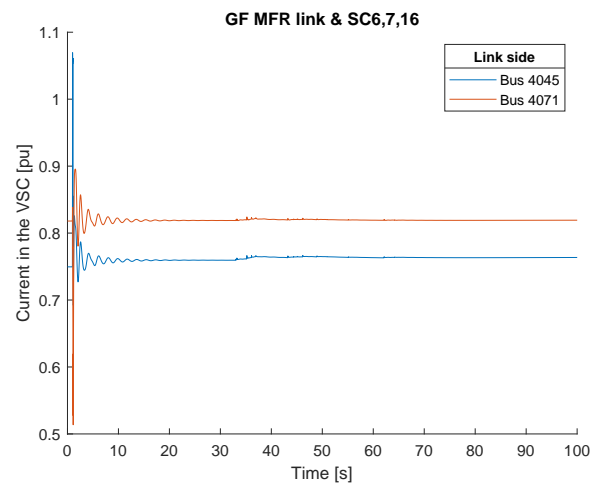
(d) Grid-forming VSC HVDC link with SC6,7,16.

Figure 4.43: Current in the VSCs after a short-circuit at bus 4032 and the tripping of line 4032-4044, with both types of HVDC links without and with synchronous condensers.

First, as in the previous figures, the current in the VSC connected to bus 4071 is not subjected to a high peak due to the electrical distance between this bus and bus 4032 where the short-circuit occurs. In the case of the grid-

following VSC HVDC, the current in the VSC connected to bus 4045 is increasing after the peak limited to 1 pu by the current limiter. This peak is due to the short-circuit after which the VSC produces reactive power to support the voltage. The current increase in the long term is directly linked to the voltage drop caused by the activation of the LTCs in the network during the whole time span of the simulation. With the addition of the synchronous condensers, the network gets rid of this harmful effect caused by the LTCs and the current is more stable with time. For the grid-forming VSC HVDC link, the current is characterized by a peak due to the delay of the activation of the virtual impedance but is lower than 1.1 pu anyway. The peak is due to the fact that the VSC provides some current after the occurrence of the fault to support the voltage at bus 4045 to which it is connected. With the synchronous condensers, this peak is a bit reduced by the means of their short-circuit power capacity.

FIGURE 4.44 shows the reactive power produced by each synchronous condenser after the short-circuit at bus 4032 followed by the tripping of line 4032-4044, in the configuration where both types of VSC HVDC links are used together with synchronous condensers replacing synchronous machines $g6$, $g7$ and $g16$. TABLE C.28 in APPENDIX C presents the numerical results of this simulation.
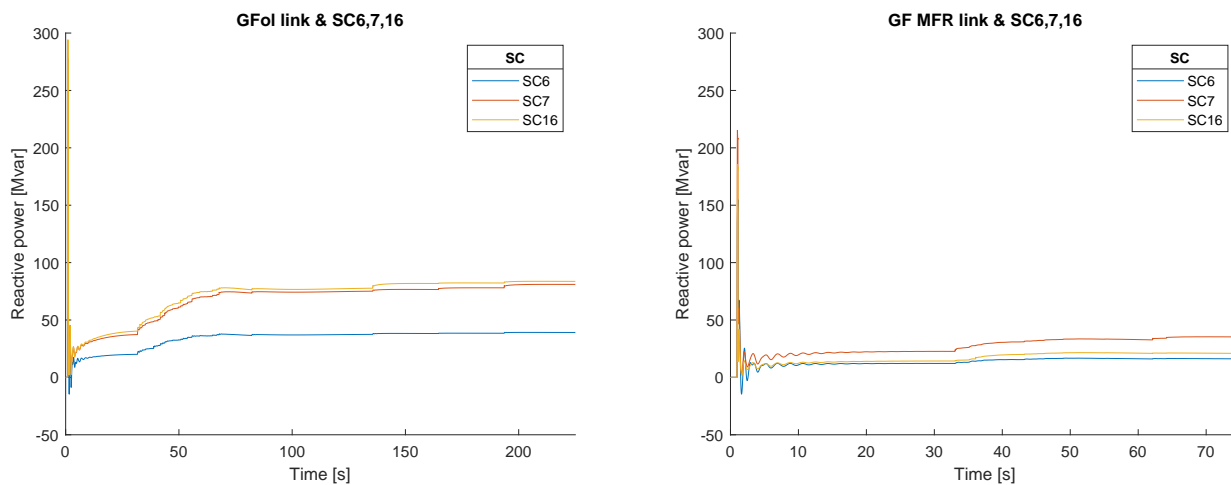


(a) Grid-following VSC HVDC link with SC6,7,16.      (b) Grid-forming VSC HVDC link with SC6,7,16.

Figure 4.44: Produced reactive power by synchronous condensers after the a short-circuit at bus 4032 and tripping of line 4032-4044, with both types of HVDC links with synchronous condensers.

In both figures, the reactive power produced by each synchronous condenser is first characterized by a peak following the short-circuit at bus 4032. This shows that the synchronous condensers provide reactive power to support the voltage in the central part of the network. Then, when the fault is cleared, the reactive power produced by each synchronous condenser is reduced and stabilizes to a steady-state value. The peaks as well as the steady-state values are higher with the grid-following VSC HVDC link since the grid-forming VSC HVDC link is more suited for voltage support. Indeed, with the grid-following VSC HVDC link, the peak reached by the reactive power produced by each synchronous condenser ranges from 202.37 to 294.16 Mvar compared to the values ranging from 154.74 and 215.22 Mvar for the grid-forming VSC HVDC link. The steady-state values are equal to 39.14, 81.02 and 83.66 Mvar for SC6, SC7 and SC16 respectively with the grid-following VSC HVDC link. With the grid-

forming one, these values become equal to 16.36, 35.75 and 21.18 Mvar for each respective synchronous condenser. The effect of the grid-forming connected to bus 4045 can also be noticed by the fact that the synchronous condenser that produce the highest amount of reactive power is not SC16 anymore, connected to bus 4042 which is close to bus 4045, but SC7.

As it can be noticed, both the peak and the steady-state value of the reactive power produced by SC6 are the lowest values compared to SC7 and SC16. This synchronous condenser could be removed and the same study could have been performed with SC7 and SC16 only. Indeed, adding a synchronous condenser imply a certain cost and this machine has to be really necessary. However, this is especially the case in this situation but a short-circuit could arise at any bus in the network where SC6 could potentially be necessary for the voltage support. The choice of leaving SC6 has also been taken by consistency since in the previous chapter the study in SECTION 4.3.3 has been carried out with synchronous condensers replacing every removed synchronous machine from the central part of the network.

### 4.4.5.1    Conclusions of the simulations

It can be concluded that the best configuration uses the grid-forming VSC HVDC link together with synchronous condensers. This configuration is similar to the one analysed in the previous section where each synchronous machine is replaced with a grid-forming converter in parallel with a synchronous condenser. In these configurations, the voltage support is optimal because of the topology of the VSC and thanks to the short-circuit power provided by the synchronous condensers. The second best configuration is the initial one where synchronous machines also provide short-circuit power while the worst configuration is when the grid-following VSC HVDC link is used without any other technology. The topology of the grid-following converters acting as current sources is not strong enough to support the voltage and in the long term the LTCs are activated causing the network to collapse. This result is similar to the one obtained in the voltage control analysis. This confirms that if the grid-following VSC HVDC link is used, modifications should be carried out in the network. The other three configurations give changing results depending on the bus that is considered and each of them has some advantages. The configuration with the grid-forming VSC HVDC has the grid-forming VSC connected in the central part of the network. Then the configurations with the grid-following VSC HVDC link used either with synchronous condensers or with grid-forming VSCs in the central part of the network show that the presence of a technology helping in the voltage support allows to use the grid-following VSC HVDC link without causing the network collapse. Nevertheless, the configurations are characterized by different load flows. This makes the comparison not very relevant in terms of the exact values reached during the voltage drop or in steady state.

Regarding the current in each VSC, they are all characterized by a peak due to the short-circuit. When comparing the peaks reached by the VSCs at both ends of the HVDC link, the peak reached by the one connected in the equiv. part at bus 4071 is not significant because of the long electrical distance between this bus and bus 4032 where the short-circuit occurs. Because of this short-circuit, the current limiter is activated in most of the configurations. The grid-following VSCs limit to 1 pu the current they produce while the grid-forming ones activate their virtual impedance when the current is higher than 1 pu. This takes a certain delay and causes a non-physical peak due to the phasor approximation. In all cases, after the tripping of the line clearing the short-circuit, the current is reduced except in the configuration where the grid-following VSC HVDC link is used alone. In that situation, the network collapse visible in the voltage curves caused by the activation of the LTCs makes the VSCs increase their current in the long term.

Finally, the reactive power produced by each synchronous condenser reaches a peak after the occurrence of the short-circuit to support the voltage in the central part of the network. Then it reaches a steady state where it produces a finite amount of reactive power. The configuration using the grid-forming VSC HVDC link better supports the voltage compared to the grid-following one that allows the synchronous condensers to produce less reactive power during the whole time span.

# Chapter 5

# Challenges

Reaching a 100 % renewable grid is complex and some challenges are still to be met by TSOs.

First, TSOs have to define the new grid code, standards and limits when moving towards a low or zero inertia network. By means of deep studies, these new criteria would take into account that the frequency regulation and the voltage control provided by renewable energy sources in an effective and intelligent way. These studied should also consider the limits and the delays of the converters that connect RES to the grid [8]. Moreover, as the dynamics differs between synchronous machines and converters, the overall response to grid faults including the response time, the Rate of Change of Frequency or the depth of the voltage drop is different as well. Depending on these new grid codes, a further analysis should be launched to tune the parameters of each network component. For instance, the implementation of virtual inertia has been studied but there are still some questions about the exact inertia value to assign to converters, if this inertia should be distributed amongst all of them or if it should be concentrated somewhere in the network. In parallel, the exact role of the system operator and the power market should be revised as well [25, 27].

Then, additional studies and economic analyses should focus on the reserve policy. Indeed, in these simulations, the energy buffer behind each converter is not considered. It is assumed that the power produced by the RES can replace the power initially produced by the synchronous machine that is removed. In practice, this change depends on the weather conditions, the geographic location, the power coming from the interconnections, the balance between cost and technical performance and other parameters. This deeper analysis should take into account all these parameters for each specific network and a certain reserve margin [8].

Finally, the type of energy buffer behind the converters should be carefully chosen as well. Either PV, batteries or wind power plants, this RES should be able to respond to the grid services. Grid-following or grid-forming converters should be properly sized, allocated and organized in the network to make it safe and stable all the time. They should be able to operate with existing grid components and synchronize with interconnected systems [26]. This change in the grid topology, i.e. moving from synchronous machines to an inverter-based power network, will take time and will require the installation of millions of inverter-interfaced variable renewable energy units [16].

# Conclusion

The main purpose of this master thesis is to analyse the dynamics and the control of low inertia networks with high penetration of renewable energy sources. Connected to the grid through converters, these renewable energy sources are expected to participate in the frequency regulation and voltage control to ensure the network stability. These services should be provided to the grid even though changes occur while moving towards a zero inertia grid. Solutions have been proposed not only to manage the energy buffer behind the converters, typically wind power plants, PV or batteries, but also to find solutions to participate in frequency reserves and support the voltage after the occurrence of a grid fault. In this work, the comparison between grid-following and grid-forming converters is studied in various situations. These are modelled as injectors and the RES connected to the grid through these converters is not considered. Their general topology is compared : grid-following converters acting as a current source produce active and reactive powers depending on the active power and voltage set-points while grid-forming converters act as a voltage source and implement both virtual inertia and a frequency droop.

Two different situations have been studied in the simulation part of this thesis. The first one is the modification of the central part of the existing Nordic network where synchronous machines are replaced with RES connected either through grid-following or grid-forming converters. The other situation is when several synchronous machines initially placed in this network part are removed. The active power that they initially produce is compensated by power coming from an interconnection transferred through a VSC HVDC link. Three specific analyses have been carried out in both situations : the frequency response, the voltage control of the modified network and an analysis focusing on the effect of various technologies added to the network, including VSCs, synchronous condensers and/or the VSC HVDC link.

Concerning the frequency response, the conclusions drawn are different in each situation. In the first one, the frequency drop is deeper and the RoCoF is higher with VSCs compared to synchronous machines but the frequency recovery is faster. In the second situation including the VSC HVDC link, connecting it with a grid-following VSC in the central part improves the frequency response of the network since the voltage is less supported making the loads consume less active power, which has the effect opposite to a grid-forming VSC. The PLL of the grid-forming VSCs correctly estimates the system frequency except for the computation at the occurrence of the fault. When these VSCs have a 4 % droop instead of an infinite one, the frequency regulation is improved but the current flowing in the VSCs increases proportionally to the active power generated by the RES. In both situations and for all configurations, the system frequency does not deviate from its nominal value by more than 5 % and the current in the VSCs does not exceed 1.1 pu, even during the transient period, which makes all configurations safe and acceptable.

Regarding the voltage control, it has been analysed in both situations. In the first situation, the voltage is better supported with VSCs compared to synchronous machines : the voltage drops are less deep, the voltage is more stable in the long term and the oscillations due to the synchronous machines are removed. Nevertheless, these changes are visible only at the bus electrically close to the replacement of synchronous machines with VSCs. In this first situation, no significant changes occur whatever the VSC type, which is not the case in the second situation.

Indeed, with the VSC HVDC link, the network collapses if the connection in the central part is achieved through a grid-following VSC. Removing LTCs from the network allows to get rid of this effect and use either link. This collapse does not occur with the grid-forming VSC HVDC link that better supports the bus voltages during the transient period and in the long term. By modifying the configuration with the grid-following VSC HVDC link, all configurations are acceptable since the voltages reach admissible steady-state values between 0.9 and 1.1 pu and the current in the VSCs is always lower than 1.1 pu.

Finally, the third analysis considers different configurations and compares their voltage control after the occurrence of a short-circuit cleared 100 milliseconds later. Both the grid-following VSCs and the VSC HVDC link give rise to the network collapse and are not able to operate safely standalone. They need the voltage support of grid-forming VSCs or the short-circuit power provided by synchronous condensers. As a confirmation, the best configuration in both situations is using all VSCs in grid-forming mode, putting either the injectors or the HVDC link connection in the central part, used together with synchronous condensers. Any other configuration yields to deeper bus voltage drops compared to the initial configuration of the Nordic network. The results obtained with the grid-forming VSCs or VSC HVDC link operating standalone are similar to those obtained with the grid-following VSCs or VSC HVDC link used together with synchronous condensers. Finally, a mix of the grid-following VSCs or VSC HVDC link and grid-forming VSCs is stable but not as good as the other configurations. The current in the VSCs connected to the bus in the central part reaches a peak higher than 1 pu causing the activation of their current limiter. This considerably limits the performance of the VSC itself compared to synchronous machines which transient current can reach very high values during the transient period.

# Appendices

# Appendix A

# Acronyms

| | |
|---|---|
| **ALS** | Automatic Load Shedding |
| **AGC** | Automatic Generation Control |
| **ASE** | Aggregated Swing Equation |
| **AVR** | Automatic Voltage Regulator |
| **DFIG** | Doubly Fed Induction Generator |
| **ESS** | Energy System Storage |
| **FCSG** | Full Converter Synchronous Generator |
| **FFR** | Fast Frequency Response |
| **LTC** | Load Tap Changer |
| **MPP** | Maximum Power Point |
| **PCC** | Point of Common Coupling |
| **PLL** | Phased-Locked Loop |
| **PV** | Photovoltaic |
| **RES** | Renewable Energy Sources |
| **RoCoF** | Rate of Change of Frequency |
| **SC** | Synchronous Condenser |
| **SM** | Synchronous Machine |
| **SG** | Synchronous Generator |
| **SOC** | State Of Charge |
| **SVC** | Static Var Compensator |
| **TSO** | Transmission System Operator |
| **VSC** | Voltage-Source Converter |

# Appendix B

# Operation of grid-following and grid-forming converters

This appendix consists in the presentation of the basic operation of the model of both types of VSCs. The simple grid model used in the simulations is represented in FIGURE B.1, where $v_{dc}$, $i_{dc}$, $\bar{I}$, $R_{pr}$ and $L_{pr}$ are the same quantities as the ones described in SECTION 3.3.4. The VSC, acting as an injector, is connected to the left side of a line characterized by an impedance $R_g + j \cdot X_g$, which is connected to an ideal voltage source on the other side, with a constant voltage $V_R$. $P_L$ and $Q_L$ are respectively the active and reactive powers injected from the left side of the line, while $P_R$ and $Q_R$ are those coming from the right side.
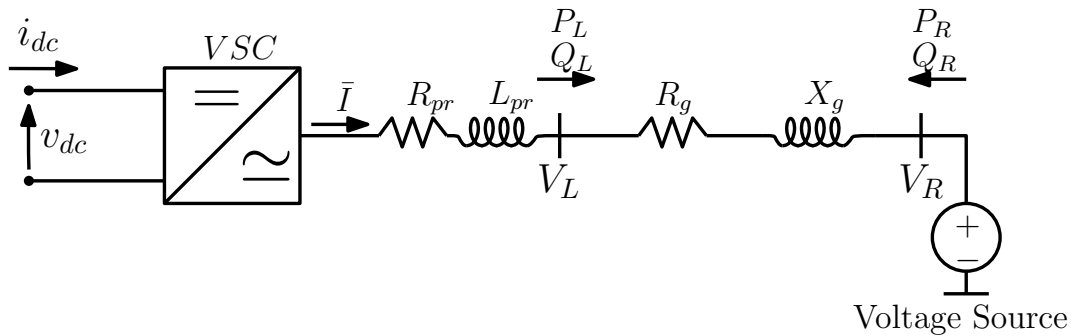


Figure B.1: Simple grid model supplied by a Voltage-Source Converter [3].

The data used for the simulation is the following :

- Voltage-source converter : apparent and active nominal powers are respectively $S_{nom} = 1000$ MVA and $P_{nom} = 900$ MW ;

- Phase reactor : $R_{pr} = 0.005$ pu and $L_{pr} = 0.15$ pu ;

- AC line : rated at 400 kV, with an impedance $R_g + j \cdot X_g = 0.033 + j \cdot 0.33$ pu ;

- $P_L = 200$ MW and $Q_L = -13.24$ Mvar ;

- $P_R = -198.66$ MW and $Q_R = 26.62$ Mvar ;

- $V_R = V_L = 1$ pu (bus at voltage $V_R$ is the slack bus) ;

- $S_{base} = 1000$ MVA and $V_{base} = 400$ kV ;

- Grid-forming VSC : $m_p = 0.0033$ pu and $\omega_c = 33.33$ pu/s. These parameters have been tuned so that no oscillation occurs in the produced power after a disturbance and are kept for all the simulations using this model of grid-forming VSCs. Their value gives rise to a virtual inertia of $H = \frac{1}{2m_p\omega_c} = 4.5$ s using EQ. 3.6.

Simulations have been carried out with a change in the active power set-point $\Delta P^*$ set to 0.2 pu. Results are shown in FIGURE B.2, including the produced power and the current in each VSC, the frequency estimated by the PLL of grid-forming VSC and the bus voltages at both line ends $V_R$ and $V_L$.
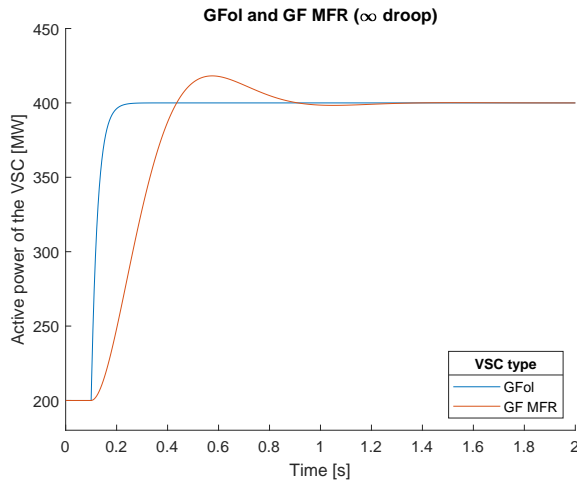


(a) Produced active power of both types of VSCs.
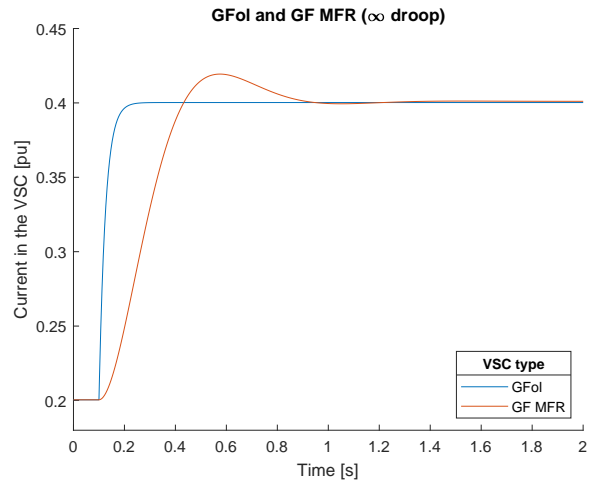


(b) Current in the VSC.
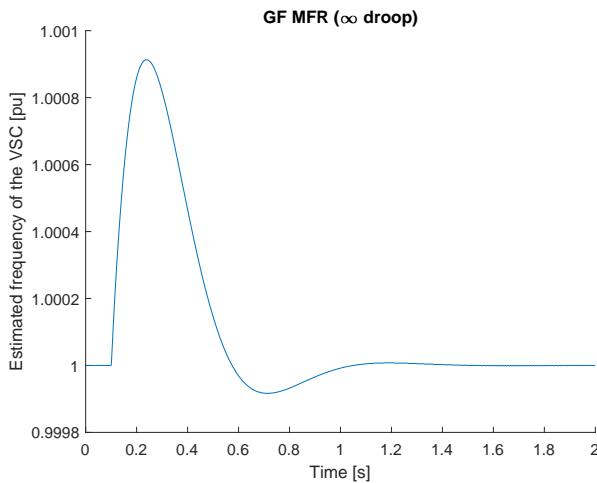


(c) Frequency estimated by the grid-forming VSC.
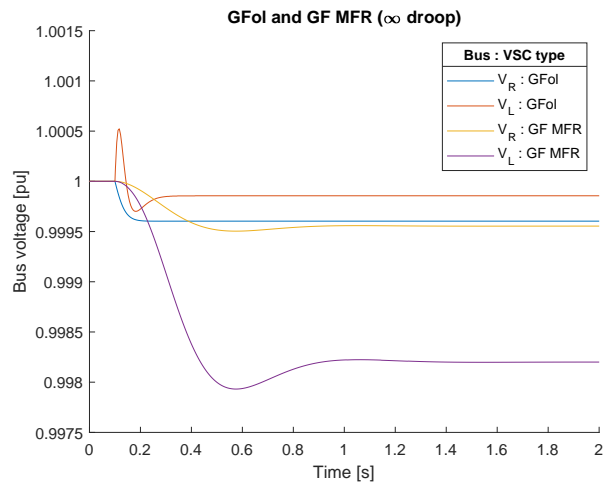


(d) Bus voltages $V_R$ and $V_L$, for both types of VSCs.

Figure B.2: Results of the dynamic simulation of the simple grid model supplied by a grid-following or grid-forming VSC with $\Delta P^* = 0.2$ pu.

Some comments arise from the results of the simulations. First, in both cases, the converter reacts to the difference in the active power set-point $P^*$ by increasing its produced power from 200 to 400 MW. The grid-following VSC reacts more rapidly to the disturbance since it is characterized by faster dynamics while the grid-forming VSC has a certain inertia that slows its dynamics down. It can obviously be noticed that the curves related to the produced power are similar to those representing the current in the VSC, for both types of converters. This effect is directly related to the relation :

$$I = \frac{\sqrt{P^2 + Q^2}}{V_m},$$

where $Q \ll P$ thus $\sqrt{P^2 + Q^2} \approx P$ and $V_m = 1$ pu, which gives $I \approx P$, if both are taken in per-unit and for both types of VSCs. The evolution of the estimated frequency is directly related to the evolution of the produced power of the VSC and it thus takes the same time to reach the steady-state value of 1 pu. The peak comes from the imbalance in active power during the transient period where the VSC has not produced the right amount of active power yet. Finally, the time the voltages takes to reach a steady state is also greater with the grid-forming compared to the grid-following VSC.

# Appendix C

# Application to the Nordic network

Since lots of curves are shown in a same graph in CHAPTER 4, tables are presented below to give the main characteristics of each curve : the deviation between the initial value and the minimal or maximal value reached during the transient period mentioned as "Maximum transient deviation", the minimum or maximum value and the steady-state value reached by the measure.

## C.1  Initial configuration of the Nordic network

Table C.1: Characteristics of rotor speeds $\omega_{g12}$ and voltages $V_{bus}$ in the central part after different events (loss of $g1$ or $g15$, tripping of line 4032-4044 and the short-circuit at bus 4032 cleared by the tripping of line 4032-4044), with the initial configuration of the Nordic network.

| Event | Measure | Maximum transient deviation [%] | Minimum value [pu] | Steady-state value [pu] |
|---|---|---|---|---|
| Loss of $g1$ | $\omega_{g12}$ | 0.93 | 0.9907 | 0.9968 |
| Loss of $g15$ | $\omega_{g12}$ | 0.69 | 0.9931 | 0.9969 |
| Tripping of line 4032-4044 | $V_{1042}$ | 2.22 | 0.9939 | 1.0061 |
| | $V_{1043}$ | 3.52 | 0.9980 | 1.0051 |
| | $V_{4042}$ | 3.60 | 1.0583 | 1.0650 |
| | $V_{4047}$ | 2.92 | 1.0559 | 1.0698 |
| | $V_{4051}$ | 2.33 | 1.0748 | 1.0892 |
| Short-circuit at bus 4032 and tripping of line 4032-4044 | $V_{1042}$ | 27.48 | 0.7372 | 1.0061 |
| | $V_{1043}$ | 44.72 | 0.5718 | 1.0051 |
| | $V_{4042}$ | 55.04 | 0.4937 | 1.0650 |
| | $V_{4047}$ | 39.17 | 0.6616 | 1.0698 |
| | $V_{4051}$ | 28.76 | 0.7840 | 1.0892 |

## C.2 Replacement of synchronous machines in the central part with Voltage-Source Converters

### C.2.1 Frequency response

Table C.2: Characteristics of the rotor speed of $g12$ after the loss of $g1$, with the replacement of SMs in the central part with VSCs, for different droops.

| Configuration | GF MFR droop | Maximum transient deviation [%] | Minimum value [pu] | Steady-state value [pu] |
|---|---|---|---|---|
| Initial configuration | - | 0.93 | 0.9907 | 0.9968 |
| GFol | - | 1.33 | 0.9867 | 0.9968 |
| GF MFR | $\infty$ | 1.23 | 0.9877 | 0.9968 |
| | 4 % | 0.45 | 0.9955 | 0.9979 |

Table C.3: Characteristics of the frequency estimated by each VSC after the loss of $g1$, with the replacement of SMs in the central part with grid-forming converters, for different droops.

| VSC | GF MFR droop | Maximum transient deviation [%] | Minimum value [pu] | Steady-state value [pu] |
|---|---|---|---|---|
| VSC6 | $\infty$ | 1.23 | 0.9877 | 0.9968 |
| | 4 % | 0.45 | 0.9955 | 0.9979 |
| VSC7 | $\infty$ | 1.23 | 0.9877 | 0.9968 |
| | 4 % | 0.45 | 0.9955 | 0.9979 |
| VSC14 | $\infty$ | 1.23 | 0.9877 | 0.9968 |
| | 4 % | 0.45 | 0.9955 | 0.9979 |
| VSC15(b) | $\infty$ | 1.23 | 0.9877 | 0.9968 |
| | 4 % | 0.45 | 0.9955 | 0.9979 |
| VSC16(b) | $\infty$ | 1.23 | 0.9877 | 0.9968 |
| | 4 % | 0.45 | 0.9955 | 0.9979 |

Table C.4: Characteristics of the current in each VSC after the loss of $g1$, with the replacement of SMs in the central part with VSCs, for different droops.

| VSC | VSC type | GF MFR droop | Maximum value [pu] | Steady-state value [pu] |
|---|---|---|---|---|
| | GFol | - | 0.9213 | 0.9061 |
| VSC6 | GF MFR | $\infty$ | 0.9520 | 0.9061 |
| | GF MFR | 4 % | 1.0138 | 0.9516 |
| | GFol | - | 0.9167 | 0.8781 |
| VSC7 | GF MFR | $\infty$ | 0.9248 | 0.8781 |
| | GF MFR | 4 % | 0.9817 | 0.9196 |
| | GFol | - | 0.8396 | 0.8211 |
| VSC14 | GF MFR | $\infty$ | 0.8606 | 0.8211 |
| | GF MFR | 4 % | 0.9260 | 0.8677 |
| | GFol | - | 0.8383 | 0.8272 |
| VSC15(b) | GF MFR | $\infty$ | 0.8687 | 0.8272 |
| | GF MFR | 4 % | 0.9321 | 0.8729 |
| | GFol | - | 0.7865 | 0.7789 |
| VSC16(b) | GF MFR | $\infty$ | 0.8241 | 0.7789 |
| | GF MFR | 4 % | 0.8851 | 0.8253 |

Table C.5: Characteristics of the frequency estimated by each VSC after the loss of $g1$, with the replacement of SMs in the central part with grid-forming converters, for different droops.

| VSC having a 4 % droop | Maximum transient deviation [%] | Minimum value [pu] | Steady-state value [pu] |
|---|---|---|---|
| - | 1.23 | 0.9877 | 0.9968 |
| VSC6 | 0.94 | 0.9906 | 0.9970 |
| VSC6,7 | 0.89 | 0.9911 | 0.9971 |
| VSC6,7,14 | 0.72 | 0.9928 | 0.9973 |
| VSC6,7,14,15 | 0.61 | 0.9939 | 0.9975 |
| VSC6,7,14,15,15b | 0.54 | 0.9946 | 0.9976 |
| VSC6,7,14,15,15b,16 | 0.47 | 0.9953 | 0.9978 |
| VSC6,7,14,15,15b,16,16b | 0.45 | 0.9955 | 0.9979 |

Table C.6: Characteristics of the produced active power of each VSC after the loss of $g1$, with the replacement of SMs in the central part with VSCs, for different droops.

| VSC | VSC type | GF MFR droop | Maximum transient deviation [%] | Maximum value [MW] | Steady-state value [MW] |
|---|---|---|---|---|---|
| | GFol | - | 0.13 | 360.4840 | 359.9998 |
| VSC6 | GF MFR | ∞ | 5.54 | 379.9384 | 359.9998 |
| | GF MFR | 4 % | 12.82 | 406.1463 | 380.6554 |
| | GFol | - | 0.12 | 180.2166 | 179.9995 |
| VSC7 | GF MFR | ∞ | 5.05 | 189.0821 | 179.9995 |
| | GF MFR | 4 % | 12.79 | 203.0178 | 190.3272 |
| | GFol | - | 0.10 | 630.6350 | 630.0019 |
| VSC14 | GF MFR | ∞ | 4.87 | 660.6864 | 630.0019 |
| | GF MFR | 4 % | 12.80 | 710.6463 | 666.1491 |
| | GFol | - | 0.05 | 540.2440 | 540 |
| VSC15(b) | GF MFR | ∞ | 5.16 | 567.8901 | 540 |
| | GF MFR | 4 % | 12.81 | 609.1578 | 570.9833 |
| | GFol | - | 0.03 | 600.1999 | 599.9999 |
| VSC16(b) | GF MFR | ∞ | 5.75 | 634.4821 | 599.9999 |
| | GF MFR | 4 % | 13.48 | 680.8899 | 636.1471 |

## C.2.2  Voltage control

Table C.7: Characteristics of bus voltages in the central part after the tripping of line 4032-4044, with the replacement of SMs in the central part with VSCs.

| Measure | VSC type | Maximum transient deviation [%] | Minimum transient value [pu] | Steady-state value [pu] |
|---|---|---|---|---|
| $V_{1042}$ | GF MFR | 0.68 | 1.0096 | 1.0080 |
| | GFol | 0.89 | 1.0074 | 1.0081 |
| $V_{1043}$ | GF MFR | 1.89 | 1.0148 | 1.0083 |
| | GFol | 1.74 | 1.0163 | 1.0085 |
| $V_{4042}$ | GF MFR | 2.59 | 1.0695 | 1.0680 |
| | GFol | 2.16 | 1.0741 | 1.0682 |
| $V_{4047}$ | GF MFR | 1.20 | 1.0746 | 1.0727 |
| | GFol | 1.18 | 1.0748 | 1.0729 |
| $V_{4051}$ | GF MFR | 0.73 | 1.0925 | 1.0912 |
| | GFol | 0.88 | 1.0908 | 1.0913 |

Table C.8: Characteristics of voltage at bus 1042 after the tripping of line 4032-4044, with the replacement of SMs in the central part with VSCs.

| VSCs replacing SMs | VSC type | Maximum transient deviation [%] | Minimum transient value [pu] | Steady-state value [pu] |
|---|---|---|---|---|
| - | - | 2.22 | 0.9939 | 1.0061 |
| VSC6 | GF MFR | 0.97 | 1.0066 | 1.0074 |
| | GFol | 0.96 | 1.0067 | 1.0075 |
| VSC6,7 | GF MFR | 0.92 | 1.0071 | 1.0075 |
| | GFol | 0.90 | 1.0074 | 1.0076 |
| VSC6,7,14 | GF MFR | 0.74 | 1.0089 | 1.0078 |
| | GFol | 0.75 | 1.0089 | 1.0079 |
| VSC6,7,14,15 | GF MFR | 0.71 | 1.0093 | 1.0078 |
| | GFol | 0.73 | 1.0090 | 1.0080 |
| VSC6,7,14,15,15b | GF MFR | 0.69 | 1.0094 | 1.0079 |
| | GFol | 0.76 | 1.0087 | 1.0080 |
| VSC6,7,14,15,15b,16 | GF MFR | 0.68 | 1.0095 | 1.0080 |
| | GFol | 0.78 | 1.0085 | 1.0081 |
| VSC6,7,14,15,15b,16,16b | GF MFR | 0.68 | 1.0096 | 1.0080 |
| | GFol | 0.89 | 1.0074 | 1.0081 |

Table C.9: Characteristics of voltage at bus 4042 after the tripping of line 4032-4044, with the replacement of SMs in the central part with VSCs.

| VSCs replacing SMs | VSC type | Maximum transient deviation [%] | Minimum value [pu] | Steady-state value [pu] |
|---|---|---|---|---|
| - | - | 3.60 | 1.0583 | 1.0650 |
| VSC6 | GF MFR | 3.56 | 1.0588 | 1.0650 |
| | GFol | 3.57 | 1.0587 | 1.0650 |
| VSC6,7 | GF MFR | 3.52 | 1.0592 | 1.0651 |
| | GFol | 3.48 | 1.0597 | 1.0651 |
| VSC6,7,14 | GF MFR | 2.57 | 1.0697 | 1.0675 |
| | GFol | 2.49 | 1.0706 | 1.0676 |
| VSC6,7,14,15 | GF MFR | 2.56 | 1.0698 | 1.0677 |
| | GFol | 2.43 | 1.0712 | 1.0679 |
| VSC6,7,14,15,15b | GF MFR | 2.50 | 1.0704 | 1.0679 |
| | GFol | 2.35 | 1.0721 | 1.0681 |
| VSC6,7,14,15,15b,16 | GF MFR | 2.57 | 1.0697 | 1.0680 |
| | GFol | 2.30 | 1.0726 | 1.0681 |
| VSC6,7,14,15,15b,16,16b | GF MFR | 2.59 | 1.0695 | 1.0680 |
| | GFol | 2.16 | 1.0741 | 1.0682 |

Table C.10: Characteristics of the current in each VSC after the tripping of line 4032-4044, with the replacement of SMs in the central part with VSCs.

| VSC | VSC type | Maximum value [pu] | Steady-state value [pu] |
|---|---|---|---|
| VSC6 | GF MFR | 0.9548 | 0.9272 |
| | GFol | 0.9273 | 0.9271 |
| VSC7 | GF MFR | 0.9972 | 0.9403 |
| | GFol | 0.9409 | 0.9405 |
| VSC14 | GF MFR | 0.8571 | 0.8550 |
| | GFol | 0.8554 | 0.8551 |
| VSC15(b) | GF MFR | 0.8751 | 0.8459 |
| | GFol | 0.8459 | 0.8458 |
| VSC16(b) | GF MFR | 0.8233 | 0.7869 |
| | GFol | 0.7869 | 0.7868 |

### C.2.3    Mix of various technologies

Table C.11: Characteristics of bus voltages in the central part after a short-circuit at bus 4032 and the tripping of line 4032-4044, with the replacement of SMs in the central part with grid-following converters.

| Measure | Grid-following VSCs replacing SMs | Maximum transient deviation [%] | Minimum transient value [pu] | Steady-state value [pu] |
|---|---|---|---|---|
| $V_{1042}$ | - | 27.48 | 0.7372 | 1.0061 |
| | VSC6 | 56.55 | 0.4416 | 1.0075 |
| | VSC6,7 | 58.34 | 0.4235 | 1.0076 |
| | VSC6,7,14 | 63.22 | 0.3739 | 1.0079 |
| | VSC6,7,14,15 | 68.11 | 0.3242 | 1.0080 |
| | VSC6,7,14,15,15b | 83.99 | 0.1627 | 1.0080 |
| $V_{1043}$ | - | 44.72 | 0.5718 | 1.0051 |
| | VSC6 | 46.77 | 0.5505 | 1.0052 |
| | VSC6,7 | 52.80 | 0.4882 | 1.0070 |
| | VSC6,7,14 | 56.16 | 0.4534 | 1.0079 |
| | VSC6,7,14,15 | 59.39 | 0.4201 | 1.0081 |
| | VSC6,7,14,15,15b | 71.64 | 0.2933 | 1.0083 |
| $V_{4042}$ | - | 55.04 | 0.4937 | 1.0650 |
| | VSC6 | 55.75 | 0.4859 | 1.0650 |
| | VSC6,7 | 56.12 | 0.4818 | 1.0651 |
| | VSC6,7,14 | 63.23 | 0.4037 | 1.0676 |
| | VSC6,7,14,15 | 66.75 | 0.3651 | 1.0679 |
| | VSC6,7,14,15,15b | 79.54 | 0.2246 | 1.0681 |
| $V_{4047}$ | - | 39.17 | 0.6616 | 1.0698 |
| | VSC6 | 39.80 | 0.6548 | 1.0698 |
| | VSC6,7 | 40.12 | 0.6513 | 1.0699 |
| | VSC6,7,14 | 43.43 | 0.6153 | 1.0708 |
| | VSC6,7,14,15 | 53.35 | 0.5074 | 1.0719 |
| | VSC6,7,14,15,15b | 82.93 | 0.1856 | 1.0728 |
| $V_{4051}$ | - | 28.76 | 0.7840 | 1.0892 |
| | VSC6 | 29.70 | 0.7736 | 1.0892 |
| | VSC6,7 | 30.18 | 0.7684 | 1.0893 |
| | VSC6,7,14 | 31.84 | 0.7501 | 1.0897 |
| | VSC6,7,14,15 | 33.32 | 0.7338 | 1.0898 |
| | VSC6,7,14,15,15b | 39.66 | 0.6640 | 1.0899 |

Table C.12: Characteristics of the current in each grid-following VSC after a short-circuit at bus 4032 and the tripping of line 4032-4044, with the replacement of SMs in the central part with grid-following converters.

| VSCs replacing SMs | VSC | Maximum value [pu] | Steady-state value [pu] |
|---|---|---|---|
| VSC6 | VSC6 | 1 | 0.9288 |
| VSC6,7 | VSC6 | 1 | 0.9285 |
| | VSC7 | 1 | 0.9450 |
| VSC6,7,14 | VSC6 | 1 | 0.9277 |
| | VSC7 | 1 | 0.9424 |
| | VSC14 | 1 | 0.8562 |
| VSC6,7,14,15 | VSC6 | 1 | 0.9275 |
| | VSC7 | 1 | 0.9418 |
| | VSC14 | 1 | 0.8557 |
| | VSC15 | 1 | 0.8475 |
| VSC6,7,14,15,15b | VSC6 | 1 | 0.9274 |
| | VSC7 | 1 | 0.9413 |
| | VSC14 | 1 | 0.8553 |
| | VSC15(b) | 1 | 0.8459 |

Table C.13: Characteristics of bus voltages in the central part after a short-circuit at bus 4032 and the tripping of line 4032-4044, with the replacement of SMs in the central part with grid-following converters and synchronous condensers.

| Measure | Configuration | Maximum transient deviation [%] | Minimum transient value [pu] | Steady-state value [pu] |
|---|---|---|---|---|
| $V_{1042}$ | GFol & SC6 | 62.36 | 0.3826 | 1.0113 |
| | GFol & SC6,7 | 58.58 | 0.4210 | 1.0120 |
| | GFol & SC6,7,14 | 50.61 | 0.5020 | 1.0123 |
| | GFol & SC6,7,14,15 | 42.57 | 0.5837 | 1.0124 |
| | GFol & SC6,7,14,15,16 | 36.29 | 0.6476 | 1.0125 |
| $V_{1043}$ | GFol & SC6 | 93.46 | 0.0677 | 1.0087 |
| | GFol & SC6,7 | 79.17 | 0.2155 | 1.0203 |
| | GFol & SC6,7,14 | 69.83 | 0.3121 | 1.0213 |
| | GFol & SC6,7,14,15 | 58.26 | 0.4317 | 1.0215 |
| | GFol & SC6,7,14,15,16 | 49.27 | 0.5247 | 1.0219 |
| $V_{4042}$ | GFol & SC6 | 93.46 | 0.0718 | 1.0682 |
| | GFol & SC6,7 | 96.04 | 0.0435 | 1.0704 |
| | GFol & SC6,7,14 | 82.17 | 0.1957 | 1.0747 |
| | GFol & SC6,7,14,15 | 70.04 | 0.3289 | 1.0750 |
| | GFol & SC6,7,14,15,16 | 64.22 | 0.3928 | 1.0755 |
| $V_{4047}$ | GFol & SC6 | 81.43 | 0.2020 | 1.0729 |
| | GFol & SC6,7 | 84.30 | 0.1708 | 1.0745 |
| | GFol & SC6,7,14 | 85.59 | 0.1567 | 1.0760 |
| | GFol & SC6,7,14,15 | 64.59 | 0.3852 | 1.0776 |
| | GFol & SC6,7,14,15,16 | 57.30 | 0.4644 | 1.0779 |
| $V_{4051}$ | GFol & SC6 | 88.95 | 0.1216 | 1.0914 |
| | GFol & SC6,7 | 80.70 | 0.2124 | 1.0926 |
| | GFol & SC6,7,14 | 90.73 | 0.1020 | 1.0932 |
| | GFol & SC6,7,14,15 | 76.02 | 0.2639 | 1.0933 |
| | GFol & SC6,7,14,15,16 | 49.82 | 0.5522 | 1.0945 |

Table C.14: Characteristics of the current in each grid-following VSC after a short-circuit at bus 4032 and the tripping of line 4032-4044, with the replacement of SMs in the central part with grid-following converters and synchronous condensers.

| VSC | Configuration | Maximum value [pu] | Steady-state value [pu] |
|---|---|---|---|
| VSC6 | GFol & SC6 | 1 | 0.9183 |
| | GFol & SC6,7 | 1 | 0.9172 |
| | GFol & SC6,7,14 | 1 | 0.9164 |
| | GFol & SC6,7,14,15 | 1 | 0.9162 |
| | GFol & SC6,7,14,15,16 | 1 | 0.9159 |
| VSC7 | GFol & SC6 | 1 | 0.9350 |
| | GFol & SC6,7 | 1 | 0.9088 |
| | GFol & SC6,7,14 | 1 | 0.9065 |
| | GFol & SC6,7,14,15 | 1 | 0.9060 |
| | GFol & SC6,7,14,15,16 | 1 | 0.9050 |
| VSC14 | GFol & SC6 | 1 | 0.8524 |
| | GFol & SC6,7 | 1 | 0.8509 |
| | GFol & SC6,7,14 | 1 | 0.8437 |
| | GFol & SC6,7,14,15 | 1 | 0.8432 |
| | GFol & SC6,7,14,15,16 | 1 | 0.8425 |
| VSC15(b) | GFol & SC6 | 1 | 0.8442 |
| | GFol & SC6,7 | 1 | 0.8432 |
| | GFol & SC6,7,14 | 1 | 0.8410 |
| | GFol & SC6,7,14,15 | 1 | 0.8386 |
| | GFol & SC6,7,14,15,16 | 1 | 0.8383 |
| VSC16(b) | GFol & SC6 | 1 | 0.7862 |
| | GFol & SC6,7 | 1 | 0.7855 |
| | GFol & SC6,7,14 | 1 | 0.7849 |
| | GFol & SC6,7,14,15 | 1 | 0.7848 |
| | GFol & SC6,7,14,15,16 | 1 | 0.7836 |

Table C.15: Characteristics of the produced reactive power of each synchronous condenser after a short-circuit at bus 4032 and the tripping of line 4032-4044, with the replacement of SMs in the central part with grid-following converters and synchronous condensers.

| SC | Configuration | Maximum value [Mvar] | Steady-state value [Mvar] |
|---|---|---|---|
| SC6 | GFol & SC6 | 287.07 | 11.27 |
| | GFol & SC6,7 | 281.02 | 10.27 |
| | GFol & SC6,7,14 | 264.72 | 9.53 |
| | GFol & SC6,7,14,15 | 240.49 | 9.40 |
| | GFol & SC6,7,14,15,16 | 218.39 | 9.08 |
| SC7 | GFol & SC6,7 | 307.06 | 32.82 |
| | GFol & SC6,7,14 | 297.16 | 30.52 |
| | GFol & SC6,7,14,15 | 287.98 | 30.11 |
| | GFol & SC6,7,14,15,16 | 274.56 | 29.11 |
| SC14 | GFol & SC6,7,14 | 357.83 | 51.86 |
| | GFol & SC6,7,14,15 | 347.82 | 51.20 |
| | GFol & SC6,7,14,15,16 | 345.00 | 50.24 |
| SC15 | GFol & SC6,7,14,15 | 315.95 | 22.32 |
| | GFol & SC6,7,14,15,16 | 312.85 | 21.82 |
| SC16 | GFol & SC6,7,14,15,16 | 281.41 | 13.46 |

Table C.16: Characteristics of bus voltages in the central part after a short-circuit at bus 4032 and the tripping of line 4032-4044, with the replacement of SMs in the central part with various technologies.

| Measure | Configuration | Maximum transient deviation [%] | Minimum transient value [pu] | Steady-state value [pu] |
|---|---|---|---|---|
| $V_{1042}$ | Initial configuration | 27.48 | 0.7372 | 1.0061 |
| | GF MFR | 32.70 | 0.6841 | 1.0083 |
| | GF MFR & SC6,7,14,15,16 | 16.41 | 0.8496 | 1.0135 |
| | GFol (VSC6,15b,16,16b) & GF MFR (VSC7,14,15) | 82.94 | 0.1734 | 1.0085 |
| | GFol & SC6,7,14,15,16 | 36.29 | 0.6476 | 1.0125 |
| $V_{1043}$ | Initial configuration | 44.72 | 0.5718 | 1.0051 |
| | GF MFR | 50.40 | 0.5130 | 1.0103 |
| | GF MFR & SC6,7,14,15,16 | 33.61 | 0.6867 | 1.0252 |
| | GFol (VSC6,15b,16,16b) & GF MFR (VSC7,14,15) | 69.23 | 0.3182 | 1.0106 |
| | GFol & SC6,7,14,15,16 | 49.27 | 0.5247 | 1.0219 |
| $V_{4042}$ | Initial configuration | 55.04 | 0.4937 | 1.0650 |
| | GF MFR | 60.31 | 0.4358 | 1.0687 |
| | GF MFR & SC6,7,14,15,16 | 50.35 | 0.5451 | 1.0785 |
| | GFol (VSC6,15b,16,16b) & GF MFR (VSC7,14,15) | 69.09 | 0.3393 | 1.0688 |
| | GFol & SC6,7,14,15,16 | 64.22 | 0.3928 | 1.0755 |
| $V_{4047}$ | Initial configuration | 39.17 | 0.6616 | 1.0698 |
| | GF MFR | 42.45 | 0.6260 | 1.0733 |
| | GF MFR & SC6,7,14,15,16 | 31.30 | 0.7472 | 1.0795 |
| | GFol (VSC6,15b,16,16b) & GF MFR (VSC7,14,15) | 60.77 | 0.4267 | 1.0735 |
| | GFol & SC6,7,14,15,16 | 57.30 | 0.4644 | 1.0779 |
| $V_{4051}$ | Initial configuration | 28.76 | 0.7840 | 1.0892 |
| | GF MFR | 32.73 | 0.7403 | 1.0903 |
| | GF MFR & SC6,7,14,15,16 | 22.48 | 0.8531 | 1.0951 |
| | GFol (VSC6,15b,16,16b) & GF MFR (VSC7,14,15) | 80.97 | 0.2094 | 1.0916 |
| | GFol & SC6,7,14,15,16 | 49.82 | 0.5522 | 1.0945 |

Table C.17: Characteristics of the current in each VSC after a short-circuit at bus 4032 and the tripping of line 4032-4044, with the replacement of SMs in the central part with various technologies.

| Configuration | VSC | Maximum transient value [pu] | Steady-state value [pu] |
|---|---|---|---|
| GF MFR | VSC6 | 1.1051 | 0.9113 |
| | VSC7 | 1.2892 | 0.8998 |
| | VSC14 | 1.3619 | 0.1125 |
| | VSC15(b) | 1.0106 | 0.0391 |
| | VSC16(b) | 0.7513 | 0.0248 |
| GF MFR & SC6,7,14,15,16 | VSC6 | 1.0776 | 0.9071 |
| | VSC7 | 1.2583 | 0.8909 |
| | VSC14 | 1.4904 | 0.8316 |
| | VSC15(b) | 1.1904 | 0.8298 |
| | VSC16(b) | 1.0907 | 0.9071 |
| GFol (VSC6,15b,16,16b) & GF MFR (VSC7,14,15) | VSC6 | 1 | 0.9263 |
| | VSC7 | 1.3884 | 0.9336 |
| | VSC14 | 1.5674 | 0.8532 |
| | VSC15 | 1.3117 | 0.8444 |
| | VSC15b | 1 | 0.8448 |
| | VSC16(b) | 1 | 0.7866 |

Table C.18: Characteristics of the produced reactive power of each synchronous condenser after a short-circuit at bus 4032 and the tripping of line 4032-4044, with the replacement of SMs in the central part with grid-forming converters and synchronous condensers.

| SC | Maximum value [Mvar] | Steady-state value [Mvar] |
|---|---|---|
| SC6 | 117.70 | 6.92 |
| SC7 | 231.18 | 21.31 |
| SC14 | 335.33 | 42.58 |
| SC15 | 239.78 | 18.01 |
| SC16 | 170.61 | 12.03 |

## C.3   HVDC connection between equiv. and central parts

### C.3.1   Frequency response

Table C.19: Characteristics of the rotor speed of $g12$ after the loss of $g15$, with both types of HVDC links.

| Configuration | Maximum transient deviation [%] | Minimum value [pu] | Steady-state value [pu] |
|---|---|---|---|
| Initial configuration | 0.69 | 0.9931 | 0.9969 |
| GFol link | 0.51 | 0.9949 | 0.9982 |
| GF MFR link | 0.89 | 0.9911 | 0.9976 |

Table C.20: Characteristics of the frequency estimated by each VSC after the loss of $g15$, with both types of HVDC links and without the LTCs.

| HVDC link type | Maximum transient deviation [%] | Minimum value [pu] | Steady-state value [pu] |
|---|---|---|---|
| GFol link | 0.51 | 0.9949 | 0.9982 |
| GF MFR link | 1.95 | 0.9805 | 0.9976 |

Table C.21: Characteristics of the current in the VSCs after the loss of $g15$, with both types of HVDC links and without the LTCs.

| HVDC link type | Bus to which the VSC is connected | Maximum value [pu] | Steady-state value [pu] |
|---|---|---|---|
| GFol link | 4045 | 0.7983 | 0.7761 |
| | 4071 | 0.8266 | 0.8218 |
| GF MFR link | 4045 | 0.8343 | 0.7630 |
| | 4071 | 0.9148 | 0.8233 |

## C.3.2 Voltage control

Table C.22: Characteristics of bus voltages in the central part after the tripping of line 4032-4044, with both types of HVDC links.

| Measure | HVDC link type | Maximum transient deviation [%] | Minimum transient value [pu] | Steady-state value [pu] |
|---------|---------------|--------------------------------|------------------------------|-------------------------|
| $V_{1042}$ | GFol link | 6.78 | 0.9335 | 0.7730 |
| | GF MFR link | 2.98 | 0.9716 | 0.9479 |
| $V_{1043}$ | GFol link | 6.07 | 0.9606 | 0.8268 |
| | GF MFR link | 2.68 | 0.9952 | 0.9820 |
| $V_{4042}$ | GFol link | 4.61 | 1.0427 | 0.9904 |
| | GF MFR link | 3.24 | 1.0577 | 1.0593 |
| $V_{4047}$ | GFol link | 3.86 | 1.0429 | 1.0188 |
| | GF MFR link | 2.36 | 1.0591 | 1.0668 |
| $V_{4051}$ | GFol link | 5.64 | 1.0307 | 0.8860 |
| | GF MFR link | 1.340 | 1.0771 | 1.0714 |

Table C.23: Characteristics of bus voltages in the central part after the tripping of line 4032-4044, with both types of HVDC links and without the LTCs.

| Measure | HVDC link type | Maximum transient deviation [%] | Minimum transient value [pu] | Steady-state value [pu] |
|---------|---------------|--------------------------------|------------------------------|-------------------------|
| $V_{1042}$ | GFol link | 6.78 | 0.9335 | 0.9616 |
| | GF MFR link | 2.98 | 0.9716 | 0.9811 |
| $V_{1043}$ | GFol link | 6.07 | 0.9606 | 0.9862 |
| | GF MFR link | 2.68 | 0.9952 | 1.0040 |
| $V_{4042}$ | GFol link | 4.61 | 1.0427 | 1.0664 |
| | GF MFR link | 3.24 | 1.0577 | 1.0711 |
| $V_{4047}$ | GFol link | 3.86 | 1.0429 | 1.0693 |
| | GF MFR link | 2.36 | 1.0591 | 1.0738 |
| $V_{4051}$ | GFol link | 5.64 | 1.0307 | 1.0562 |
| | GF MFR link | 1.40 | 1.0771 | 1.0819 |

Table C.24: Characteristics of the current in each VSC after the tripping of line 4032-4044, with both types of HVDC links.

| HVDC link type | Bus to which the VSC is connected | Maximum value [pu] | Steady-state value [pu] |
|---|---|---|---|
| GFol link | 4045 | 0.8862 | 0.8852 |
|  | 4071 | 0.8200 | 0.8197 |
| GF MFR link | 4045 | 0.8210 | 0.7742 |
|  | 4071 | 0.8922 | 0.8196 |

Table C.25: Characteristics of the current in each VSC after the tripping of line 4032-4044, with both types of HVDC links and without the LTCs.

| HVDC link type | Bus to which the VSC is connected | Maximum value [pu] | Steady-state value [pu] |
|---|---|---|---|
| GFol link | 4045 | 0.7920 | 0.7738 |
|  | 4071 | 0.8182 | 0.8178 |
| GF MFR link | 4045 | 0.8210 | 0.7612 |
|  | 4071 | 0.8922 | 0.8184 |

### C.3.3  Mix of various technologies

Table C.26: Characteristics of bus voltages in the central part after a short-circuit at bus 4032 and the tripping of line 4032-4044, with both types of HVDC links and various technologies.

| Measure | Configuration | Maximum transient deviation [%] | Minimum transient value [pu] | Steady-state value [pu] |
|---|---|---|---|---|
| $V_{1042}$ | Initial configuration | 27.48 | 0.7372 | 1.0061 |
| | GFol link | 62.67 | 0.3738 | 0.7730 |
| | GF MFR link | 49.54 | 0.5053 | 0.9479 |
| | GFol link & SC6,7,16 | 35.25 | 0.6484 | 0.9841 |
| | GF MFR link & SC6,7,16 | 24.47 | 0.7564 | 0.9942 |
| | GFol link & GF MFR6,7,16,16b | 36.24 | 0.6443 | 0.9901 |
| $V_{1043}$ | Initial configuration | 44.72 | 0.5718 | 1.0051 |
| | GFol link | 60.84 | 0.4005 | 0.8268 |
| | GF MFR link | 47.69 | 0.5349 | 0.9820 |
| | GFol link & SC6,7,16 | 45.93 | 0.5529 | 0.9873 |
| | GF MFR link & SC6,7,16 | 35.13 | 0.6633 | 1.0071 |
| | GFol link & GF MFR6,7,16,16b | 50.07 | 0.5143 | 0.9881 |
| $V_{4042}$ | Initial configuration | 55.04 | 0.4937 | 1.0650 |
| | GFol link | 58.31 | 0.4557 | 0.9904 |
| | GF MFR link | 55.15 | 0.4903 | 1.0594 |
| | GFol link & SC6,7,16 | 56.65 | 0.4738 | 1.0501 |
| | GF MFR link & SC6,7,16 | 53.79 | 0.5051 | 1.0642 |
| | GFol link & GF MFR6,7,16,16b | 55.99 | 0.4826 | 1.0593 |
| $V_{4047}$ | Initial configuration | 39.17 | 0.6616 | 1.0698 |
| | GFol link | 41.99 | 0.6293 | 1.0188 |
| | GF MFR link | 39.59 | 0.6553 | 1.0669 |
| | GFol link & SC6,7,16 | 40.50 | 0.6454 | 1.0603 |
| | GF MFR link & SC6,7,16 | 38.47 | 0.6674 | 1.0702 |
| | GFol link & GF MFR6,7,16,16b | 40.00 | 0.6520 | 1.0659 |
| $V_{4051}$ | Initial configuration | 28.76 | 0.7840 | 1.0892 |
| | GFol link | 58.44 | 0.4539 | 0.8860 |
| | GF MFR link | 36.25 | 0.6964 | 1.0714 |
| | GFol link & SC6,7,16 | 46.22 | 0.5875 | 1.0546 |
| | GF MFR link & SC6,7,16 | 27.72 | 0.7896 | 1.0828 |
| | GFol link & GF MFR6,7,16,16b | 35.05 | 0.7149 | 1.0808 |

Table C.27: Characteristics of the current in each VSC after a short-circuit at bus 4032 and the tripping of line 4032-4044, with both types of HVDC links and various technologies.

| Configuration | Measure | Maximum transient value [pu] | Steady-state value [pu] |
|---|---|---|---|
| GFol link | $I_{4045}$ | 1 | 0.8852 |
| | $I_{4071}$ | 0.8840 | 0.8200 |
| GF MFR link | $I_{4045}$ | 1.0816 | 0.7742 |
| | $I_{4071}$ | 0.9688 | 0.8196 |
| GFol link & SC6,7,16 | $I_{4045}$ | 1 | 0.7823 |
| | $I_{4071}$ | 0.8846 | 0.8199 |
| GF MFR link & SC6,7,16 | $I_{4045}$ | 1.0694 | 0.7638 |
| | $I_{4071}$ | 0.8955 | 0.8193 |
| GFol link & GF MFR (VSC6,7,16,16b) | $I_{4045}$ | 0.6990 | 0.3882 |
| | $I_{4071}$ | 0.4550 | 0.4005 |
| | $I_{VSC6}$ | 1.1277 | 0.9359 |
| | $I_{VSC7}$ | 1.3537 | 0.9121 |
| | $I_{VSC16(b)}$ | 1.1572 | 0.7939 |

Table C.28: Characteristics of the produced reactive power of each synchronous condenser after a short-circuit at bus 4032 and the tripping of line 4032-4044, with both types of HVDC links with synchronous condensers.

| Configuration | SC | Maximum value [Mvar] | Steady-state value [Mvar] |
|---|---|---|---|
| GFol link & SC6,7,16 | SC6 | 202.37 | 39.14 |
| | SC7 | 277.58 | 81.02 |
| | SC16 | 294.16 | 83.66 |
| GF MFR link & SC6,7,16 | SC6 | 154.74 | 16.36 |
| | SC7 | 215.22 | 35.75 |
| | SC16 | 185.37 | 21.18 |

# Bibliography

[1] ABB. Synchronous condensers for power grid stability. `https://new.abb.com/motors-generators/synchronous-condensers`.

[2] B. Bastin and T. Van Cutsem. Modelling and simulation of grid following converters under the phasor approximation. *University of Liege*, 2020.

[3] B. Bastin and T. Van Cutsem. Modelling and simulation of grid forming converters under the phasor approximation. *University of Liege*, 2020.

[4] H. Bevrani and J. Raisch. On virtual inertia application in power grid frequency control. *Energy Procedia*, 141:681–688, 2017.

[5] General Electric company. Hybrid high-inertia synchronous condenser facility. `https://patentimages.storage.googleapis.com/5e/59/8e/39299ec0cfd7e9/US20150168981A1.pdf`, 2015.

[6] J. Dai, Y. Phulpin, A. Sarlette, and D. Ernst. Coordinated primary frequency control among non-synchronous systems connected by a multi-terminal high-voltage direct current grid. *Generation, Transmission & Distribution, IET*, 6:99–108, Feb 2012.

[7] M.-S. Debry, G. Denis, T. Prevost, F. Xavier, and A. Menze. Maximizing the penetration of inverter-based generation on large transmission systems: the migrate project. In *6th Solar Integration Workshop*, 2017.

[8] M. Dreidy, H. Mokhlis, and S. Mekhilef. Inertia response and frequency control techniques for renewable energy sources: A review. *Renewable and Sustainable Energy Reviews*, 69:144–155, 2017.

[9] D. Ernst. Energy markets: system security and ancillary services. *University of Liege*, slides 2019.

[10] A. Fernández-Guillamón, E. Gómez-Lázaro, E. Muljadi, and Á. Molina-García. Power systems with high renewable energy sources: A review of inertia and frequency control strategies over time. *Renewable and Sustainable Energy Reviews*, 115:109369, 2019.

[11] D. Gross, S. Bolognani, B. K. Poolla, and F. Dörfler. Increasing the resilience of low-inertia power systems by virtual inertia and damping. In *Proceedings of IREP'2017 Symposium*, page 64, s.l., 2017-08-31. International Institute of Research and Education in Power System Dynamics (IREP).

[12] ENTSO-E Technical Group. High penetration of power electronic interfaced power sources and the potential contribution of grid forming converters. Jan 2020.

[13] B. Hartmann, I. Vokony, and I. Táczi. Effects of decreasing synchronous inertia on power system dynamics - overview of recent experiences and marketisation of services. *International Transactions on Electrical Energy Systems*, 29(12):e12128, 2019.

[14] H. Jóhannsson. Stability and control in power systems, introduction to the power system stability problem. *Technical University of Denmark*, slides 2019.

[15] Electropaedia : Battery and energy technologies. `https://www.mpoweruk.com/life.htm`, 2005.

[16] B. Kroposki, B. Johnson, Y. Zhang, V. Gevorgian, P. Denholm, B.-M. Hodge, and B. Hannegan. Achieving a 100% renewable grid: Operating electric power systems with extremely high levels of variable renewable energy. *IEEE Power and Energy Magazine*, 15(2):61–73, 2017.

[17] U. Markovic, O. Stanojev, P. Aristidou, and G. Hug. Partial grid forming concept for 100% inverter-based transmission systems. In *2018 IEEE Power & Energy Society General Meeting (PESGM)*, pages 1–5. IEEE, 2018.

[18] J. Matevosyan, B. Badrzadeh, T. Prevost, E. Quitmann, D. Ramasubramanian, H. Urdal, S. Achilles, J. Mac-Dowell, S. H. Huang, V. Vital, et al. Grid-forming inverters: Are they the key for high renewable penetration? *IEEE Power and Energy Magazine*, 17(6):89–98, 2019.

[19] F. Milano, F. Dörfler, G. Hug, D. J Hill, and G. Verbič. Foundations and challenges of low-inertia systems. In *2018 Power Systems Computation Conference (PSCC)*, pages 1–25. IEEE, 2018.

[20] J. G. Møller. Stability and control in power systems, active power and frequency control: Frequency stability. *Technical University of Denmark*, slides 2019.

[21] L. Papangelis. *Local and centralized control of multi-terminal DC grids for secure operation of combined AC/DC systems*. PhD thesis, Université de Liège, Liège, Belgique, 2018.

[22] D. Pattabiraman, R.H. Lasseter, and T.M. Jahns. Comparison of grid following and grid forming control for a high inverter penetration power system. In *2018 IEEE Power & Energy Society General Meeting (PESGM)*, pages 1–5. IEEE, 2018.

[23] M. Sanduleac, L. Toma, M. Eremia, V. A Boicea, D. Sidea, and A. Mandis. Primary frequency control in a power system with battery energy storage systems. In *2018 IEEE International Conference on Environment and Electrical Engineering and 2018 IEEE Industrial and Commercial Power Systems Europe (EEEIC/I&CPS Europe)*, pages 1–5. IEEE, 2018.

[24] C. Seneviratne and C. Ozansoy. Frequency response due to a large generator loss with the increasing penetration of wind/pv generation–a literature review. *Renewable and Sustainable Energy Reviews*, 57:659–668, 2016.

[25] U. Tamrakar, D. Shrestha, M. Maharjan, B. Bhattarai, T. Hansen, and R. Tonkoski. Virtual inertia: Current trends and future directions. *Applied Sciences*, 7(7):654, Jun 2017.

[26] A. Tayyebi, F. Dörfler, F. Kupzog, Z. Miletic, and W. Hribernik. Grid-forming converters–inevitability, control strategies and challenges in future grids application. *AIM*, 2018.

[27] P. Tielens and D. Van Hertem. Grid inertia and frequency control in power systems with high penetration of renewables. In *Young Researchers Symposium in Electrical Power Engineering, Date: 2012/04/16-2012/04/17, Location: Delft, The Netherlands*, 2012.

[28] P. Tielens and D. Van Hertem. The relevance of inertia in power systems. *Renewable and Sustainable Energy Reviews*, 55:999–1009, Mar 2016.

[29] A. Ulbig, T. S. Borsche, and G. Andersson. Impact of low rotational inertia on power system stability and operation. *IFAC Proceedings Volumes*, 47(3):7290 – 7297, 2014. 19th IFAC World Congress.

[30] T. Van Cutsem. Introduction to electric power and energy systems. *University of Liege*, 2019.

[31] T. Van Cutsem. Power system dynamics, control and stability - long-term voltage instability: dynamic aspects and countermeasures - course lectures. *University of Liege*, 2019.

[32] T. Van Cutsem and X. Guillaud. High voltage direct current grids - course lectures. *University of Liege*, 2019.

[33] T. Van Cutsem and L. Papangelis. Description, modeling and simulation results of a test system for voltage stability analysis (version 6). *University of Liege*, 2013.

[34] J. Yu, K. Bakic, A. Kumar, A. Iliceto, L. Beleke Tabu, J.L. Ruaud, J. Fan, B. Cova, H. Li, D. Ernst, et al. Global electricity network-feasibility study. 2019.